UNIVERSITY OF HOUSTON

MECHANICAL ENGINEERING DEPARTMENT

Nondestructive Characterization of Two-Phase Metal - Matrix Materials

DAAL03-88-K-0096

Final Report

SUBMITTED TO
U. S. ARMY RESEARCH OFFICE
MATERIALS SCIENCE DIVISION

December, 1991

UNCLASSIFIED

SECU

AD-A249 912

RT DOCUMENTATION PAGE

1a. F
Ur

1b. RESTRICTIVE MARKINGS

2a. S

3. DISTRIBUTION / AVAILABILITY OF REPORT
Approved for public release; distribution unlimited.

2b. DECLASSIFICATION / DOWNG ING SCHEDULE

MAY 04 1992

S D

4. PERFORMING ORGANIZATION EPORT NUMBER(S)

5. MONITORING ORGANIZATION REPORT NUMBER(S)
ARO 25397.9-MS

6a. NAME OF PERFORMING ORGANIZATION	6b. OFFICE SYMBOL (If applicable)	7a. NAME OF MONITORING ORGANIZATION
University of Houston		U. S. Army Research Office

6c. ADDRESS (City, State, and ZIP Code)	7b. ADDRESS (City, State, and ZIP Code)
4800 Calhoun Houston, Texas 77204-4792	P. O. Box 12211 Research Triangle Park, NC 27709-2211

8a. NAME OF FUNDING / SPONSORING ORGANIZATION	8b. OFFICE SYMBOL (If applicable)	9. PROCUREMENT INSTRUMENT IDENTIFICATION NUMBER
U. S. Army Research Office		DAAL03-88-K-0096

8c. ADDRESS (City, State, and ZIP Code)	10. SOURCE OF FUNDING NUMBERS			
	PROGRAM ELEMENT NO.	PROJECT NO.	TASK NO.	WORK UNIT ACCESSION NO.
P. O. Box 12211 Research Triangle Park, NC 27709-2211				

11. TITLE (Include Security Classification)
Nondestructive Characterization of Two-Phase Metal-Matrix Materials

12. PERSONAL AUTHOR(S)
Professor Kamel Salama

13a. TYPE OF REPORT	13b. TIME COVERED	14. DATE OF REPORT (Year, Month, Day)	15. PAGE COUNT
Final	FROM 6/88 TO 10/91	December, 1991	

16. SUPPLEMENTARY NOTATION The view, opinions and/or findings contained in this report are those of the author(s) and should not be construed as an official Department of the Army position, policy, or decision, unless so designated by other documentation.

17. COSATI CODES			18. SUBJECT TERMS (Continue on reverse if necessary and identify by block number)
FIELD	GROUP	SUB-GROUP	

19. ABSTRACT (Continue on reverse if necessary and identify by block number)

The Major goal of this program is to study methods for the nondestructive characterization of mechanical properties of two-phase metal-matrix composites such as discontinuous SiC-reinforced aluminum alloys. The methods to be studied are based on the physical nonlinear elastic behavior of solids and utilized measurements of the elastic as well as the accoustoelastic constants. The objectives are to establish both experimentally and theoretically relationships between those parameters which can be measured nondestructively and the percentages of second phase in two-phase systems. Mechanical properties of these systems are derived from the presence of reinforcement second phase in the matrix.

The research accomplished during contract No. DAAL03-88-K-0096 of the Army Research Office program is documented in details in 4 theses (1 - 4) and 8 papers (5 - 12). Abstracts of these theses and reprints or preprints of these papers are attached in appendix A.

20. DISTRIBUTION / AVAILABILITY OF ABSTRACT	21. ABSTRACT SECURITY CLASSIFICATION
☒ UNCLASSIFIED/UNLIMITED ☐ SAME AS RPT. ☐ DTIC USERS	Unclassified

22a. NAME OF RESPONSIBLE INDIVIDUAL	22b. TELEPHONE (Include Area Code)	22c. OFFICE SYMBOL
Professor Kamel Salama	(713) 749-4455	

DD FORM 1473, 84 MAR 83 APR edition may be used until exhausted. All other editions are obsolete

SECURITY CLASSIFICATION OF THIS PAGE
UNCLASSIFIED

U. S. ARMY RESEARCH OFFICE
MATERIALS SCIENCE DIVISION

Nondestructive Characterization of Two-Phase Metal - Matrix Materials
DAAL03-88-K-0096

Final Report

The Major goal of this program is to study methods for the nondestructive characterization of mechanical properties of two-phase metal-matrix composites such as discontinuous SiC-reinforced aluminum alloys. The methods to be studied are based on the physical nonlinear elastic behavior of solids and utilize measurements of the elastic as well as the acoustoelastic constants. The objectives are to establish both experimentally and theoretically relationships between those parameters which can be measured nondestructively and the percentages of second phase in two-phase systems. Mechanical properties of these systems are derived from the presence of reinforcement second phase in the matrix.

The research accomplished during contract No. DAALO3-88-K-0096 of The Army Research Office program is documented in details in 4 theses (1 - 4) and 8 papers (5 - 12). Abstracts of these theses and reprints or preprints of these papers are attached in appendix A. The major accomplishments obtained under this program are, however, summarized in the following.

A. Texture

Texture is the reason for the direction dependence of materials properties. It is developed during the plastic deformation and heat treatment during manufacturing. It is characterized by the fourth-order expansion coefficients of the orientation distribution function (ODF), $C^{11}{}_4$ and $C^{12}{}_4$ and $C^{13}{}_4$. In two-phase materials, however, the situation is more complicated where the properties, the shape, the volume fraction and the orientation of each phase influence the macroscopic behavior.

In this study (1, 5, 6), an ultrasonic method is developed for the nondestructive characterization of texture in metal-matrix composites. The method utilizes the measurements of

the six independent ultrasonic velocities Vij and the formulation given by Bunge. The examined composites are the siicon carbide (Si-C)-particle-reinforced aluminum 8091, 7094, and 6061 metal-matrix composites. The fourth-order expansion coefficients of the orientation distribution function are found to change linearly as a function of the SiC content. Also in this study, the relationship between elastic anistropy and texture in metal-matrix composites has been developed under certain conditions. Linear correlations between anisotropy described by Young's moduli and texture determined by orientation distribution function expansion coefficients are obtained, and found to confirm developed relationships for two-phase metal-matrix composites. These results show that ultrasonic measurements provide a viable technique for the characterization of texture and elastic anisotropy in these materials.

B. **Elastic Properties and Elastic Anisotropy**

In this investigation (2, 7, 8, 11), longitudinal and shear ultrasonic velocities have been measured in aluminum based metal matrix composites containing either SiC-particles or alumina fibers and particles as the reinforcements. Three types (extruded, pressed, squeeze cast) of composites have been investigated. Also, based on microstructural studies, models have been developed in order to predict and explain the elastic properties of these composites. From the experimental measurements as well as the comparison between measured and calculated elastic moduli the following conclusions are obtained.

1. Extruded Composites

a) For relatively low volume percentage of reinforcement, up to 20%, the elastic moduli increase linearly with SiC-particle content.

b) The overall increase in elastic moduli due to the reinforcement can be well predicted by a model assuming dilute concentration of particles.

c) The extrusion direction is elastically stiffer than the other two directions.

d) The higher value of Young's modulus along the extrusion direction is partly due to the aligned particle free regions created during manufacturing, and partly due to texture in the aluminum matrix.

2. Pressed Composites

a) For the high volume fraction of SiC-particles, up to 40%, the increase in elastic moduli with particle content is not linear and deviates significantly towards higher values.

b) The model assuming dilute concentration of particles fails completely to predict the increase in elastic moduli.

c) The high values in elastic moduli can be attributed to the increased interaction between particles as the particle content becomes higher.

d) The elastic moduli in the compression direction is lower than in the directions in the plane of the plate.

3. Squeeze Cast Composites

a) The elastic moduli increase with the alumina particle content, whereas the elastic anisotropies between directions in the plane of fibers and normal to this plane decrease with the particle content.

b) The overall increase in elastic moduli as well as the elastic anisotropies can be predicted by a model assuming no interaction between particles and fibers.

c) The planar-random alignment of fibers makes the composites stiffer in that plane.

C. Manufacturing

In this work, the powder metallurgy process has been successfully implemented in the processing of aluminum metal matrix composites containing up to 30 volume percent of silicon carbide particulate, and up to 20 volume percent silicon carbide whiskers (3). The composites processed have been densified to above 97 percent of their theoretical density, which is comparable to those obtained from commercial sources. The stiffness properties of these composites have been evaluated using flexure and compression mechanical tests as well as ultrasonic measurements, and are found to match those of commerical composites.

Theoretical calculations of the Young's modulus based on the Hashin-Strikman and the Eshelby models are found to be in good agreement with the experimental results for particulate content of 15 percent or less. At higher percentages of reinforcement, however, both models

underpredict the stiffnesses. For the whisker reinforced composites, the Eshelby model predicts the stiffnesses better than the shear large model. The stiffnesses predicted by the composite cylinders model are also found to agree pretty well with experimental results.

D. **Nonlinear elastic Effects**

In this study, the temperature dependances of nonlinear effects effects are investigated by measuring the acoustoelastic constants at different temperatures using ultrasonic time of flight measurements (4, 9, 12). These constants are determined in the aluminum alloys AlMg 3, 7064, and 8091 as well as in SiC-particle reinforced metal matrix composites based on the aluminum alloys 7064 and 8091. In the metal matrix composite specimens, the acoustic nonlinearity parameter is also measured using the harmonic generation technique. The results show the following.

a) In all materials investigated, the acoustoelastic constants show a linear temperature dependance. In single phase alloys, the third order elastic constants, calculated from acoustoelastic constants show an increase in magnitude for the constants l and m with temperature. However, the increase in the constant l is stronger. The third order elastic constant n is not significantly influenced by temperature. In the case of the two phase metal matrix composites, temperature changes affect the three third order elastic constants decreases with increasing temperature.

b) The temperature dependence of the acoustoelastic effect confirms the linear relationship between stresses in the material and the temperature dependance of the longitudinal velocity found by Salama and Long. The parameter K, which characterizes the magnitude of the stress-temperature dependance of ultrasonic velocities, is found to be significantly influenced by the base material as well as the alloying elements contained.

c) The acoustic nonlinearity parameter, which is a measure for the material's deviation from the ideal Hookean behavior, is calculated using the second and third order elastic constants for all specimens investigated. Similar to the behavior of the parameter K, the value of the nonlinearity parameter is found to depend strongly on the base material as well as the reinforcements.

d) In two phase materials, it is not sufficient to realate changes in the nonlinearity parameter to lattice distortions only. Since the determination of β involves the ratio between third and second order elastic constants, changes in the elastic moduli, due to the presence of second phase, are to be taken into account. In the case of coherent precipitates, where increases in the elastic moduli are negligible, the behavior of the nonlinearity parameter is dominated by the lattice distortions. Earlier studies by Razvi et al. revealed an increase in the nonlinearity parameter with the volume fraction of second phase particles in such materials. However, in the metal matrix composites investigated in the present study, the behavior of the nonlinearity parameter is dominated by the increase of the elastic moduli.

e) Values of calculated nonlinearity parameters as well as those directly measured are found to decrease linearly with increasing content of second phase particles. Also the presence of reinforcement particles changes the temperature dependance of the nonlinearity parameter in the metal-matrix composites. In contrast to the behavior in single phase alloys, its value decreases with increasing temperature. Changes in the distortion of the matrix are believed to be responsible for this opposite behavior. A temperature increase leads to relaxation of the thermal stresses which are always present in metal matrix composites, due to the mismatch of the coefficients of thermal expansion of the matrix and the reinforcement materials. The relaxation of these stresses reduces the distortion of the matrix and, thus, the value of the nonlinearity parameter decreases.

E. Scanning Acoustic Microscope (SAM) Studies

In addition to the above macroscopic studies, preliminary acoustic microscopy studies (13) on samples of Al-8091 and Al-7064 show that the SAM has no difficulty at 1.0 GHz in resolving the particles in both composites. The resolution in the GHz range is on the order of a micron, so that detection of the particles is not a difficulty. In the characterization of the interface the assumption is made that changes in the stress field will produce measurable changes in the region of the interface and there will be a corresponding change in the stress between the two phases due to the difference in the thermally induced strain between them. This will cause changes in the sound propagation properties in the stressed regions. Although these changes are small they

depend on the properties of the interface and can be measured.

The affected region can range from nanometers to micrometers in thickness even in the GHz range and the properties will vary throughout only one acoustic wavelength. Point to point changes along the boundary, however, cause significant changes in the shape of the fringe pattern due to the changing of the boundary conditions at the reflecting interface. In addition, many of the particles exhibit surface wave scattering fringes over several wavelengths, indicating higher phase sensitivity.

REFERENCES

1. M. Spies, "Nondestructive Determination of Materials' Textures by Ultrasonic Techniques", M. S. Thesis, University of Houston, Dec. 1988.

2. B. Grelsson, "Ultrasonic Determination and Modeling of Elastic Properties of Metal-Matrix Composites", M.S. Thesis, University of Houston, Aug. 1990.

3. S. Jayashankar, "Processing and Characterization of Aluminum/Silicon Carbide Composites", M.S. Thesis, University of Houston, Dec. 1990.

4. H. P. Mohrbacher, "Temperature Dependence of Nonlinear Ultrasonic Effects", M.S. Thesis, University of Houston, May 1991.

5. M. Spies and K. Salama, Res. Nondestructive Evaluation, 1, p. 99 (1989).

6. M. Spies and K. Salama, Ultrasonics, 28, p. 370 (1990).

7. B. Grelsson and K. Salama, Proc. QNDE, 9B, p. 1441 (1990).

8. B. Grelsson and K. Salama, Res. Nondestructive Evaluation, 2, p. 83 (1990).

9. M. Mohrbacher, E. Schneider and K. Salama, Proc. QNDE, 10,(1991), in press.

10. J. H. Cantrell and K. Salama, Internation Metal Rev. (1991), in press.

11. B. Grelsson and K. Salama, Proc. IMC6 (1991), submitted.

12. M. Mohrbacher and K. Salama, Res. Nondestructive Evaluation, (1991), submitted.

13. T. Miller, "Characterization of the Microstructure in Al/SiC Metal Matrix Composites Using Acoustic Microscope Technique", M.S. Thesis, University of Houston, Aug. 1988.

APPENDIX

Temperature Dependance of Nonlinear Ultrasonic Effects

An Abstract of a Thesis
Presented to
The Faculty of the Materials Engineering Program
Cullen College of Engineering
University of Houston

In Partial Fulfillment
of the Requirements for the Degree
Master of Science in Materials Engineering

---

by
Hardy P. Mohrbacher
May 1991

Abstract

Many important material properties are of nonlinear nature. Among them are the stress-temperature dependance of ultrasonic velocities, the distortion of elastic waves by the generation of higher harmonics, and the thermal expansion. These effects are characterized quantitatively by measurements of the acoustoelastic constants, the acoustic nonlinearity parameter, and the coefficient of thermal expansion.

In this study, the temperature dependances of nonlinear ultrasonic effects are investigated in the cemented carbide WC-Co, the ferritic steel 24 CrMoV 5 5, the austenitic steel X6 CrNi 18 11, the aluminum alloys AlMg 3, Al 7064 and Al 8091 as well as in metal-matrix composites consisting of Al 7064 and Al 8091 matrices and SiC-particles. The results show that the magnitude of acoustic nonlinearity depends on the base material, alloying elements, and microstructure. It increases with the temperature in single phase materials whereas it decreases in metal-matrix composites. The various contributions to the acoustic nonlinearity are analyzed qualitatively and possible explanations for its behavior in metal-matrix composites are discussed.

Nondestructive Determination of Materials' Textures by Ultrasonic Techniques

---

An Abstract of A Thesis

Presented to

The Faculty of the Interdisciplinary Program in Materials Engineering

University of Houston

In Partial Fulfillment

of the Requirements for the Degree

Master of Science in Materials Engineering

---

by

Martin Spies

December 1988

Abstract

Textures or preferred orientations of single crystals in polycrystalline materials are developed by heat treatment and deformation processes like rolling, drawing and extrusion. Thus magnetic, elastic and plastic properties become directionally dependent. This can yield desirable behavior, but it can have also negative effects. In both cases a nondestructive determination of the texture and its consequences for materials behavior is of great interest.

In this study texture is analyzed by determining the fourth-order expansion coefficients of the orientation distribution function from the measured ultrasonic velocities of different wave modes. The results obtained for rolled ferritic steel sheets, rolled ferritic steel plates and for extruded metal-matrix composites of the aluminium alloys Al-8091, Al-7064 and Al-6061 with silicon carbide particle reinforcements show that ultrasonics provide an efficient nondestructive method of texture analysis in the bulk as well as on the surface of these materials. The expansion coefficients determined for the ferritic steels agree qualitatively with those determined by x-ray diffraction which is a common nondestructive technique for texture analysis. For the metal-matrix composites the expansion coefficients have been determined under the assumption that only the Al-matrix is textured. The results also show that the fourth-order expansion coefficients allow the evaluation of the elastic and the plastic behavior of the examined specimens.

PROCESSING AND CHARACTERIZATION OF

ALUMINUM/SILICON CARBIDE COMPOSITES

An Abstract

of a

Thesis

Presented to

The Faculty of the Department of Mechanical Engineering

University of Houston

In Partial Fulfillment

of the Requirements for the Degree

Master of Science in Mechanical Engineering

S. Jayashankar

December 1990

ABSTRACT

The effects of varying the reinforcement type and content on the elastic behavior of aluminum / silicon carbide composites have been investigated in order to develop relationships to be used in controlling the integrity of the composites. A canless powder metallurgy (PM) process was successfully developed for the in-house manufacture of the MMC specimens . Composite specimens with up to 30 v/o particulates and up to 20 v/o whiskers were fabricated using Al 6061 as the base metal. The elastic moduli of these MMCs were characterized using ultrasonic velocity measurements as well as mechanical testing involving flexural and compressive tests. The measured moduli were also compared with model predictions.

The results indicate that the addition of the particulate or the whisker reinforcements increase the elastic moduli as well as the elastic anisotropy of the MMCs. The composites were elastically stiffer in the plane perpendicular to the hot pressing direction than in the pressing direction and also exhibited transverse isotropy about the pressing axis. While the anisotropy of the particulate reinforced MMCs is attributed to the uneven distribution of the reinforcement along the different directions, the anisotropy of the whisker reinforced MMC is traced to the planar orientation of the whiskers in the plane perpendicular to the pressing direction. Also, it is found that the substitution of particulate reinforcement by whiskers does not improve the elastic stiffness of the MMCs for this method of composite manufacture.

ULTRASONIC DETERMINATION AND MODELING OF ELASTIC PROPERTIES OF METAL MATRIX COMPOSITES

An Abstract

of a

Thesis

Presented to

The Faculty of the Department of Mechanical Engineering

University of Houston

In Partial Fulfillment

of the Requirements for the Degree

Master of Science in Materials Engineering

Bertil Grelsson

August 1990

ABSTRACT

Conventionally, metal matrix composites (MMC) are reinforced with either particles or fibers, but lately, a new class of composites has emerged, where a mixture of particles and fibers is used as a reinforcement. The particles are present to improve the overall mechanical and thermal properties, whereas the fibers introduce the directionality often desired in some applications.

The elastic behavior of three composites with different matrices and volume fraction of particles (9,13 and 17%), but the same fiber content (6%), has been characterized using ultrasonic velocity measurements. The results show that the elastic moduli increase with particle content and that the composites are elastically stiffer in the directions of the plane of the fibers than in the direction normal to that plane.

A model is developed to explain the observed elastic moduli of these composites. This model uses the results of theories presented by Ledbetter and Datta, for spherical inclusions, and by Hashin and Rosen, for aligned fibers. It also includes an average procedure suggested by Christensen and Waals. The agreement between measured and calculated elastic moduli is found to be very good and the elastic anisotropies observed in these composites could also be predicted.

Elastic moduli are also determined using ultrasonic velocity measurements for two series of extruded MMC's and one series of pressed MMC's. These composites are reinforced with SiC-particles only. The elastic moduli as well as the elastic anisotropies in these composites could be explained using combinations and/or special cases of the theories mentioned above.

Res Nondestr Eval (1989) 1:99–109

Texture of Metal-Matrix Composites by Ultrasonic Velocity Measurements

M. Spies* and K. Salama

Department of Mechanical Engineering, University of Houston, Houston, TX 77204, USA

Abstract. An ultrasonic method is developed for the nondestructive characterization of texture in metal-matrix composites. In this approach, it is assumed that the presence of reinforcement particles changes the elastic properties of the composite but only the texture of the matrix. The method utilizes the measurements of the six independent ultrasonic velocities V_{ij} and the formulation given by Bunge. The examined composites are the silicon carbide (SiC)-particle-reinforced aluminum 8091, 7064, and 6061 metal-matrix composites. The fourth-order expansion coefficients of the orientation distribution function are determined as a function of the SiC content in these composites. The results show that the expansion coefficients change with the presence of SiC where the coefficients C_4^{11} and C_4^{13} increase as the volume fraction of SiC is increased and the coefficient C_4^{12} is zero in all composites examined. The analysis of these results indicates that ultrasonics can provide a promising technique for the texture characterization of metal-matrix composites.

Introduction

Texture is the orientation distribution of the single crystals in the polycrystalline aggregate. A textured polycrystal is elastically anisotropic because the elastic properties of a single crystal are directionally dependent. Because of the texture, the single crystal anisotropies do not vanish when averaged, thus the polycrystal looses its quasi-isotropy. Most structural materials are polycrystalline aggregates and their exposure to plastic deformation and heat treatment during manufacturing leads to the alignment of single crystals relative to the forming geometry. This development of preferred orientation is the main reason for the anisotropic behavior in these materials. The texture is characterized by the fourth-order expansion coefficients of the orientation distribution function (ODF). These three coefficients allow a satisfactory evaluation of the elastic as well as the plastic behavior of polycrystalline aggregates, as has been

* *Permanent address:* Institut für zerstörungsfreie Prüfverfahren, Saarbrücken, FRG.

shown by several studies (e.g., [1–5]). This situation, however, is more complicated in the case of two-phase or multiphase materials, where the properties, the shape, the volume fraction, and the orientation of each phase influence the macroscopic behavior.

In metal-matrix composites a ductile metal and a high strength reinforcement are combined to provide a composite of high strength and toughness. Since many of these properties are characteristic of the bulk, ultrasonics have been shown to provide promising nondestructive methods for the characterization of metal-matrix composites [6].

In this study, an ultrasonic method is developed for the nondestructive characterization of texture in metal-matrix composites. Measurements of ultrasonic velocities are used to determine the texture in the silicon carbide (SiC)-reinforced 8091, 7064, and 6061 aluminum composites.

Quantitative Texture Analysis Using Ultrasonics

Orientation Distribution Function

Texture is mathematically described by the ODF. This function determines the probability of finding a single crystal in the polycrystalline sample with a certain orientation with respect to the sample orientations, given by the axes of the sample fixed coordinate system. According to Bunge [7], the ODF can be written as a series expansion into symmetrical generalized spherical harmonics as

$$f(g) = \sum_{l=0}^{\infty} \sum_{\mu=1}^{M(l)} \sum_{\nu=1}^{N(l)} C_l^{\mu\nu} \dot{T}_l^{\mu\nu}(g) \tag{1}$$

where g is the orientation, the $T_l^{\mu\nu}$ are symmetrical generalized spherical harmonics and the $C_l^{\mu\nu}$ are the expansion coefficients. The upper limits $M(l)$ and $N(l)$ depend on l as well as the crystal and sample symmetry, respectively. The orthonormal function system $T_l^{\mu\nu}$ is invariant towards all rotations of the sample symmetry (indicated by the right dot) and the crystal symmetry (indicated by the left two dots). In first approximation only the three fourth-order expansion coefficients C_4^{11}, C_4^{12} and C_4^{13} need to be considered for texture evaluation in cubic materials with orthorhombic sample symmetry [1, 8]. These three coefficients can be used to characterize both the elastic and the plastic behavior of these materials. The fourth-order coefficients in the Roe-notation [9] are called W_{400}, W_{420}, and W_{440} and are related to Bunge's coefficients by the following expression:

$$\begin{aligned} W_{400} &= \frac{1}{24\pi^2} \sqrt{\frac{7}{6}}\, C_4^{11} \\ W_{420} &= \frac{1}{24\pi^2} \sqrt{\frac{7}{12}}\, C_4^{12} \\ W_{440} &= \frac{1}{24\pi^2} \sqrt{\frac{7}{12}}\, C_4^{13}. \end{aligned} \tag{2}$$

Ultrasonic Velocity Relationships

Inserting the elastic constants of the textured polycrystal, given by Bunge [1] for cubic crystal structure, into Christoffel's equation for the orthorhombic sample, the following relationships between the velocities of ultrasonic waves V_{ij} and the expansion coefficients C_4^{lr} result as

$$\begin{aligned}
\rho V_{11}^2 &= c_{11} - c\left[\frac{2}{5} - \frac{1}{70}\sqrt{\frac{7}{3}}\left(C_4^{11} - \frac{2}{3}\sqrt{5}\,C_4^{12} + \frac{1}{3}\sqrt{35}\,C_4^{13}\right)\right] \\
\rho V_{22}^2 &= c_{11} - c\left[\frac{2}{5} - \frac{1}{70}\sqrt{\frac{7}{3}}\left(C_4^{11} + \frac{2}{3}\sqrt{5}\,C_4^{12} + \frac{1}{3}\sqrt{35}\,C_4^{13}\right)\right] \\
\rho V_{33}^2 &= c_{11} - c\left(\frac{2}{5} - \frac{1}{70}\sqrt{\frac{7}{3}}\frac{8}{3}\,C_4^{13}\right) \qquad (3) \\
\rho V_{12}^2 &= c_{44} + c\left[\frac{1}{5} + \frac{1}{70}\sqrt{\frac{7}{3}}\left(\frac{1}{3}\,C_4^{11} - \frac{1}{3}\sqrt{35}\,C_4^{13}\right)\right] = \rho V_{21}^2 \\
\rho V_{23}^2 &= c_{44} + c\left[\frac{1}{5} - \frac{1}{70}\sqrt{\frac{7}{3}}\left(\frac{4}{3}\,C_4^{11} + \frac{2}{3}\sqrt{5}\,C_4^{12}\right)\right] = \rho V_{32}^2 \\
\rho V_{31}^2 &= c_{44} + c\left[\frac{1}{5} - \frac{1}{70}\sqrt{\frac{7}{3}}\left(\frac{4}{3}\,C_4^{11} - \frac{2}{3}\sqrt{5}\,C_4^{12}\right)\right] = \rho V_{13}^2,
\end{aligned}$$

where ρ is the density and c_{11}, c_{12}, and c_{44} are the elastic constants of the cubic single crystal and $c = c_{11} - c_{12} - 2c_{44}$. In these relationships the velocity is characterized by two subscripts. The first indicates the propagation direction, while the second indicates the polarization direction of the wave. 1, 2, and 3 designate the axes in a right-handed coordinate system as shown in Fig. 1.

The Lamé constants λ and μ for the untextured polycrystal ($C_4^{11} = C_4^{12} = C_4^{13} = 0$) can be expressed as

$$\mu = c_{44} + \frac{1}{5}c,\ \lambda + 2\mu = c_{11} - \frac{2}{5}c,\ \lambda = c_{12} + \frac{1}{5}c.$$

For the isotropic case ($c = 0$), the shear wave velocity V_S as well as the longitudinal wave velocity V_L will be the same in all directions, and

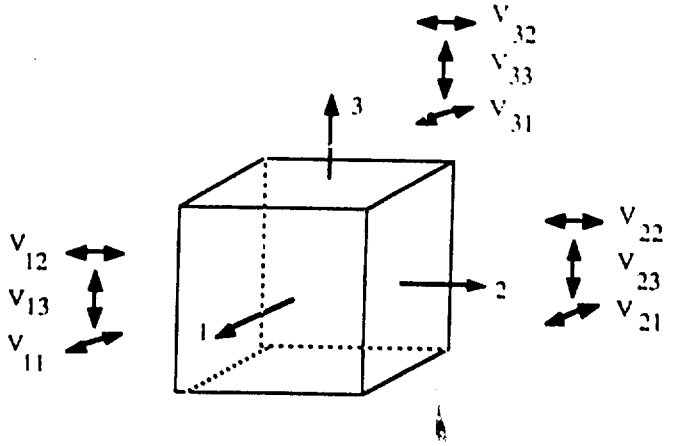

Fig. 1. Velocity designations for free ultrasonic waves.

Table 1. Chemical composition of aluminium alloys and volume percentage of SiC reinforcement of the MMC-specimens

	Alloying Elements									
Alloy	Si	Fe	Cu	Mg	Zr	Li	Zn	Cr	Co	Al
8091	0.02	0.01	1.90	0.80	0.11	2.70	—	—	—	rem
7064	0.05	0.10	2.00	2.30	0.20	—	7.10	0.12	0.22	rem
6061	0.71	0.29	0.21	0.86	—	—	0.10	0.06	—	rem

Specimens		
8091 + 0% SiC	8091 + 10% SiC	8091 + 15% SiC
7064 + 0% SiC	7064 + 15% SiC	7064 + 20% SiC
	6061 + 15% SiC	6061 + 20% SiC

$$\rho V_1^2 = c_{11} = \lambda + 2\mu,$$

$$\rho V_2^2 = c_{44} = \mu.$$

A further useful expression which can be obtained from Eqs. (3) is

$$\rho(V_{31}^2 + V_{32}^2 + V_{33}^2) = c_{11} + 2c_{44}. \tag{4}$$

Experiment

The metal-matrix composites examined in this investigation are the aluminium alloys Al-8091, Al-7064, and Al-6061 containing up to 20% volume fraction of SiC particles. The chemical compositions of these alloys and the volume percentages of the SiC reinforcement are shown in Table 1. The Al-8091 and Al-7064 composites were received as extruded rods of 25 mm in diameter, while the Al-6061 composites were received as extruded bars of 16 mm in thickness and 50 mm in width. Prismatic specimens 15 to 18 mm wide and 30 mm long were machined such that the length direction was parallel to the extrusion direction. Opposite faces were machined flat and parallel to within ±0.025 mm. All these specimens were examined in the as-received condition.

In order to determine the ODF-expansion coefficients, ultrasonic velocity measurements are performed using the pulse-echo-overlap method, which is described in detail by Papadakis [10]. The system used in this investigation consists of an ultrasound apparatus which generates pulses of approximately 1 μs duration and of variable repetition rate. These pulses are impressed on a commercial transducer of a fundamental frequency of 5 MHz which is acoustically bonded to the specimen. The reflected echoes, *rf*, are received by the same transducer, amplified, and displayed on a screen of an oscilloscope. Two of the displayed echoes are then chosen and exactly overlapped by critically adjusting the frequency of a C.W. oscillator and the division factor on a decade divider. The frequency, *f*, accurately determined by an electronic counter is employed to compute the ultrasonic velocity using the relationship $V = sf$, where s is the path length of the ultrasonic wave. The system is capable of

measuring changes in the ultrasonic velocity to an accuracy of better than 1 part in 10^5, while the inaccuracy of measuring both the longitudinal and the shear velocities is estimated to be 0.3%.

Results

Reduction of Data

The conversion of the measured velocity data to the texture expansion coefficients is very critical. Equations (3), which relate the velocities V_{ij} of shear and longitudinal waves with different polarization and propagation directions to the fourth-order expansion coefficients, provide a variety of relationships to determine these coefficients. These relationships are shown in Table 2. In order to select the relationships from which the coefficients are to be determined, the propagation of errors involved in the procedure of reducing the measured data to the physically significant quantities becomes very important.

From Table 2 one can see that there are three relationships which determine C_4^{11} and four equations to determine each of C_4^{12} and C_4^{13}. The usual procedure to determine these coefficients from the relationships shown in Table 2 is to use the least-squares analysis. However, in order to keep the number of velocities to be measured low and to reduce the effect of propagation of errors, the following procedure is employed:

1. We select relationships which do not require the absolute values of velocities and only require the differences in these velocities. Thus errors in the

Table 2. Different relationships for the determination of the expansion coefficients C_4^{lr}

$C_4^{11} = A_1[\rho V_{33}^2 - (\lambda + 2\mu)]$	(a)
$C_4^{11} = A_1[2\mu - \rho(V_{31}^2 + V_{32}^2)]$	(b)
$C_4^{11} = A_1[\rho(V_{11}^2 + V_{22}^2 + 2V_{12}^2) - 2(\lambda + 2\mu)]$	(c)
$C_4^{12} = A_2\rho(V_{31}^2 - V_{32}^2)$	(d)
$C_4^{12} = A_2\rho(V_{22}^2 - V_{11}^2)$	(e)
$C_4^{12} = A_2[\lambda + 4\mu - \rho(V_{33}^2 + 2V_{32}^2)]$	(f)
$C_4^{12} = A_2[2(\lambda + 4\mu) - \rho(V_{11}^2 + V_{22}^2 + 2V_{12}^2 + 2V_{32}^2)]$	(g)
$C_4^{13} = A_3[6\mu - \lambda + \rho(V_{33}^2 - 8V_{12}^2)]$	(h)
$C_4^{13} = A_3[10\mu - \rho(V_{31}^2 + V_{32}^2 + 8V_{12}^2)]$	(i)
$C_4^{13} = A_3[\rho(4V_{11}^2 + 4V_{22}^2 - 3V_{33}^2) - 5(\lambda + 2\mu)]$	(j)
$C_4^{13} = A_3[\rho(4V_{11}^2 + 4V_{22}^2 + 3V_{31}^2 + 3V_{32}^2) - 2(4\lambda + 11\mu)]$	(k)

where $A_1 = \frac{210}{8c}\sqrt{\frac{3}{7}}$, $A_2 = \frac{2}{\sqrt{5}}A_1$, $A_3 = \frac{1}{\sqrt{35}}A_1$.

velocity calculations, which are due to measurements of the path length, are cancelled out.
2. We use relationships which involve the lowest number of velocities.
3. We select relationships which require only ratios of elastic constants. If this is not possible (as in the cases of C_4^{11} and C_4^{13}) the equations which require the lowest number of elastic constants are used.
4. We use the set of relationships which requires the lowest number of measurements necessary to determine the coefficient.

The relationships which best satisfy the above procedure are:

$$C_4^{11} = \frac{210}{8c}\sqrt{\frac{3}{7}}\,[2\mu - \rho(V_{31}^2 + V_{32}^2)], \tag{5}$$

$$C_4^{12} = \frac{210}{4\sqrt{5}c}\sqrt{\frac{3}{7}}\,\rho(V_{31}^2 - V_{32}^2), \tag{6}$$

$$C_4^{13} = \frac{210}{8\sqrt{35}c}\sqrt{\frac{3}{7}}\,[6\mu - \lambda + \rho(V_{33}^2 - 8V_{12}^2)]. \tag{7}$$

Replacing the density ρ by the expression in Eq. (4) yields

$$C_4^{11} = \frac{210}{8c}\sqrt{\frac{3}{7}}\left[2\mu - (c_{11} - 2c_{44})\frac{V_{31}^2 + V_{32}^2}{V_{31}^2 + V_{32}^2 + V_{33}^2}\right], \tag{8}$$

$$C_4^{12} = \frac{210}{4\sqrt{5}c}\sqrt{\frac{3}{7}}\,(c_{11} - 2c_{44})\frac{V_{31}^2 - V_{32}^2}{V_{31}^2 + V_{32}^2 + V_{33}^2}, \tag{9}$$

$$C_4^{13} = \frac{210}{8\sqrt{35}c}\sqrt{\frac{3}{7}}\left[6\mu - \lambda + (c_{11} - 2c_{44})\frac{V_{33}^2 - 8V_{12}^2}{V_{31}^2 + V_{32}^2 + V_{33}^2}\right]. \tag{10}$$

It must be noted that Eq. (A) of Table 2 also satisfies options 1–4 listed above. Replacing the density ρ by the expression in Eq. (4), the resulting expression for C_4^{11} leads to the same values obtained from Eq. (8).

Equations (8–10) are valid only for materials with cubic crystal structure, and in order to apply these equations to the composites examined in this work, the following assumptions are made: 1) The presence of the SiC-particles changes the elastic properties of the composite but only the texture of the matrix; 2) The SiC-particles are randomly distributed in the specimen without any preferred orientation; 3) The ultrasonic wavelength (frequency used is 5 MHz) is much larger than the average particle dimension (2–4 μm) so that no dispersion effects occur.

Determination of the Expansion Coefficients C_4^{ij}

The geometry of the specimens used in this investigation allows the measurements of all nine ultrasonic wave velocities V_{ij} (3 different waves in 3 orthogonal directions). In these measurements the 3-direction is taken to be parallel to the extrusion direction of the samples (see Fig. 1). The velocities measured are

Table 3. Ultrasonic velocities of the Al-8091, Al-7064, and Al-6061 MMC specimens[1]

	8091 +0% SiC	8091 +10% SiC	8091 +15% SiC	7064 +0% SiC	7064 +15% SiC	7064 +20% SiC	6061 +15% SiC	6061 +20% SiC
V_{11}	6612	6922	7050	6238	6731	6911	6817	7165
V_{22}	6606	6913	7011	6233	6734	6937	6780	7103
V_{33}	6564	7043	7168	6194	6920	7108	6869	7207
V_{12}	3484	3708	3816	3059	3435	3584	3413	3695
V_{21}	3477	3702	3805	3066	3440	3567	3418	3701
V_{13}	3467	3728	3834	3082	3479	3641	3438	3731
V_{31}	3480	3736	3842	3057	3469	3636	3442	3733
V_{23}	3472	3733	3848	3051	3470	3617	3446	3740
V_{32}	3482	3736	3844	3062	3469	3640	3435	3774

[1] Velocities are shown in units of m/s.

listed in Table 3 and are found to be reproducible to within 0.3%. Because of the rotational axis, the corresponding velocities V_{11} and V_{22}, V_{12} and V_{21}, V_{31} and V_{13}, and V_{23} and V_{32} are averaged according to the rotational symmetry around the extrusion axis.

The ultrasonic velocities in the textured Al-matrix (which has a face-centered cubic crystal structure) are then computed using the equal stress condition and the velocities measured. This condition assumes that the Al-crystallites and the SiC-particles are subjected to the same stress. With x denoting the volume percentage of SiC, the equal stress condition can be written as

$$M_{\text{comp}} = \frac{M_{\text{Al}} M_{\text{SiC}}}{xM_{\text{Al}} + (1 - x)M_{\text{SiC}}}, \tag{11}$$

where M_{comp}, M_{Al}, and M_{SiC} are the elastic moduli of the composite, the matrix and the reinforcement, respectively. Using Eq. (11) and the well-known relationships between elastic moduli and ultrasonic velocities, the velocities V_{ij} in the Al-matrix can be expressed as

$$V_{ij}^{\text{Al}} = \left[\frac{1}{\rho_{\text{Al}}} \frac{(1 - x)\rho_{\text{comp}}(V_{ij}^{\text{comp}})^2 \rho_{\text{SiC}} V_{\text{SiC}}^2}{\rho_{\text{SiC}} V_{\text{SiC}}^2 - x\rho_{\text{comp}}(V_{ij}^{\text{comp}})^2}\right]^{1/2}. \tag{12}$$

In the calculations of V^{Al} the density of the composite is determined according to the law of mixture

$$\rho_{\text{comp}} = (1 - x)\rho_{\text{Al}} + x\rho_{\text{SiC}}. \tag{13}$$

Only small deviations of the densities calculated using Eq. (13) and of the measured densities are found for the specimens examined in this work [11]. The densities used in the calculations are 2524 kg/m^3 for Al-8091, 2864 kg/m^3 for Al-7064, 2710 kg/m^3 for Al-6061 [12], and 3200 kg/m^3 for SiC [13]. The shear and

Table 4. Expansion coefficients C_4^{ij} of the Al-8091, Al-7064 and Al-6061 MMC specimens[1]

	8091 +0% SiC	8091 +10% SiC	8091 +15% SiC	7064 +0% SiC	7064 +15% SiC	7064 +20% SiC	6061 +15% SiC	6061 +20% SiC
C_4^{11}	2.205	1.573	3.532	2.358	3.155	5.352	3.295	7.404
C_4^{12}	0	0	0	0	0	0	0	0
C_4^{13}	2.194	−0.431	1.034	1.962	1.267	2.175	1.913	4.636

[1] 3-direction ∥ extrusion direction.

the longitudinal wave velocities V_S and V_l for SiC are obtained from the relationships $V_S^2 = \mu/\rho$, $V_l^2 = (\lambda + 2\mu)/\rho$ and $v = \lambda/[2(\lambda + \mu)]$, where v is the Poisson's ratio = 0.19 and μ = 165.5 GPa [13].

The single crystal values used in Eqs. (8)–(10) are:

c_{11} = 111.1 GPa, c_{12} = 52.5 GPa, c_{44} = 32.5 GPa, c = −6.4 GPa for Al-8091 [14].

c_{11} = 107.3 GPa, c_{12} = 60.3 GPa, c_{44} = 28.0 GPa, c = −9.0 GPa for Al-7064 [15].

c_{11} = 108.0 GPa, c_{12} = 62.0 GPa, c_{44} = 28.3 GPa, c = −10.6 GPa for Al-6061 [16].

The expansion coefficients C_4^{ij} are then determined using Eqs. (8–10), and their results are shown in Table 4. Because of the rotational symmetry of the samples, the coefficient C_4^{12} is found to be zero for all specimens.

Discussion

The expansion coefficients C_4^{11} and C_4^{13} are plotted versus the volume percentage of SiC in Fig. 2. From the figure one can see that there is first a slight decrease in these coefficients followed by a linear increase up to 20 volume percent of SiC. These plots also show that the presence of SiC leads to considerable changes in these expansion coefficients and thus in the texture of the Al-matrix.

The determination of C_4^{11} is known to be critical because it requires absolute velocity measurements. Therefore it must be established whether the determined values for C_4^{11} are reasonable. This can be done by considering the two extreme cases of a ⟨111⟩-fiber texture and a ⟨100⟩-fiber texture, which are usually observed in extruded aluminium [17]. Because of their rotational symmetry, fiber textures are sufficiently described by one expansion coefficient, namely, C_4^{11}, whereas C_4^{12} and C_4^{13} are zero [18]. In the case of an ideal ⟨111⟩-fiber texture, where the crystallographic directions with the highest ultrasonic velocity lie along the extrusion direction, the value of C_4^{11} is found to be equal to −4.575. On the other hand, for ani deal ⟨100⟩-fiber texture, where the crystallographic direction with the lowest ultrasonic velocity lies along the extrusion direction, the value of C_4^{11} is +6.887. These values, which are obtained from the

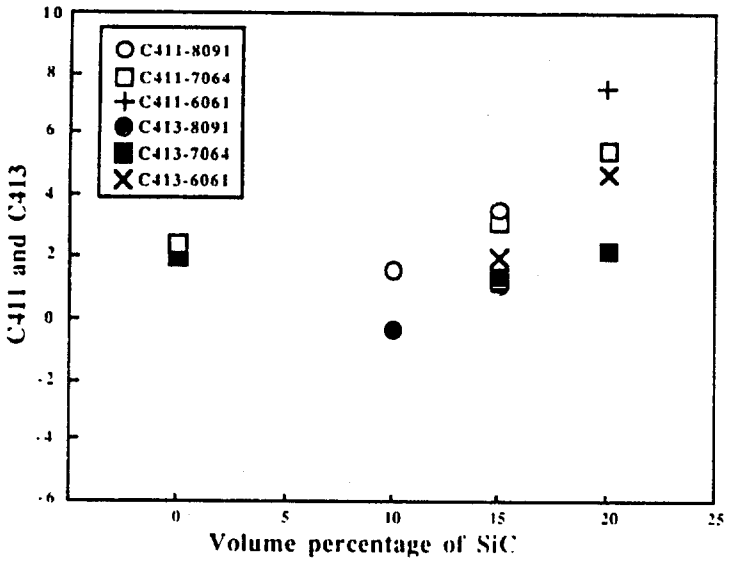

Fig. 2. Expansion coefficients C_4^{II} and C_4^{III} (bulk values) determined for the MMC specimens plotted versus the volume percentage of SiC.

results of pure aluminium, agree very well with $C_4^{II} \approx -4.570$ and $C_4^{III} \approx +6.770$ given by Bunge [18]. These two "extreme" values constitute the upper and the lower bounds for C_4^{II} of any texture in extruded aluminium.

The values obtained in this work (Table 4) lie within these bounds, except for the Al-6061 + 20% SiC composite. This agrees with the results reported in reference [11] which show that the elastic behavior of all Al-SiC composites examined in this work can be approximately described by the equal stress condition represented by Eq. (11), with the exception of the Al-6061 + 20% SiC composite which shows a large deviation from that condition. The velocities V_i in the Al-matrix were also determined using the equal strain condition

$$M_{comp} = (1 - x)M_{Al} + xM_{SiC},$$

which assumes that the Al-crystallites and the SiC-particles undergo the same strain. The coefficients resulting from these calculations are found to lie far outside the bounds given above, which again agrees with the results in reference [11].

The departure of the elastic behavior of the Al-6061 + 20% SiC composite from the equal stress condition may be due to some degree of hydrostatic stress generated within the MMC specimen. In this case, the matrix material in the composite tends to deform at a lower stress than the reinforcement because the matrix material is softer than the reinforcing material. If the matrix material is rigidly coupled with the reinforcement, it is restricted from deforming in the way it would if it were alone and causes hydrostatic stresses to be generated within the matrix material. The exact magnitude of this effect is unknown and rather complex, but it is a function of the mean free path in the matrix and the ratio of the elastic constants of the constituents [19]. In general the mean free path in the matrix varies from region to region, and therefore no simple ratio

can be predicted. Thus the extent of deviation of the elastic moduli form the equal stress condition can vary from specimen to specimen.

Since the mean free path in the matrix decreases with increasing volume percentage of the reinforcing phase, the limitation of the approach presented in this work to composites with "small" fractions of reinforcements is apparent. Nevertheless, in these cases reasonable results are obtained up to a volume fraction of 20%. From Table 4 and Fig. 2 one can see that the coefficients determined lie within the bounds given above and that the coefficients of these specimens, which contain the same volume percentage of SiC lie close together, indicating that these specimens contain similar textures. Figure 2 also indicates that the textures, which are only due to the extrusion process (0% SiC), are modified by the addition of the SiC-reinforcements in a similar way. If it is assumed that the examined specimens contain a mixture of a ⟨111⟩- and a ⟨100⟩-fiber texture, which is usually observed in extruded aluminium [17], the increase in the expansion coefficient C_4^{11} with increasing volume percentage of SiC indicates that the ⟨100⟩-directions of the Al-crystallites align more and more towards the extrusion direction as the SiC-concentration is increased.

From above, it can be seen that ultrasonic velocity measurements can be used for the nondestructive characterization of texture in metal-matrix composites. The results also indicate that the assumptions made concerning the effects of reinforcement particles on the texture in these materials are reasonable.

Acknowledgments. This work is sponsored by the National Science Foundation under contract No. MSM-8521830, and by the Army Research Office under contract No. DAAL03-88-K-0096.

References

1. H.J. Bunge, *Krist. u. Tech.* **3**:431 (1968)
2. H.J. Bunge, *Krist. u. Tech.* **5**:145 (1971).
3. G.J. Davies, D.J. Goodwill, and J.S. Kallend, *Metallurg. Trans.* **3**:1627 (1972)
4. M. Spies and H. Schneider, To be published in *Proceedings of the 3rd Int. Symposium on the Nondestr. Char. of Materials*, Saarbrücken, FRG, October 3–6, 1988
5. O. Cassier, C. Donadille, and B. Bacroix, *Review of Progress in Quant. NDE 8*, La Jolla, CA, USA (1988)
6. D. Lee, S. Razvi, K. Salama and E. Schneider, In *Proceedings of the 16th Symposium on NDE*, San Antonio, TX, USA, April 1987
7. H.J. Bunge, *Z. Metallkunde* **56**:872 (1965)
8. H. Pursey and H.L. Cox, *Phil. Mag.* **45**:295 (1954)
9. R.J. Roe, *J. Appl. Phys.* **37**:2069 (1966)
10. E.P. Papadakis, *J. Acoust. Soc. Am.* **42**:1045 (1967)
11. D.F. Lee, Master's Thesis, University of Houston, USA (1987)
12. F. Beer and E. Johnston, *Mechanics of Materials*, McGraw-Hill, New York (1981)
13. *Engineering Properties of Selected Ceramic Materials*, American Ceramic Society, Columbus, OH, USA (1966)
14. W. Müller, E. Bubeck, and V. Gerold, In *Proceedings of the 3rd Int. Al-Li Conference*, The Institute of Metals, London (1986)

15. G. Tempus, Dissertation, University of Stuttgart, FRG (1982)
16. C. M. Sayers, *J. Appl. Phys.* 17:1179 (1984)
17. G. Wassermann and J. Grewen, *Texturen metallischer Werkstoffe*, Springer-Verlag, Berlin Göttingen/Heidelberg (1962)
18. H.J. Bunge, *Texture Analysis in Materials Science*, Butterworth, London (1982)
19. L.J. Broutman and R.H. Krock (eds.), *Modern Composite Materials*, Addison-Wesley, Read, MA (1967)

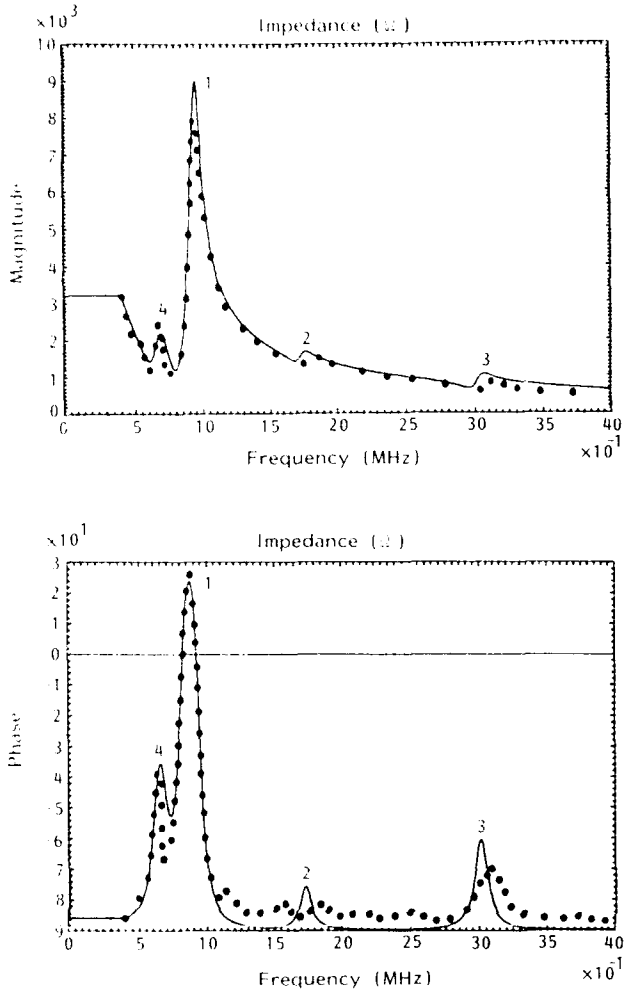

Figure 9 Experimental (●) and simulated ( ) operational impedance characteristics for a three-layered lateral structure. Frequency range: 400 kHz 4 MHz

Concluding remarks

A model has been presented for predicting the response from multilayered piezoelectric structures which demonstrate two, loosely coupled, compressional modes of vibration. Good agreement between theoretical and experimental results was achieved over a range of structural configuration ratios. Provided that the underlying physical assumptions are appreciated, the model is useful for providing a first order approximation to electrical mechanical and piezoelectric interaction in ultrasonic array structures. For example, the model will provide a good approximation for thickness mode behaviour within individual elements in a diced array. The influence of bond lines, mechanical matching layers and electrical loading on transducer response may be investigated in both time and frequency domains. In addition, lateral mode propagation may be studied in conjunction with factors such as element periodicity, inter-element loading and electrical cross coupling. This approach is also suitable for modelling of pure thickness mode structures which are subject to independent electrical loading by setting the appropriate mechanical and piezoelectric cross coupling constants to zero. An extension of the method for the simulation of stacked piezoelectric structures which possess common or parallel electrical loading has also been developed and will be reported at a later date.

References

1 **Hayward, G., Macleod, C.J. and Durrani, T.S.** A systems model of the thickness mode piezoelectric transducer *J Acoust Soc Am* (1984) **76** 369–375

2 **Hayward, G. and Jackson, M.N.** A lattice model of the thickness mode piezoelectric transducer *IEEE Trans. UFFC* (1986) **33** 41–50

3 **Hayward, G.** Using a linear systems model to assess the influence of some design, constructional and measurement parameters on the performance of ndt probe assemblies *NDT Int* (1986) **19** 67–75

4 **Hayward, G. and Gillies, D.** Block diagram modelling of tall, thin, parallelepiped, piezoelectric structures *J Acoust Soc Am* (1989) **86** 1643–1653

5 **Hayward, G., Gillies, D. and Hossack, J.** A model for the operational impedance of piezoelectric structures exhibiting two, loosely coupled modes of vibration, *J Acoust Soc Am* (in press)

6 **Sato, J., Kawabuchi, M. and Fukomoto, J.** Dependence of electro-mechanical coupling coefficient on the width to thickness ratio of plank shaped piezoelectric transducers used for electronically scanned ultrasound diagnostic systems *J Acoust Soc Am* (1979) **66** 1609–1611

7 **Naillon, M., Coursant, R.H. and Besnier, F.** Analysis of piezoelectric structures by a finite element method. *Acta Electronica* (1983) **25** 341–362

Relationship between elastic anisotropy and texture in metal–matrix composites

M. Spies* and K. Salama

Department of Mechanical Engineering, University of Houston, Houston, TX 77004, USA

Received 23 June 1989; revised 7 November 1989

The relationship between elastic anisotropy and texture in two-phase metal matrix composites has been developed under certain conditions. Using measurements of the six independent ultrasonic velocities V_{ij} in samples of the aluminium alloys 8091 and 7064 containing up to 20% SiC particles and the formulation given by Bunge, the fourth-order expansion coefficients of the orientation distribution function are determined. The Young's moduli in different directions are also obtained from ultrasonic velocity measurements. Linear correlations between anisotropy described by Young's moduli and texture determined by orientation distribution function expansion coefficients are obtained, and confirm developed relationships for two-phase metal matrix composites. This result shows that ultrasonic measurements provide a technique for the characterization of texture and elastic anisotropy in these materials.

Keywords: metal–matrix composites; elastic anisotropy; texture

Introduction

Most structural materials are polycrystalline aggregates and their exposure to plastic deformation and heat treatment during manufeturing leads to the alignment of the single crystals relative to the forming geometry. This development of preferred orientation or texture is the main reason for the anisotropic behaviour of these materials. The texture is mathematically described by the orientation distribution function (ODF), which determines the probability of finding a single crystal in the aggregate with a certain orientation with respect to the sample geometry. The elastic behaviour of polycrystalline materials is determined by the three fourth-order expansion coefficients of the ODF. The situation, however, is more complicated in the case of two-phase materials, where the macroscopic properties are strongly influenced by the properties, the shape, the volume fraction and the orientation of each phase.

In a recent study an ultrasonic method has been developed for the nondestructive determination of texture in metal matrix composites[1]. Measurements of ultrasonic velocities have been used to determine the three fourth-order ODF-expansion coefficients in 8091, 7064 and 6061 aluminium matrix composites. The examined composites are reinforced with up to 20% silicon carbide (SiC) particles of about 2–4 μm in diameter and of approximately spherical shape. Under the assumptions of homogeneous distribution of the SiC particles and that the Al crystallites and the SiC particles are subjected to the same stress, the expansion coefficients of fourth-order have been determined as a function of the volume percentage of SiC-reinforcement, and found to lie within given bounds.

In this study the fourth-order expansion coefficients obtained by this technique are used to examine relationships between texture and Young's modulus in the SiC reinforced 8091 and 7064 aluminium composites. Measurements of ultrasonic velocities are used to determine the Young's modulus in different directions of the composites.

Ultrasonic texture analysis

Orientation distribution function

Texture is described by the (ODF), which determines the probability of finding a single crystal in the polycrystalline sample with a certain orientation with respect to the sample orientations, as shown in *Figure 1*. According to Bunge[2] the ODF can be written as a series expansion into symmetrical generalized spherical harmonics as

$$f(g) = \sum_{l=0}^{L} \sum_{\mu=1}^{M(l)} \sum_{\nu=1}^{N(l)} C_l^{\mu\nu} \hat{T}_l^{\mu\nu}(g) \qquad (1)$$

where g is the orientation, the $\hat{T}_l^{\mu\nu}$ are symmetrical generalized spherical harmonics and the $C_l^{\mu\nu}$ are the expansion coefficients. The upper limits $M(l)$ and $N(l)$ depend on l as well as the crystal and sample symmetry, respectively. The orthonormal function system $\hat{T}_l^{\mu\nu}$ is invariant towards all rotations of the sample symmetry (indicated by the right dot) and the crystal symmetry (indicated by the left two dots). In first approximation only the three fourth-order expansion coefficients C_4^{11}, C_4^{13} and C_4^{13} need to be considered for texture evaluation in cubic materials with orthorhombic sample symmetry[3,4].

* Permanent address: Fraunhofer Institut für zerstörungsfreie Prüfverfahren, Saarbrücken, FRG

0041 624X/90/060370-05

The modified relationships which allow the determination of the fourth-order expansion coefficients C_4^{lv} for the SiC particle-reinforced aluminium matrix composites are described in detail in reference 1. With $c = c_{11} + c_{12} + 2c_{44}$, where c_{11}, c_{12} and c_{44} are the elastic constants of the aluminum single crystals, the expansion coefficients C_4^{lv} are related to the ultrasonic velocities V_{ij}^{comp} as follows

$$C_4^{11} = \frac{210}{8c}\left(\frac{3}{7}\right)\left[2\mu_{Al} - (c_{11} + 2c_{44})\frac{\tilde{\Gamma}_{31}^2 + \tilde{\Gamma}_{32}^2}{\tilde{\Gamma}_{31}^2 + \tilde{\Gamma}_{32}^2 + \tilde{\Gamma}_{33}^2}\right] \quad (2)$$

$$C_4^{12} = \frac{210}{4\sqrt{5}c}\left(\frac{3}{7}\right)\left[(c_{11} + 2c_{44})\frac{\tilde{\Gamma}_{31}^2 - \tilde{\Gamma}_{32}^2}{\tilde{\Gamma}_{31}^2 + \tilde{\Gamma}_{32}^2 + \tilde{\Gamma}_{33}^2}\right] \quad (3)$$

$$C_4^{13} = \frac{210}{8\sqrt{35}c}\left(\frac{3}{7}\right)\left[6\mu_{Al} - 2\lambda_{Al} + (c_{11} + 2c_{44})\frac{\tilde{\Gamma}_{33}^2 - 8\tilde{\Gamma}_{12}^2}{\tilde{\Gamma}_{31}^2 + \tilde{\Gamma}_{32}^2 + \tilde{\Gamma}_{33}^2}\right] \quad (4)$$

where

$$(\tilde{\Gamma}_{3j})^2 = \left(\frac{1}{(\Gamma_{3j}^{comp})^2} - \frac{x\rho_{comp}}{M_j}\right)^{-1} \qquad j = 1, 2, 3 \quad (5)$$

$$(\tilde{\Gamma}_{12})^2 = \left(\frac{1}{(\Gamma_{12}^{comp})^2} - \frac{x\rho_{comp}}{M_1}\right)^{-1} \quad (6)$$

and

$$M_j = \mu_{SiC} + (\mu_{SiC} + \lambda_{SiC})b_{3j}^2 \qquad j = 1, 2, 3 \quad (7)$$

(ρ is the density and M is the elastic modulus)

In these equations x designates the volume fraction of SiC; μ_{Al}, λ_{Al}, μ_{SiC} and λ_{SiC} are the Lamé constants for Al and SiC, respectively. Also in the calculation of the coefficients C_4^{lv}, the density of the composite can be determined according to the law of mixture $\rho_{comp} = (1 - x)\rho_{Al} + x\rho_{SiC}$.

The above equations are derived under the following assumptions. The presence of the SiC particles changes both the elastic properties of the composite and the texture of the matrix. The SiC particles are randomly distributed in the specimen without any preferred orientation. The ultrasonic wavelength is much larger than the average particle dimension (2–4 μm) so that no dispersion effects may occur.

Relationship between texture and Young's modulus

The direction dependence of Young's modulus E in materials with cubic crystal structure containing textures with orthorhombic symmetry can be described by

$$E(\theta) = e_1 + e_2 \cos 2\theta + e_3 \cos 4\theta \quad (8)$$

where θ is the angle to the deformation direction (rolling or extrusion) coinciding with the 1-direction of the sample fixed coordinate system (*Figure 1*). The quantities e_1, e_2 and e_3 in equation (8) are constants determined from equation (10).

According to Bunge[3-5], equation (8) can also be expressed as

$$E(\theta) = E_r + E_1 C_4^{11} + E_2 C_4^{12} \cos 2\theta + E_3 C_4^{13} \cos 4\theta \quad (9)$$

where E_r is the Voigt average of Young's modulus for random orientation distribution and E_1, E_2 and E_3 are combinations of the elastic constants of the single crystals. Equation (8) will then provide the expressions

$$e_1 = 1/4[E(0°) + 2E(45°) + E(90°)] = E_m \quad (10a)$$

$$e_2 = 1/2[E(0°) - E(90°)] = E_A \quad (10b)$$

$$e_3 = 1/4[E(0°) - 2E(45°) + E(90°)] = 1/2\Delta E \quad (10c)$$

and from equation (9) we can obtain

$$E_m = E_1 C_4^{11} + E_r \quad (11a)$$

$$E_A = E_2 C_4^{12} \quad (11b)$$

$$\Delta E = E_3 C_4^{13} \quad (11c)$$

Experimental

The metal matrix composites examined in this investigation are the aluminium alloys 8091 and 7064 containing up to 20% volume fraction of silicon carbide particles. The chemical compositions of these alloys and the volume percentages of the SiC reinforcement are shown in *Table 1*. The composites were received as extruded rods of 25 mm in diameter. Prismatic specimens 15 to 18 mm wide and 30 mm long were machined out of these rods such that the length direction is parallel to the extrusion direction. Opposite faces are machined flat and parallel to within ±0.025 mm on these specimens.

In order to determine the ODF expansion coefficients, ultrasonic velocity measurements are performed using the pulse-echo-overlap method, which is described in detail by Papadakis[10]. The system used in this investigation consists of an ultrasound apparatus which generates pulses of approximately 1 μs duration of a variable repetition rate. These pulses are impressed on a commercial transducer of a fundamental frequency of 5 MHz which is acoustically bonded to the specimen. The reflected r.f. echoes are received by the same transducer, amplified and displayed on a screen of an oscilloscope. Two of the displayed echoes are then chosen and exactly overlapped by critically adjusting the frequency of a CW oscillator and the division factor on a decade divider. The frequency,

Table 1 Chemical composition of aluminium alloys and volume percentage of SiC reinforcement of the MMC specimens

Alloy	Alloying Elements									
	Si	Fe	Cu	Mg	Zr	Li	Zn	Cr	Co	Al
8091	0.12	0.04	1.90	0.80	0.11	2.70				rem
7064	0.05	0.10	2.10	2.30	0.20		7.10	0.12	0.22	rem

Specimens		
8091 + 0% SiC	8091 + 10% SiC	8091 + 15% SiC
7064 + 0% SiC	7064 + 15% SiC	7064 + 20% SiC

f, accurately determined by an electronic counter is employed to compute the ultrasonic velocity using the relationship $V = sf$, where s is the path length of the ultrasonic wave. The system is capable of measuring changes in the ultrasonic velocity to an accuracy of better than one part in 10^5, while the inaccuracy of measuring both the longitudinal and the shear velocities is estimated to be 0.3%.

Results and discussion

The geometry of the specimens used in this investigation allows the measurements of all nine ultrasonic wave velocities V_{ij}^{comp} (three different waves in three orthogonal directions). The velocities measured are listed in *Table 2*. In these measurements the 3-direction is taken to be parallel to the extrusion direction of the sample (see *Figure 1*). The relationship between texture and Young's modulus, described by equation (11), is valid for a cubic crystal structure containing textures with orthorhombic symmetry, such as those generated by rolling. In this arrangement θ is the angle to the rolling direction, which is taken to be parallel to the 1-direction.

Because the extruded samples under examination also exhibit textures with orthorhombic symmetry[5-7], equation (11) can be applied if the extrusion direction is parallel to the 1-direction. Rearranging the sample-fixed coordinate system in this way leads to a renaming of the composite-velocities V_{ij}^{comp} (*Table 2*) by changing the subscripts i and j such that $1 \rightarrow 2$, $2 \rightarrow 3$, $3 \rightarrow 1$.

The velocities which should be equal because of the rotational symmetry around the extrusion axis are then averaged to provide the velocities $(V_{31}^{comp})_{av}$, $(V_{32}^{comp})_{av}$, $(V_{33}^{comp})_{av}$ and $(V_{12}^{comp})_{av}$. The expansion coefficients C_4^{ij} are calculated using these velocities and equations (2)–(4). Their values are plotted *versus* the volume percentage of SiC in *Figures 2*, *3* and *4*. In these calculations the following Al-single crystal constants are used[9]: $c_{11} = 111.1$ GPa, $c_{12} = 52.5$ GPa, $c_{44} = 32.5$ GPa for Al-8091 [8]; $c_{11} = 107.3$ GPa, $c_{12} = 60.3$ GPa, $c_{44} = 28.0$ GPa for Al-7064. The density values used are[10] 2524 kg m^{-3} for Al-8091 and 2864 kg m^{-3} for Al-7064.

The Young's moduli in the 0°, 45° and 90°-directions are determined using the relationship

$$E(\theta) = \frac{\mu(\theta)(3\lambda(\theta) + 2\mu(\theta))}{\lambda(\theta) + \mu(\theta)} \qquad (12)$$

where the Lamé constants $\lambda(\theta)$ and $\mu(\theta)$ are determined by

$$\mu(\theta) = \rho V_{ij}^2(\theta) \qquad \lambda(\theta) + 2\mu(\theta) = \rho V_{ij}^2 \qquad (13)$$

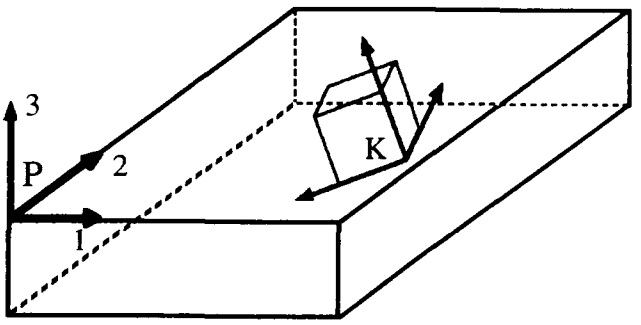

Figure 1 Sample fixed coordinate system P and crystal fixed system K for characterization of orientation

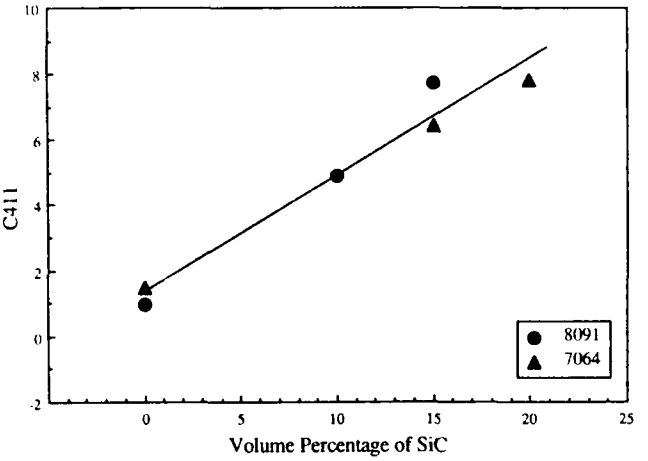

Figure 2 Expansion coefficients C_4^{11} of the MMC specimens plotted *versus* volume percentage of SiC (1-direction parallel to extrusion direction)

for the angles $\theta = 0°$, 45°, 90°, $E(0°)$ and $E(90°)$ are computed using the velocity data shown in *Table 2*. The shear velocities at 45° to the extrusion direction have also been measured and their values are used to determine $E(45°)$. The values of $E(0°)$, $E(45°)$ and $E(90°)$ as well as those of E_m, E_Δ and ΔE for the Al-8091 and Al-7064 composites are included in *Table 3*. The plots of E_m *versus* C_4^{11}, E_Δ *versus* C_4^{12} and ΔE *versus* C_4^{13} are also shown in *Figures 5* to *7* and indicate linear correlations as given by equation (11). The regression equations for these relationships can then be written as

Al-8091

$E_m = (2.238\ C_4^{11} + 78.17)$ GPa $\quad r = 0.992$

$E_\Delta = (0.451\ C_4^{12} - 0.003)$ GPa $\quad r = 1$

$\Delta E = (0.143\ C_4^{13} - 0.115)$ GPa $\quad r = 0.995$

Table 2 Ultrasonic velocities of the Al 8091 and Al-7064 MMC specimens. Velocities are shown in units of m s^{-1}

	8091 + 0% SiC	8091 + 10% SiC	8091 + 15% SiC	7064 + 0% SiC	7064 + 15% SiC	7064 + 20% SiC	6061 + 15% SiC	6061 + 20% SiC
V_{11}	6612	6922	7050	6238	6731	6911	6817	7165
V_{22}	6606	6913	7011	6232	6734	6937	6780	7103
V_{33}	6564	7043	7168	6194	6920	7108	6869	7207
V_{12}	3484	3708	3816	3059	3435	3584	3413	3695
V_{21}	3477	3702	3805	3066	3440	3567	3418	3701
V_{13}	3467	3728	3834	3082	3479	3641	3438	3731
V_{31}	3480	3736	3842	3057	3469	3636	3442	3733
V_{23}	3472	3733	3848	3051	3470	3617	3446	3740
V_{32}	3482	3736	3844	3062	3469	3640	3435	3774

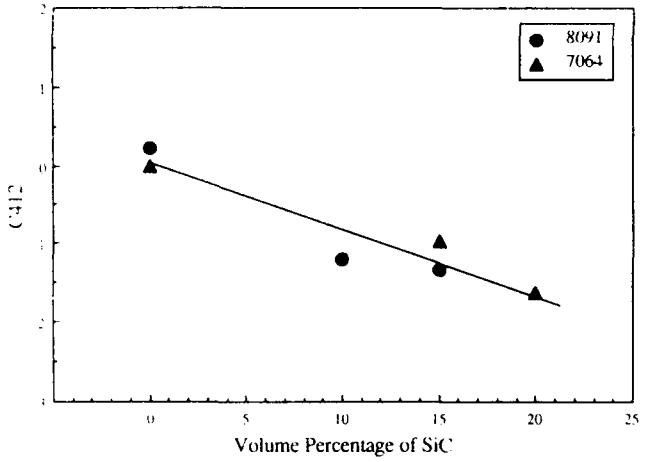

Figure 3 Expansion coefficient C_4^{12} of the MMC specimens plotted *versus* volume percentage of SiC (1-direction parallel to extrusion direction)

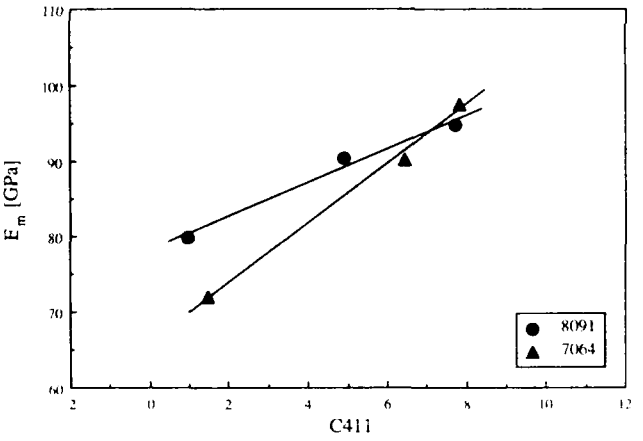

Figure 5 Elastic parameter E_m plotted *versus* the expansion coefficient C_4^{11} for the Al-8091 and Al-7064 MMC specimens

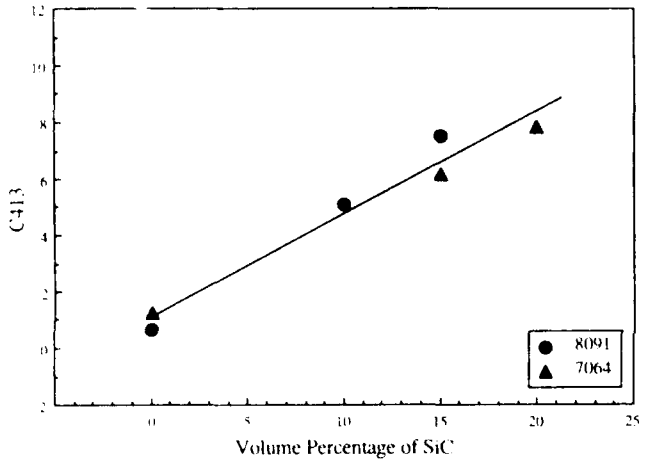

Figure 4 Expansion coefficients C_4^{13} of the MMC specimens plotted *versus* volume percentage of SiC (1-direction parallel to extrusion direction)

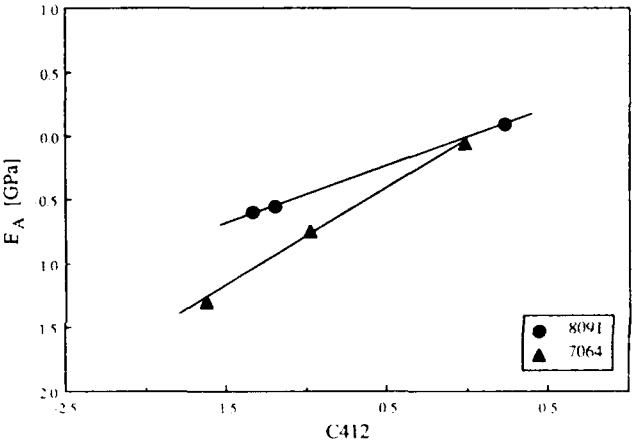

Figure 6 Elastic anisotropy parameter E_A plotted *versus* the expansion coefficient C_4^{12} for the Al-8091 and Al-7064 MMC specimens

Al-7064

E_m (3.925 C_4^{11} + 65.95) GPa $r = 0.998$

E_A (0.772 C_4^{12} − 0.027) GPa $r = 0.999$

ΔE (0.062 C_4^{13} + 0.050) GPa $r = 0.943$

The fact that the regression lines for E_A and ΔE do not cross the ordinate at the origin is due to measuring errors. Nevertheless, the high correlation coefficients confirm the validity of the relationships between texture and Young's modulus (equations (11)) for the Al SiC composites examined. It is important to note that in these relationships C_4^{1y} are the texture coefficients determined for the Al-matrix, whereas E_m, E_A and ΔE characterize the elastic anisotropy of the whole composite. From this it can be concluded that the elastic anisotropy of the composites is influenced only by the texture of the Al matrix, which is in turn influenced by the extrusion process and the presence of the SiC particles. Also from the linear correlation of E_A with C_4^{12}, shown in *Figure 6*, it is seen, that E_A, which represents the difference of the Young's modulus in the extrusion direction and the Young's

Table 3 Young's moduli $E(0°)$, $E(45°)$ and $E(90°)$ and the resulting parameters E_m, E_A and ΔE for the Al 8091 and Al 7064 MMC specimens. The values are shown in units of GPa

	8091 · 0% SiC	8091 · 10% SiC	8091 · 15% SiC	7064 · 0% SiC	7064 · 15% SiC	7064 · 20% SiC
$E(0°)$	79.8	91.1	95.9	72.1	91.1	99.1
$E(45°)$	79.9	90.0	94.3	71.9	90.0	97.2
$E(90°)$	80.0	90.0	94.7	72.0	89.6	96.5
E_m	79.9	90.3	94.8	72.0	90.2	97.5
E_A	0.10	0.55	0.60	0.05	0.75	1.30
ΔE	0	0.55	1.00	0.15	0.35	0.60

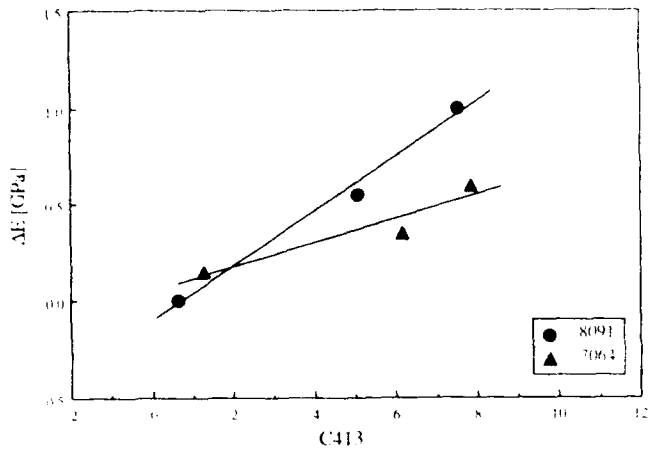

Figure 7 Elastic anisotropy parameter ΔE plotted *versus* the expansion coefficient $C_{\frac{1}{3}}$ for the Al 8091 and Al 7064 MMC specimens

modulus perpendicular to that direction, is equal to zero when $C_{\frac{1}{3}}$ goes to zero. Since the addition of SiC reinforcement modifies textures during the extrusion process (0% SiC)[5], the texture of the composite can be changed by modifying manufacturing parameters such as extrusion velocity and temperature[7]. This will then provide a means to control the anisotropy of the composite, and its mechanical properties.

Acknowledgements

The authors would like to thank D.F. Lee, Department of Mechanical Engineering, University of Houston, for many valuable discussions. This work is sponsored by the Army Research Office under contract No. DAAL03-88-K-0096.

References

1 **Spies, M. and Salama, K.** Texture of metal-matrix composites by ultrasonic velocity measurements *Res Nondestr Eval* (1989) **1** 99–109

2 **Bunge, H.J.** Zur Darstellung allgemeiner Texturen *Z Metallkunde* (1965) **56** 872–874

3 **Bunge, H.J.** Über die elastischen Konstanten kubischer Materialien mit beliebiger Textur *Krist u Tech* (1968) **3** 431–438

4 **Pursey, H. and Cox, H.L.** The correction of elasticity measurements on slightly anisotropic materials *Phil Mag* (1954) **45** 295–304

5 **Bunge, H.J.** *Texture Analysis in Materials Science* Butterworths London (1982)

6 **Spies, M.** Nondestructive Determination of Materials' Textures by Ultrasonic Technique. *MS Thesis*, University of Houston, Texas, USA; *Diploma Thesis*, Universität des Saarlandes, Saarbrücken, FRG (1989)

7 **Wassermann, G. and Grewen, J.** *Texturen Metallischer Werkstoffe*. Springer-Verlag, Berlin (1962)

8 **Müller, W., Bubeck, E. and Gerold, V.** Elastic Constants of Al-Li solid solutions and δ' precipitates. In: *Proc. 3rd Int. Al-Li Conf.* The Institute of Metals, London (1986) 382–387

9 **Tempus, G.** *Dissertation* Universität Stuttgart, FRG (1982)

10 **Lee, D.F.** Ultrasonic Nondestructive Characterization of SiC-Reinforced Aluminum Metal Matrix Composites. *MS Thesis*, University of Houston, Texas, USA (1987)

ELASTIC ANISOTROPY IN PARTICLE/FIBER REINFORCED ALUMINUM METAL MATRIX COMPOSITES

B.Greisson and K.Salama

Department of Mechanical Engineering
University of Houston
Houston, TX 77204

INTRODUCTION

Metal matrix composites hold high promises as engineering materials. In order to take full advantage of their promising properties, the complex nature of the composites must be understood. Some questions thus arising; how do different manufacturing processes influence the microstructure and how can the mechanical properties of the composites be explained and predicted from knowledge of their microstructure.

The elastic properties of a composite material depend on many parameters: volume fraction, geometrical shape, size distribution, orientation and distribution of the reinforcement and the properties of the matrix. Mathematical models have been developed for some specific shapes and distributions of the reinforcement. Christensen [1] derived the effective shear and bulk moduli for a dilute suspension of elastic spherical particles in a continuous phase of another elastic material. Ledbetter et al. [2] used a scattering theory to explain the elastic behavior of a particle reinforced composite in which randomly oriented ellipsoidal particles were nonhomogeneously distributed. Experimental work by Lee et al. [3] showed that in particle-reinforced composites the second-order elastic constants increase linearly with the particle content. Their results suggested that the dominant factor in influencing the anisotropy is the content of reinforcement. Spies & Salama [4] investigated the influence of the reinforcing phase on the texture and found that the fourth-order expansion coefficients change linearly with the particle content. Their results indicate that the presence of particles in the composites leads to considerable changes in the texture of the aluminum matrix.

The objective of this study is to obtain information about what features in the microstructure of the composites are causing their anisotropic behavior. This was accomplished by comparing the particle size distribution in three orthogonal directions, with the ultrasonic velocities measured along the same directions. Three series of SiC-particle reinforced composites were examined. Two series comprised of extruded samples while the third consisted of pressed specimens. Each series included samples of different particle content. Also, three squeeze-cast samples with different particle/fiber content were

Review of Progress in Quantitative Nondestructive Evaluation, Vol. 9
Edited by D.O. Thompson and D.E. Chimenti
Plenum Press, New York, 1990

examined. In the extruded composites, the properties along the extrusion direction were found to be different from those in the directions perpendicular to the extrusion direction. This behavior is explained in terms of the presence of texture in the matrix. The squeeze-cast specimens also showed an anisotropic behavior which is induced by preferred orientation of the fiber reinforcement.

MEASUREMENTS

Specimens

The metal matrix composites (MMC) used in this investigation comprised of aluminum alloys as the matrix material and either SiC-particles or alumina fibers and particles as the reinforcement. The specimens which have Al-6061 as matrix were received as pressed plates, whereas the composites containing Al-7064 and Al-8091 were obtained as extruded rods. The alumina reinforced specimens were all squeeze-cast. The volume fractions of reinforcement in the composites used are shown in table 1.

The coordinate systems were chosen such that in pressed samples the x_1 and x_2-axes are in the plate at right angles to each other and the x_3-axis is along the compression direction (normal to the plate). In the extruded specimens the x_1 and x_2-axes are perpendicular to the extrusion direction and orthogonal to each other. The x_3-axis is along the extrusion direction. In the squeeze-cast samples the x_1 and x_2-directions are in the fiber rich layers at right angles to each other, and the x_3-direction is perpendicular to the fiber rich layers.

Microstructure

The particle size distribution and the area fraction covered by the reinforcement in each plane were estimated in each specimen. This was accomplished by scanning the faces of the specimen under an optical microscope and taking photographs at several "representative" locations along the three chosen directions. The particle size distributions were obtained from these micrographs by counting the particles and estimating their size. The size of a particle was estimated using its projected area on the face which, in turn, is equal to the area of a circle having the diameter d. The particle was considered to belong to the size range

Table 1. Metal-Matrix Composites used in investigations

Manufacturing method	% Reinforcement in Composites
Pressed plates	Al-6061 + 0% SiC
	Al-6061 + 25% SiC
	Al-6061 + 40% SiC
Extruded rods	Al-7064 + 0% SiC
	Al-7064 + 15% SiC
	Al-7064 + 20% SiC
	Al-8091 + 0% SiC
	Al-8091 + 10% SiC
	Al-8091 + 15% SiC
Squeeze-cast	Al-Si-Cu-Ni-Mg + 20% Al_2O_3 (Mat A)
	Al-Si + 20% Al_2O_3 (Mat B)
	Hüttenaluminum + 20% Al_2O_3 (Mat C)

where the inequalities $n < d < n+1$ are satisfied, where n and n+1 are the lower and upper limits of the size range. Also from the micrographs, features like orientation, shape and distribution of the reinforcement were examined.

Ultrasonic velocities

Measurements of the ultrasonic velocities were performed using the pulse-echo-overlap method, which is described in detail elsewhere [5]. A pulse of approximately 1-μsec duration of variable pulse-repetition rate is generated and impressed on a transducer which is acoustically bound to the specimen. The reflected echoes are received by the same transducer, amplified, and displayed on an oscilloscope. Two of the displayed echoes are then chosen and exactly overlapped by critically adjusting the frequency of the cw oscillator. This frequency f is employed to compute the ultrasonic velocity using the relation $V=2lf$, where l is the thickness of the specimen. X- and Y-cut transducers of 10 and 2.25 MHz were used for the generation of the longitudinal and transverse waves respectively.

RESULTS AND DISCUSSION

The particle size distribution and the fiber/particle content, estimated from optical micrographs, are shown in figures 1-4. Table 2 and 3 contain the area fractions covered by the reinforcement. The data are accurate to within 10% of the nominal values. Table 4,5 and 6 give the ultrasonic longitudinal and shear velocities measured. The velocities are denoted V_{ij}, where i and j are the directions of propagation and polarization respectively. The velocities are found to be reproducible to within 0.5%.

From figures 1-3 one finds that in the pressed samples, the particle size distributions as well as the area fractions covered by the reinforcement are the same in the three directions within the accuracy of the measurement. On the micrographs the reinforcement showed no features explaining the differencies in ultrasonic velocities measured. This suggests that the anisotropy is due to the texture in the aluminum matrix. The similar anisotropic behavior in the specimen without reinforcement also confirms this statement. However, the presence of SiC-particles is found to vastly enhance the anisotropy.

Table 2. Area fractions covered by the SiC-particle reinforcement.

Direction	6061+ 25% SiC	6061+ 40% SiC	7064+ 15% SiC	7064+ 20% SiC	8091+ 10% SiC	8091+ 15% SiC
1	26.3	37.7	20.6	23.9	12.7	17.5
2	22.6	36.3	18.7	23.7	12.1	16.5
3	24.0	31.7	16.5	21.0	11.8	15.3

Table 3. Area fractions covered by the alumina fiber and particle reinforcement (%).

Direction	Material A			Material B			Material C		
	Particle	Fiber	Total	Particle	Fiber	Total	Particle	Fiber	Total
1	12.0	11.9	23.9	8.5	12.6	21.1	1.0	13.2	14.2
2	20.4	2.5	22.9	15.2	2.7	17.9	12.5	3.2	15.7
3	18.7	2.9	21.6	15.7	2.0	17.7	13.7	2.7	16.4

Table 4. Ultrasonic velocities in SiC particle-Al pressed composites (m/s)

Velocity	6061+ 0% SiC	6061+ 25% SiC	6061+ 40% SiC
V_{11}	6407	7224	8058
V_{22}	6422	7287	8084
V_{33}	6358	6979	7841
V_{12}	3098	3785	4507
V_{13}	----	----	----
V_{21}	3103	3798	4505
V_{23}	----	----	----
V_{31}	3200	3676	4398
V_{32}	3195	3692	4412

Table 5. Ultrasonic velocities in SiC-particle-Al extruded composites (m/s)

Velocity	7064+ 0% SiC	7064+ 15% SiC	7064+ 20% SiC	8091+ 0% SiC	8091+ 10% SiC	8091+ 15% SiC
V_{11}	6251	6728	6935	6617	6890	7002
V_{22}	6233	6733	6875	6611	6903	7000
V_{33}	6250	6902	7071	6626	7025	7141
V_{12}	3077	3457	3591	3511	3723	3827
V_{13}	3069	3485	3667	3498	3738	3848
V_{21}	3075	3448	3593	3507	3719	3818
V_{23}	3095	3477	3625	3496	3731	3834
V_{31}	3056	3490	3666	3492	3745	3856
V_{32}	3090	3469	3595	3494	3741	3852

Table 6. Ultrasonic velocities in alumina particle and fiber-Al squeeze-cast composites (m/s)

Velocity	Composite A	Composite B	Composite C
V_{11}	7032	6967	6670
V_{22}	7033	6969	6712
V_{33}	6904	6835	6524
V_{12}	3694	3656	3419
V_{13}	3669	3578	3336
V_{21}	3681	3657	3439
V_{23}	3683	3594	3345
V_{31}	3644	3560	3325
V_{32}	3675	3606	3329

In the two series containing extruded specimens (Al-7064 and Al-8091) the reinforcement showed the same features in the three directions (compare figures 2 and 3). Nevertheless, in the reinforced samples the longitudinal velocities are higher in the extrusion direction, whereas the velocities are the same in the samples without reinforcement. This behavior further indicates that the anisotropy is caused by texture in the aluminum matrix but also indicates that the presence of the SiC-particles enhance the formation of texture.

In the squeeze-cast specimens (composites A,B,C) the ultrasonic longitudinal velocities, given in table 6, are considerably higher in the plane of the fibers than in the directions perpendicular to that

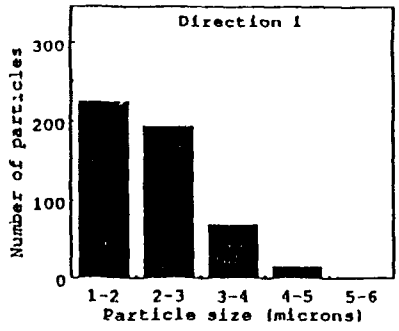

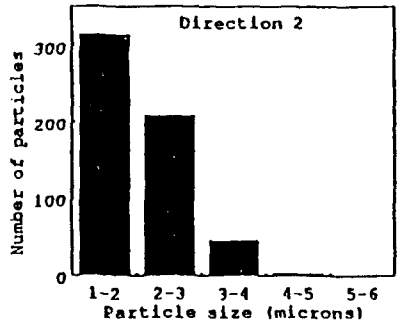

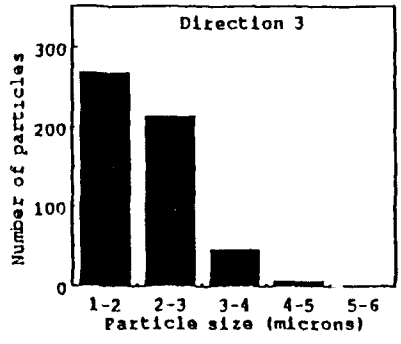

Fig.1 Particle size distribution in 25% SiC-6061 Al

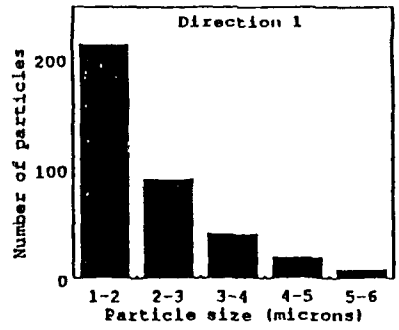

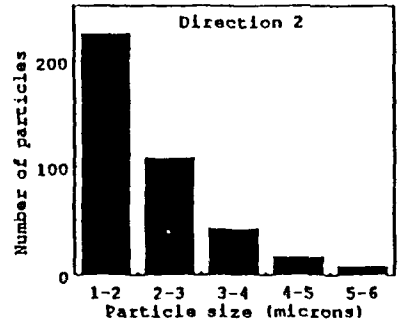

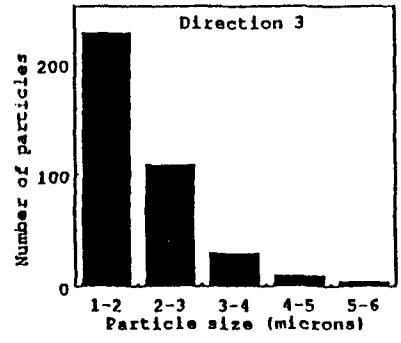

Fig.2 Particle size distribution in 20% SiC-7064 Al

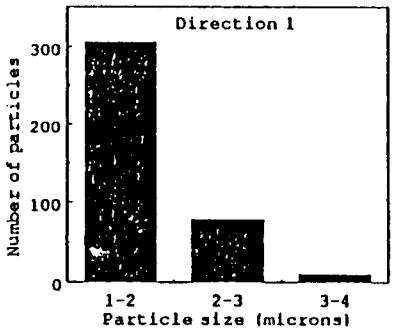

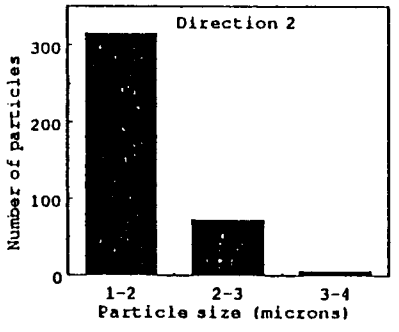

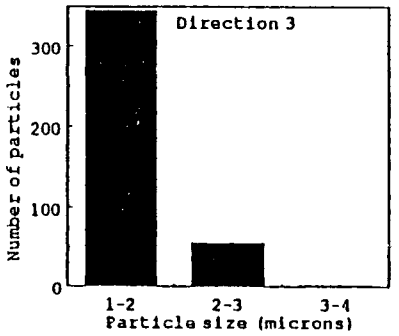

Fig.3 Particle size distribution in 15% SiC-8091 Al

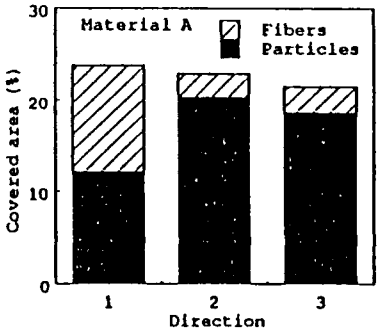

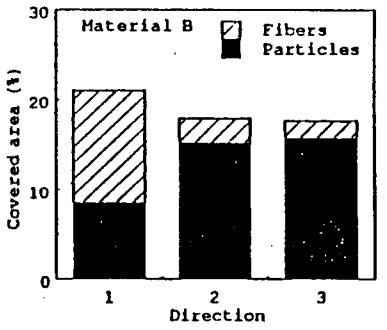

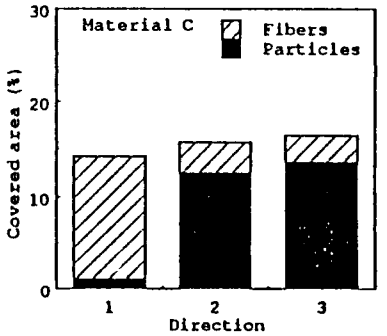

Fig.4 Area fractions covered by the reinforcement in composites A, B and C

plane and the higher the fiber content the higher the difference in velocity. No difference in longitudinal velocity was, however, found for waves propagating in the plane of the fibers having different polarization directions. Furthermore, the velocities of the shear waves propagating normal to the plane of the fibers but polarized in different directions are the same whereas the velocities of the shear waves propagating in the plane of the fibers are higher when the waves are polarized in the plane than when the waves are polarized normal to the plane. This means that the squeeze-cast specimens show a transversely isotropic behavior which is in agreement with their microstructure.

Res Nondestr Eval (1990) 2:83–96

Elastic Constants of Particle and Fiber Reinforced Metal Matrix Composites

B. Grelsson and K. Salama

Department of Mechanical Engineering, University of Houston, Houston, TX 77204, USA

Abstract. A model has been developed to predict the elastic moduli in composites reinforced with both particles and fibers. In the model the matrix material and the particles, which are assumed to be homogeneously distributed, form an effective matrix. The characteristics of this effective matrix is calculated using a theory formulated by Ledbetter and Datta. The effective matrix is then considered to be reinforced with fibers lying in one plane but randomly oriented in that plane. The effect of the 2-dimensionally random orientation of the fibers on the elastic moduli of the composites is determined in two steps. First the composite cylinders model by Hashin and Rosen for an aligned fiber system is employed, and then a geometric averaging procedure suggested by Christensen and Waals is performed. Using this model, the Young's and shear moduli were calculated for three samples with different aluminum matrices and volume fractions of particles (9, 13, and 17%) but the same fiber content (6%). The same elastic moduli were also determined using ultrasonic velocity measurements. The agreement between calculated and measured elastic moduli is found to be very good. Also, the elastic anisotropies between directions of the fiber rich plane and that normal to the plane could be predicted by the model.

Introduction

Many models have been developed to determine the effective elastic moduli of composite materials [1–7]. Most of these models deal with reinforcements in the form of spherical particles [1, 2], ellipsoidal inclusions [3, 4] or infinitely long fibers [5, 6]. However, in industrial applications the composites used are often of a more complex nature, where a mixture of particles and fibers is used as a second phase. To our knowledge no models that describe the elastic properties of these composites are available.

Ledbetter and Datta [1] used a multiple scattering theory to predict the elastic behavior of composites with a nonhomogeneous particle distribution. In the model they assume that the particles together with the matrix form an enriched "sea" that surrounds "islands" of pure matrix material. These non-spherical islands are aligned and produce anisotropy. The elastic constants predicted by the model are found to agree with those determined by ultrasonic

This article is dedicated to Professor Dr. Paul Höller on the occasion of his 65th birthday.

velocity measurements. Also, the elastic anisotropies in these composites could be explained in terms of the nonhomogeneous distribution of the particles.

On the other hand, in order to determine the effective elastic properties of fiber reinforced materials, Hashin and Rosen [5] introduced the composite cylinders model. In this model, the composite is considered to be comprised of infinitely long circular cylinders embedded in a continuous matrix phase. Each fiber has a radius, a, which is surrounded by an annulus of matrix material of radius b, and the ratio a/b is considered to be constant for all composite cylinders. In order to obtain a volume filling configuration, the absolute size of the cylinders must vary considerably. Hence, the model is expected to provide reasonable agreement with experimental measurements only if the size distribution is wide or the fiber concentration is low.

The present study is concerned with composites reinforced with both particles and fibers. In these composites, the presence of the homogeneously distributed particles improve the overall mechanical and thermal properties, whereas the fibers, randomly oriented in one plane, introduce the directionality often desirable in some applications. Due to the mixing of particles and fibers a model determining the elastic moduli of the composites is expected to be extremely extensive and complicated. In the composites investigated, however, the volume fraction of the reinforcement is relatively low, and hence we assumed no interaction between the fibers and the particles. This assumption simplified the calculations significantly since the effects of fibers and particles on the elastic properties could be evaluated independently.

In this approach we first considered the matrix material and the particles to form an effective matrix. Since the particles are homogeneously distributed in the metal, the effective matrix is considered to be homogeneous. The effective matrix was then considered to be reinforced with the fibers which are randomly oriented in one plane. The influence of the fibers on the elastic moduli of the composites was then determined first by using the composite cylinders model for an aligned fiber system [5] and second by performing a geometric average procedure which takes care of the 2-dimensionally random orientation of the fibers. A good agreement was obtained between the calculations and the experiment.

Theory

Composite with Spherical Particles

First, we consider a system that consists of an aluminum matrix and alumina particles. To find the elastic properties of this system, the results obtained by Ledbetter and Datta [1] are adopted. Using a multiple scattering approach these authors calculated the effective wave speeds of plane waves in a composite with randomly distributed particles. In their calculations they made the assumptions that the wavelength of the ultrasonic waves is long compared to the dimensions of the particles, all particles have the same shape and size, and the concentration of particles in the composite is dilute. The expressions for the effective bulk, K_{eff}, and shear moduli, G_{eff}, they obtained are

$$\frac{K_{eff} - K_m}{K_p - K_m} = \frac{\frac{1}{3} C_p \sum_{i,j} T_{iijj}}{1 - \frac{C_p (K_p - K_m)}{3K_m + 4G_m} \sum_{i,j} T_{iijj}} \tag{1}$$

$$\frac{G_{eff} - G_m}{G_p - G_m} = \frac{\frac{1}{5} C_p G_m \left(\sum_{i,j} T_{ijij} - \frac{1}{3} \sum_{i,j} T_{iijj} \right)}{G_m - \frac{6C_p}{25} \frac{(G_p - G_m)(K_m + 2G_m)}{3K_m + 4G_m} \left(\sum_{i,j} T_{ijij} - \frac{1}{3} \sum_{i,j} T_{iijj} \right)} \tag{2}$$

where the subscripts m and p refer to matrix and particles respectively, and C_p is the volume fraction of particles. The expressions for T_{iijj} and T_{ijij} are given in [1].

The system consisting of the aluminum matrix and the alumina particles is now considered as the effective matrix. In order to obtain the elastic properties of the composites under consideration, the characteristics of a composite comprised of the effective matrix and fibers randomly oriented in a plane are needed. The first step in finding these characteristics is to calculate the properties of a composite with fibers aligned in one direction.

Composite with Aligned Fibers

The most common model used for this geometry is the composite cylinders model introduced by Hashin and Rosen [5]. In this model, the fibers are assumed to be infinitely long circular cylinders embedded in a continuous matrix phase. With every fiber of radius, a, there is an annulus of matrix material of radius, b, associated with it. The ratio of these radii a/b is considered to be constant for all composite cylinders but the absolute values of the radii a and b vary such that a volume filling configuration is obtained. The effective Young's modulus E_{11}, the Poisson's ratio ν_{12}, the plane strain bulk modulus K_{23} and the shear moduli G_{12} and G_{23} of the composite can then be expressed as

$$E_{11} = C_f E_f + (1 - C_f) E_m + 4C_f(1 - C_f) G_m \left[\frac{(\nu_f - \nu_m)^2}{\frac{(1 - C_f) G_m}{K_f + G_m/3} + \frac{C_f G_m}{K_m + G_m/3} + 1} \right]$$

$$\nu_{12} = C_f \nu_f + (1 - C_f)\nu_m + \frac{C_f(1 - C_f)(\nu_f - \nu_m) \left[\frac{G_m}{K_m + G_m/3} - \frac{G_m}{K_f + G_f/3} \right]}{\frac{(1 - C_f) G_m}{K_f + G_f/3} + \frac{C_f G_m}{K_m + G_m/3} + 1}$$

$$K_{23} = K_m + \frac{G_m}{3} + \frac{C_f}{\frac{1}{K_f - K_m + (G_f - G_m)/3} + \frac{1 - C_f}{K_m + 4G_m/3}}$$

$$\frac{G_{12}}{G_m} = \frac{G_f(1 + C_f) + G_m(1 - C_f)}{G_f(1 - C_f) + G_m(1 + C_f)}$$

$$\frac{G_{23}}{G_m} = 1 + \frac{C_f}{\frac{G_m}{G_f - G_m} + \frac{(K_m + 7G_m/3)(1 - C_f)}{2(K_m + 4G_m/3)}} \tag{3}$$

where the subscripts m and f refer to matrix and fibers respectively, and C_f is the volume fraction of fibers. From these relationships the five independent components of the second order elastic constant tensor can be calculated using the relationships [7]

$$\begin{aligned} C_{11} &= E_{11} + 4\nu_{12}^2 K_{23} \\ C_{12} &= 2K_{23}\nu_{12} \\ C_{22} &= G_{23} + K_{23} \\ C_{23} &= -G_{23} + K_{23} \\ C_{66} &= G_{12} \end{aligned} \tag{4}$$

The above expressions give relationships for the elastic properties of a composite reinforced with spherical particles and aligned fibers. The characteristics of a composite where the fibers are randomly oriented in a plane are then to be determined.

Composite with 2-D Randomly Oriented Fibers

A schematic representation of the problem is shown in Fig. 1. The figure shows that all the fibers are lying in the x_1x_2-plane but randomly oriented in that plane. To determine the elastic properties of this configuration, the approach of Christensen and Waals [7] is used. In this approach, the effect of a random orientation of fibers on the stress to strain ratios σ_i'/ε_j' is analytically equivalent to finding the average value of the ratio σ_i'/ε_j' when all possible orientations are taken relative to a fixed axis as shown in Fig. 2. In the 2-dimensional case this can be expressed as

$$\left(\frac{\sigma_i'}{\varepsilon_j'}\right)_{\text{random}} = \frac{1}{\pi}\int_0^{\pi} \frac{\sigma_i'}{\varepsilon_j'}\, d\theta, \tag{5}$$

where the stress to strain ratio in the integrand refers to the aligned fiber system shown in Fig. 2 and θ is the angle between the x_1'- and the x_1-axis. The stress to strain ratios are then calculated using the tensor transformation laws for stresses and strains

$$\begin{bmatrix} \sigma_1' \\ \sigma_2' \\ \sigma_3' \\ \sigma_4' \\ \sigma_5' \\ \sigma_6' \end{bmatrix} = \begin{bmatrix} \cos^2\theta & \sin^2\theta & 0 & 0 & 0 & -\sin 2\theta \\ \sin^2\theta & \cos^2\theta & 0 & 0 & 0 & \sin 2\theta \\ 0 & 0 & 1 & 0 & 0 & 0 \\ 0 & 0 & 0 & \cos\theta & \sin\theta & 0 \\ 0 & 0 & 0 & -\sin\theta & \cos\theta & 0 \\ \frac{\sin 2\theta}{2} & -\frac{\sin 2\theta}{2} & 0 & 0 & 0 & \cos 2\theta \end{bmatrix} \begin{bmatrix} \sigma_1 \\ \sigma_2 \\ \sigma_3 \\ \sigma_4 \\ \sigma_5 \\ \sigma_6 \end{bmatrix} \tag{6}$$

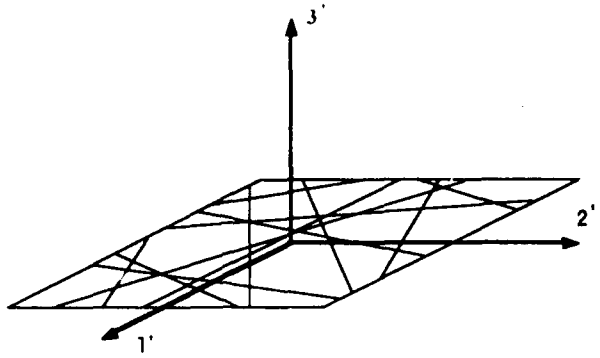

Fig. 1. Composite with fibers randomly oriented in the x_1x_2-plane.

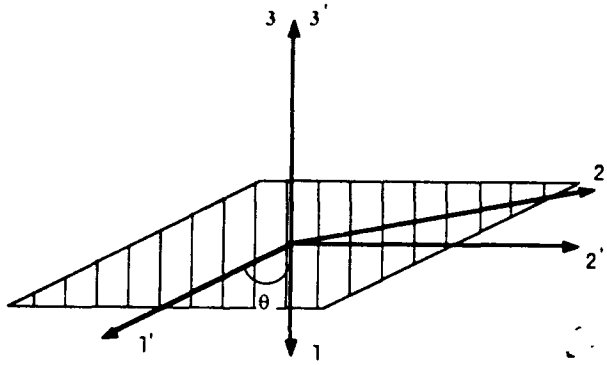

Fig. 2. Composite with fibers aligned along the x_1-direction. The x_1- and x_2-axes are rotated an angle θ with respect to the x_1'- and x_2'-axes.

$$\begin{bmatrix}\varepsilon_1\\ \varepsilon_2\\ \varepsilon_3\\ \varepsilon_4\\ \varepsilon_5\\ \varepsilon_6\end{bmatrix} = \begin{bmatrix} \cos^2\theta & \sin^2\theta & 0 & 0 & 0 & \dfrac{\sin 2\theta}{2} \\ \sin^2\theta & \cos^2\theta & 0 & 0 & 0 & -\dfrac{\sin 2\theta}{2} \\ 0 & 0 & 1 & 0 & 0 & 0 \\ 0 & 0 & 0 & \cos\theta & -\sin\theta & 0 \\ 0 & 0 & 0 & \sin\theta & \sin\theta & 0 \\ -\sin 2\theta & \sin 2\theta & 0 & 0 & 0 & \cos 2\theta \end{bmatrix} \begin{bmatrix}\varepsilon_1'\\ \varepsilon_2'\\ \varepsilon_3'\\ \varepsilon_4'\\ \varepsilon_5'\\ \varepsilon_6'\end{bmatrix} \tag{7}$$

and the stress-strain relationships for a system with aligned fibers which are given by

$$\sigma_1 = C_{11}\varepsilon_1 + C_{12}\varepsilon_2 + C_{12}\varepsilon_3$$
$$\sigma_2 = C_{12}\varepsilon_1 + C_{22}\varepsilon_2 + C_{23}\varepsilon_3$$
$$\sigma_3 = C_{12}\varepsilon_1 + C_{23}\varepsilon_2 + C_{22}\varepsilon_3$$

$$\sigma_4 = 1/2(C_{22} - C_{23})\varepsilon_4$$
$$\sigma_5 = C_{66}\varepsilon_5$$
$$\sigma_6 = C_{66}\varepsilon_6 \tag{8}$$

The stress to strain ratio σ_1'/ε_1' can then be evaluated by imposing a strain along the 1'-direction such that the conditions

$$\varepsilon_1' \neq 0$$
$$\varepsilon_i' = 0, \quad i \neq 1 \tag{9}$$

are satisfied. The transformation laws, Eqs. (6) and (7), and the stress-strain relationships, Eq. (8), then yield

$$\sigma_1' = \sigma_1 \cos^2\theta + \sigma_2 \sin^2\theta - \sigma_6 \sin 2\theta$$
$$\frac{\sigma_1}{\varepsilon_1'} = C_{11} \cos^2\theta + C_{12} \sin^2\theta$$
$$\frac{\sigma_2}{\varepsilon_1'} = C_{12} \cos^2\theta + C_{22} \sin 2\theta$$
$$\frac{\sigma_6}{\varepsilon_1'} = -C_{66} \sin^2\theta \tag{10}$$

Combining Eqs. (10) results in

$$\frac{\sigma_1'}{\varepsilon_1'} = C_{11} \cos^4\theta + 2C_{12} \sin^2\theta \cos^2\theta + C_{22} \sin^4\theta + 4C_{66} \sin^2\theta \cos^2\theta \tag{11}$$

Integration according to Eq. (5) gives

$$Q_{11} = \left(\frac{\sigma_1'}{\varepsilon_1'}\right)_{\text{random}} = \frac{1}{8}(3C_{11} + 2C_{12} + 3C_{22} + 4C_{66}) \tag{12}$$

The stress to strain ratio evaluated in Eq. (12) will correspond to one of the components, Q_{11}, in the second order elastic constant tensor for the composite in Fig. 1. The other components in this tensor can be evaluated similarly and are found to be

$$Q_{12} = \left(\frac{\sigma_2'}{\varepsilon_1'}\right)_{\text{random}} = \frac{1}{8}(C_{11} + 6C_{12} + C_{22} - 4C_{66})$$
$$Q_{13} = \left(\frac{\sigma_3'}{\varepsilon_1'}\right)_{\text{random}} = \frac{1}{2}(C_{12} + C_{23})$$

$$Q_{33} = \left(\frac{\sigma_3'}{\varepsilon_3'}\right)_{\text{random}} = C_{22}$$

$$Q_{44} = \left(\frac{\sigma_4'}{\varepsilon_4'}\right)_{\text{random}} = \frac{1}{4}(C_{22} - C_{23} + 2C_{66}) \tag{13}$$

For the composite with 2-D randomly oriented fibers, these five components fully describe the stress-strain relationships which are given by

$$\begin{aligned}
\sigma_1 &= Q_{11}\varepsilon_1 + Q_{12}\varepsilon_2 + Q_{13}\varepsilon_3 \\
\sigma_2 &= Q_{12}\varepsilon_1 + Q_{11}\varepsilon_2 + Q_{13}\varepsilon_3 \\
\sigma_3 &= Q_{13}\varepsilon_1 + Q_{13}\varepsilon_2 + Q_{33}\varepsilon_3 \\
\sigma_4 &= Q_{44}\varepsilon_4 \\
\sigma_5 &= Q_{44}\varepsilon_5 \\
\sigma_6 &= \tfrac{1}{2}(Q_{11} - Q_{12})\varepsilon_6
\end{aligned} \tag{14}$$

From the five components of the second order elastic constant tensor, the effective Young's and shear moduli of the composite can be calculated using the relationships

$$\begin{aligned}
E_{11} &= Q_{11} + \frac{Q_{13}^2(Q_{12} - Q_{11}) + Q_{12}(Q_{13}^2 - Q_{33}Q_{12})}{Q_{33}Q_{11} - Q_{13}^2} \\
E_{33} &= Q_{33} - \frac{2Q_{13}^2}{Q_{11} + Q_{12}} \\
G_{12} &= \frac{(Q_{11} - Q_{12})}{2} \\
G_{23} &= Q_{44}
\end{aligned} \tag{15}$$

Measurements

Specimens

The metal matrix composites used in this investigation are comprised of an aluminum alloy as the matrix material and alumina particles and fibers as the reinforcements. The three aluminum alloys used as matrix materials consist of Al-12% Si, Al-12% Si-Cu-Ni-Mg, and commercially pure aluminum.

The composites were manufactured using the squeeze casting method and produced in the form of bars. From these bars, blocks measuring 10 × 12 × 20 mm were cut. The blocks were machined and ground such that opposite faces were flat and parallel to within 10 μm.

The coordinate systems for the specimens were chosen such that the x_1- and x_2- directions are in the fiber rich layers at right angles to each other and the x_3-direction is perpendicular to the fiber rich layers. The volume fractions of particles and fibers in these samples were estimated using optical microscopy.

Ultrasonic velocities

Measurements of ultrasonic velocities were performed using the pulse-echo-overlap method, which is described in detail elsewhere [8]. A pulse of approximately 1-μsec duration of variable pulse-repetition rate is generated and impressed on a transducer that is acoustically bound to the specimen. The reflected echoes are received by the same transducer, amplified, and displayed on an oscilloscope. Two of the displayed echoes are then chosen and exactly overlapped by critically adjusting the frequency of the cw oscillator. This frequency f is employed to compute the ultrasonic velocity using the relation $V = 2lf$, where l is the thickness of the specimen. X- and Y-cut transducers of 10 and 2.25 MHz were used for the generation of the longitudinal and transverse waves respectively. The elastic constants were calculated using the relationship

$$C_{pp} = C_{ijij} = \rho V_{ij}^2 \qquad p = 1,2, \ldots, 6,\ i,j = 1,2,3 \tag{16}$$

where ρ is the mass density, and indices ij are contracted to index p according to Voigt's notation.

Microstructure

The microstructure of one of the composites used in this study is shown in Fig. 3. The micrographs show the microstructure in the three directions for the composite with hüttenaluminum as the matrix metal. The dark, almost circular areas are the particles, whereas the fibers appear as light grey rods, 20–50 μm in length. The micrographs clearly illustrate that the fibers are lying in one plane, with its normal in the 3-direction, but they are randomly oriented in that plane. Furthermore, the 1- and 2-directions exhibit the same features. They both show a low fraction of fibers oriented in the x_1x_2-plane and have the same particle content. These observations confirm that a transversely isotropic behavior of the composites is to be expected.

The area fractions covered by the fiber and particle reinforcements in each plane were estimated in the three specimens. This was accomplished by scanning the faces of the specimen under an optical microscope and taking photographs at several "representative" locations along the three chosen directions. The area fractions were obtained from these micrographs by adding the projected area on the face of all particles and fibers and dividing by the total area.

Results

Table 1 contains the area fractions of the fiber and particle reinforcements in the composites used in this investigation as estimated from the optical microscopy study. Table 2 includes values of the elastic constant found in literature [9] for the aluminum alloys used as matrices for the composites. It also includes the measured mass densities of the composites and the volume fractions of the

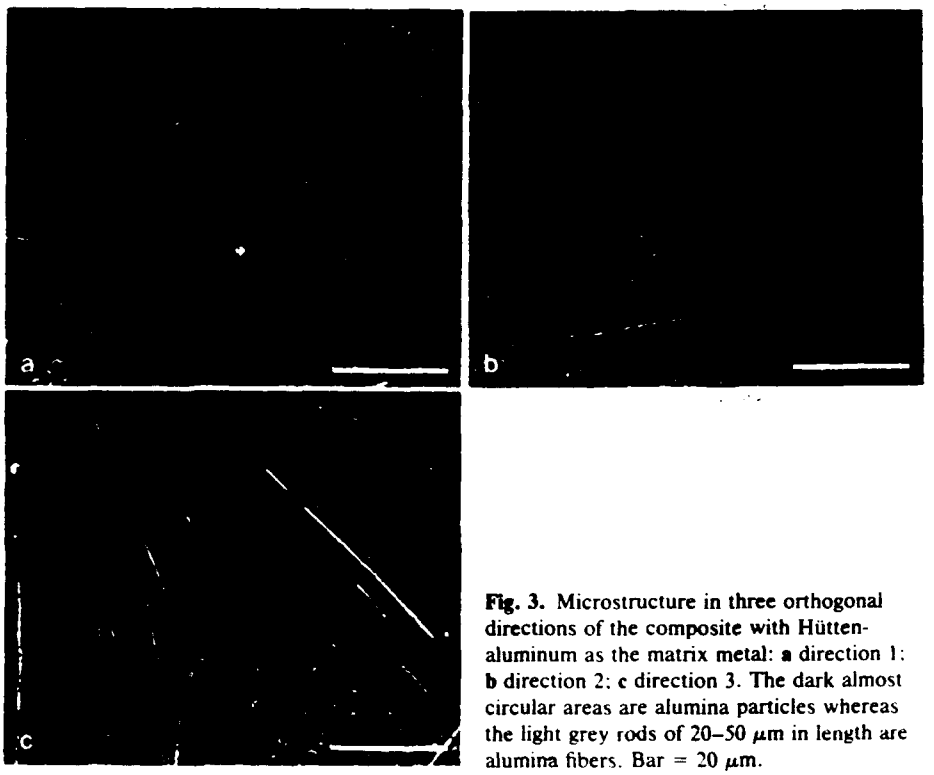

Fig. 3. Microstructure in three orthogonal directions of the composite with Hütten-aluminum as the matrix metal: **a** direction 1; **b** direction 2; **c** direction 3. The dark almost circular areas are alumina particles whereas the light grey rods of 20–50 μm in length are alumina fibers. Bar = 20 μm.

alumina reinforcements. The volume fractions of particles and fibers were obtained by taking the average of the area fractions in the three directions.

Table 3 lists the ultrasonic velocities, V_{ij}, measured, where i and j denote the directions of propagation and polarization respectively. In Table 4 the calculated and measured elastic constants are listed. Column 2 gives the elastic constants of the effective matrix, consisting of the aluminum matrix and the alumina particles. These constants were calculated using Eqs. (1) and (2). Using Eq. (3) the elastic constants of composites with aligned fibers were

Table 1. Area percentage of alumina particle and fiber reinforcements in MMC specimens

	Matrix					
	Al-Si-Cu-Ni-Mg		Al-Si		Hüttenaluminum	
Direction	Particles	Fibers	Particles	Fibers	Particles	Fibers
1	18.7	2.9	15.7	2.0	13.7	2.7
2	20.4	2.5	15.2	2.7	12.5	3.2
3	12.0	11.9	8.5	12.6	1.0	13.2

Table 2. Elastic constants, densities, and volume fractions of MMC specimens used in calculations

Material	E (GPa)	ν	ρ (kg/m^3)	C_p	C_f
Al-Si-Cu-Ni-Mg	73.1	0.33	2825	0.17	0.06
Al-Si	71.0	0.33	2760	0.13	0.06
Hüttenaluminum	68.9	0.33	2793	0.09	0.06
Alumina	372.0	0.224			

Table 3. Ultrasonic velocities measured in MMC specimens

	Matrix		
Velocity (m/s)	Al-Si-Cu-Ni-Mg	Al-Si	Hüttenaluminum
V_{11}	7032	6967	6670
V_{22}	7033	6969	6712
V_{33}	6907	6835	6524
V_{12}	3694	3656	3419
V_{13}	3669	3578	3336
V_{21}	3681	3657	3439
V_{23}	3683	3594	3345
V_{31}	3644	3560	3325
V_{32}	3675	3606	3329

Table 4. Calculated and measured elastic constants of MMC specimens with Al-Si-Cu-Ni-Mg, Al-Si, and Hüttenaluminum as the matrix metal

Matrix	Elastic constant	Effective matrix	Aligned fibers	Random fibers	Measured
Al-Si-Cu-Ni-Mg	E_{11}	92.2	109.1	102.2	100.4
	E_{22}	92.2	99.5	102.2	100.4
	E_{33}	92.2	99.5	99.6	98.7
	G_{12}	34.8	37.5	38.8	38.4
	G_{13}	34.8	37.5	37.4	37.8
	G_{23}	34.8	37.2	37.4	38.2
Al-Si	E_{11}	85.0	102.3	94.9	95.0
	E_{22}	85.0	92.0	94.9	95.4
	E_{33}	85.0	92.0	92.1	92.9
	G_{12}	32.0	34.6	35.9	36.9
	G_{13}	32.0	34.6	34.4	35.1
	G_{23}	32.0	34.2	34.4	35.8
Hüttenaluminum	E_{11}	78.1	95.8	88.0	84.6
	E_{22}	78.1	84.9	88.0	85.4
	E_{33}	78.1	84.9	85.0	81.9
	G_{12}	29.6	32.0	33.5	32.8
	G_{13}	29.6	32.0	31.9	31.0
	G_{23}	29.6	31.7	31.9	31.0

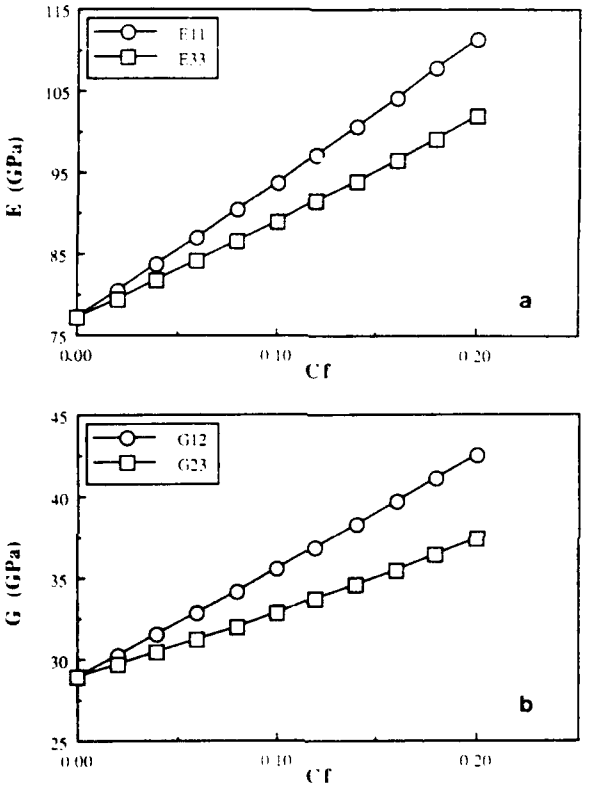

Fig. 4. Calculated effects of changing the alumina fiber content on the anisotropies in the Young's and the shear moduli of a composite containing the Al-Si alloy as the matrix metal and 6% alumina particles.

computed and the results are listed in column 3. Column 4 lists the predicted elastic constants when the fibers are randomly oriented in one plane. These results were obtained by employing Eqs. (4), (12), (13), and (15). These values are to be compared with the measured values given in column 5. The measured data were computed using the densities given in Table 2 and the ultrasonic velocities listed in Table 3 and are found to be reproducible to within 1%.

Figure 4 displays the calculated effects of changing the fiber content on the anisotropies in the Young's and the shear moduli of the composites. In these calculations the effective matrix consists of the Al-Si alloy as the matrix metal and 6% alumina particles. Figure 5 illustrates the calculated effect on the same moduli upon changing the particle content in the effective matrix. In these calculations the Al-Si alloy was also used as the matrix metal and the fiber content was 6%.

Discussion

From the metallurgical observations it is seen that the area fraction of fibers in the 3-direction is vastly higher than those measured in the two directions in the plane perpendicular to the 3-direction. In the 1- and 2-directions the fiber con-

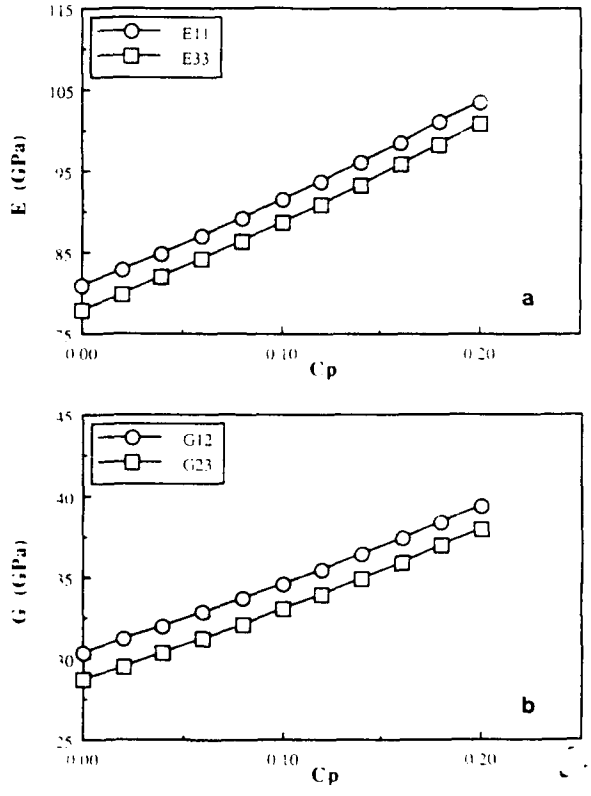

Fig. 5. Calculated effects of changing the alumina particle content on the anisotropies in the Young's and the shear moduli of a composite containing the Al-Si alloy as the matrix metal and 6% alumina fibers.

tent is the same to within ± 0.4%. Also the micrographs show that the particle content in the 3-direction is significantly lower than those in the other two directions. However, the projected area of the particles is almost circular in all three directions indicating spherical particles. Due to this result and the fact that the manufacturing process should not produce any anisotropy due to the distribution of particles, it is assumed in the calculations that the particles are spherical and that they are randomly distributed.

The experimental results in Table 3 show that the composites exhibit a transversely isotropic behavior which is in agreement with the microstructure shown in Fig. 1. This behavior requires that $E_{11} = E_{22}$ and $G_{13} = G_{23}$ which is in agreement with observations shown in Table 4, to within 2%. Furthermore, the elastic constants in the 3-direction differ from those in the 1- and 2-directions such that $E_{33} < E_{11}$ and $G_{13} < G_{12}$. This also agrees with the microstructure observed in the three samples since the fiber rich plane is expected to be elastically stiffer than the planes normal to that plane.

The general behavior of the predicted elastic moduli as a function of the fiber or particle content is shown in Figs. 4 and 5 respectively. It can be seen from these figures that the four elastic moduli increase almost linearly with the fiber content and as a consequence the anisotropy exhibit the same behavior.

As the particle content is increased the elastic moduli deviates slightly from a linear relationship. Furthermore, E_{33} and G_{13} increase at a faster rate than E_{11} and G_{12} such that the anisotrophy produced by the fibers is slightly lowered as the particle content is increased.

Since the fiber content in the three samples was the same, the anisotropy was expected to be more pronounced in the composite with the soft matrix than that with a stiffer matrix. As can be seen in Table 4, this behavior was experimentally observed in both the Young's and the shear moduli. As the stiffness of the effective matrix is increased, the difference in the moduli between the directions in the plane and normal to the plane of the fibers becomes less pronounced. The quantitative values of the anisotropies are also well predicted by the model. For the material with the lowest particle content (9%), the values agree almost exactly. As the particle content gets higher, the observed anisotropies deviate from those predicted but the agreement is still good. This trend is expected since the model assumes no interaction between the particles and the fibers, and accordingly the model will be more applicable to composites with low particle content.

The deviation from predicted anisotropies can also be explained from a microstructural point of view. When the particle content is increased it becomes more difficult to orient all the fibers in a specific plane. In addition, it seems that the presence of particles will force some of the fibers to be oriented such that they make a small angle with their ideal orientation, and the true configuration will differ from that assumed by the model. The anisotropy produced will then be lower than that predicted.

Summary

The elastic behavior of metal-matrix composites reinforced with homogeneously distributed particles and fibers randomly oriented in two dimensions, has been investigated. Using a model which assumes no interaction between particles and fibers, the elastic moduli as well as the elastic anisotropies were calculated for the composites containing 9, 13, and 17% particles and 6% fibers. The values computed by the model are found to agree very well with those determined from ultrasonic velocity measurements.

These results indicate that for relatively low volume fractions of reinforcement the interaction between particles and fibers can be neglected on determining the effective elastic properties of these composites. This simplifies the calculations significantly when these composites are to be used in applications since the effects of adding particles that improve the overall properties, and fibers that generate the directionality, can be estimated independently. This is applicable for volume fractions that are not too high.

Acknowledgment. This work is sponsored by the Army Research Office under contract No. DAAL03-88-K-0096.

References

1. H.M. Ledbetter and S.K. Datta. *J. Acoust. Soc. Am.* **79:**239 (1986)
2. B. Budiansky. *J. Mech. Phys. Solids* **13:**223 (1965)
3. J.D. Eshelby. *Proc. Roy. Soc. (London)* **241A**:376 (1957)
4. T.S. Chow. *J. Appl. Phys.* **48:**4072 (1977)
5. Z. Hashin and B.W. Rosen. *J. Appl. Mech.* **31:**223 (1964)
6. R. Hill, *J. Mech. Phys. Solids* **12:**199 (1964)
7. R.M. Christensen and F.M. Waals. *J. Comp. Mater.*, **6,** 518 (1972).
8. K. Salama and C.K. Ling, *J. Appl. Phys.* **51:**1505 (1980)
9. *Metals Handbook*, vol. 1, 8th ed. ASM (1961)

Proc. QNDE Vol 10, 1991 in Press

ACOUSTIC NONLINEARITY IN METAL - MATRIX COMPOSITES

H. Mohrbacher, D. Lee, E. Schneider * and K. Salama

Department of Mechanical Engineering
University of Houston
Houston, TX 77204, (713) 749-4455
* Fraunhofer Institute for Nondestructive Testing, Germany

INTRODUCTION

The elastic behavior of a solid consists of linear and nonlinear contributions. The linear part is represented by the well known Hooke's law which is given in tensorial notation as

$$\sigma_{ij} = C_{ijkl}\,\varepsilon_{kl} \qquad (1)$$

where σ_{ij} and ε_{kl} are the stress and strain tensors, respectively, and C_{ijkl} is the tensor of the second order elastic constants (SOEC). This relationship is sufficient for many engineering calculations since deviations from a purely linear elastic behavior are small. Hooke's law, however, is not sufficient for an advanced characterization of the elastic behavior of materials. This is due to the fact that many of the physical and mechanical properties of materials are of nonlinear nature. The nonlinear elastic behavior can be investigated using ultrasonic techniques because of their high sensitivity for small nonlinear effects. Among the nonlinear effects are the stress and the temperature dependences of ultrasonic velocities in the solid. These effects have gained considerable interest in the last decade, particularly for the nondestructive evaluation of applied and residual stresses [1], and also for the microstructural characterization of materials [2]. Another physical manifestation of the nonlinear elastic behavior of solids is the acoustic nonlinearity parameter. This parameter can be determined from measurements of the amplitudes of fundamental and second harmonic when an originally sinusoidal wave gets distorted while propagating through the solid. The nonlinearity parameter can also be calculated from a combination of second and third order elastic constants. In previous studies [3], the nonlinearity parameter was found to be sensitive to microstructural changes in aluminum alloys and in particular to the content of precipitates of the second phase.

Metal - matrix composites are a new class of materials wich contain a metallic matrix and a metallic or ceramic material as a reinforcement. The bulk properties of these composites can be tailored by changing the volume percentage, geometry, distribution, and orientation of the reinforcement. Due to the different coefficients of thermal expansion for the matrix and the reinforcement material in MMCs, the creation of thermal stresses during manufacturing is unavoidable. Therefore, the nondestructive characterization of these composites is necessary in order to monitor their mechanical properties and to guarantee their quality.

In the present study the effect of the volume content of reinforcement in metal - matrix composites (MMC) on the two nonlinear elastic quantities, namely acoustoelastic

constants and nonlinearity parameter has been investigated. The nonlinearity parameter is determined using two different methods and the results are compared.

THEORETICAL

Basically, all nonlinear elastic effects are due to the anharmonicity of the interatomic potential. Thus, relationships between quantities describing the elastic nonlinearity are expected. In order to develop quantitative parameters for the description of elastic nonlinearity, it is convenient to use the thermodynamic derivation of the elastic constants starting from the elastic potential of the solid. If the lattice arrangement of a solid is disturbed by an infinitesimal strain ε due to the presence of an elastic wave, the energy of deformation per unit volume $\Phi(\varepsilon)$ can be expanded as a power series of strains such that

$$\Phi(\varepsilon) = \phi_0 + \frac{\partial \Phi}{\partial \varepsilon_{ij}} \varepsilon_{ij} + \frac{\partial^2 \Phi}{\partial \varepsilon_{ij} \partial \varepsilon_{kl}} \varepsilon_{ij} \varepsilon_{kl} + \frac{\partial^3 \Phi}{\partial \varepsilon_{ij} \partial \varepsilon_{kl} \partial \varepsilon_{mn}} \varepsilon_{ij} \varepsilon_{kl} \varepsilon_{mn} + \ldots \qquad (2)$$

According to Brugger [4], the elastic constants of the order n are defined as the n-th partial derivatives of the elastic potential with respect to strain as

$$C_{ij\ldots} = \partial^{(n)} \Phi / \partial \varepsilon_{ij\ldots} \qquad (3)$$

If up to third order terms in ε are considered in eq.(2), the stress-strain relationship can be written as

$$\sigma_{ij} = C_{ijkl}\, \varepsilon_{kl} + C_{ijklmn}\, \varepsilon_{kl} \varepsilon_{mn} \qquad (4)$$

where the C_{ijklmn} are the third order elastic constants (TOEC) which need to be added to Hooke's law (1) to allow for nonlinear deviations.

For isotropic materials, the tensor of the second order elastic constants reduces to two independent second order elastic constants, known as Lamé constants λ and μ. These constants can be determined directly from ultrasonic experiments by measuring the wave speeds of longitudinal and shear waves using the relationships :

$$\mu = \rho\, v_T^2 \qquad \text{and} \qquad \lambda + 2\mu = \rho\, v_L^2 \qquad (5)$$

The tensor of the third order elastic constants reduces to three independent third order elastic constants in isotropic materials. These are called the Murnaghan constants l, m and n. In order to measure these constants using ultrasonic methods the propagation velocities of three different wave modes have to be determined as a function of an applied uniaxial strain. The relative change in the ultrasonic velocity of a given wave mode with the applied elastic strain normalized by the velocity of the strain-free specimen is called the acoustoelastic constant (AEC) which is a characteristic of the material. The Murnaghan constants can be evaluated from acoustoelastic constants using the relationships [6]

$$l = \frac{\lambda}{1 - 2\nu} \left[\frac{1-\nu}{\nu} \frac{\partial v_{22}/v_0}{\partial \varepsilon} + \frac{2}{1+\nu} \left(\frac{\partial v_{21}/v_0}{\partial \varepsilon} + \nu \frac{\partial v_{23}/v_0}{\partial \varepsilon} \right) + 2\nu \right]$$

$$m = 2(\lambda + \mu) \left[\frac{\nu}{1+\nu} \frac{\partial v_{23}/v_0}{\partial \varepsilon} + \frac{1}{1+\nu} \frac{\partial v_{21}/v_0}{\partial \varepsilon} + 2\nu - 1 \right] \qquad (6)$$

$$n = \frac{4\mu}{1+\nu} \left[\frac{\partial v_{21}/v_0}{\partial \varepsilon} - \frac{\partial v_{23}/v_0}{\partial \varepsilon} - 1 - \nu \right]$$

where ν is the Poisson's ratio, λ and μ are the Lamé constants, v_{ij} is the velocity of an ultrasonic wave with propagation direction i and polarization direction j, v_0 is the velocity

in the unstrained specimen and ε is a uniaxial strain applied in a direction perpendicular to the propagation direction.

Another nonlinear quantity which can be obtained if eq.(4) is inserted into the equation of motion for particles in the solid's lattice, leads to the nonlinear wave equation

$$\frac{\partial^2 u_i}{\partial t^2} - v_i^2 \frac{\partial^2 u}{\partial a^2} = -\beta_i v_i^2 \frac{\partial u_i}{\partial a} \frac{\partial^2 u_i}{\partial a^2} \tag{7}$$

where u is the particle displacement, i is a mode index depending on the polarization and the propagation direction of the wave, a is a coordinate along the direction of wave propagation and v_i is the wave velocity of the mode i. The quantity β_i is the modal acoustic nonlinearity parameter of the solid and can be expressed as a linear combination of the second and third order elastic constants [5]. The solution of the nonlinear wave equation can be given as

$$u_i = A_1 \sin(ka - \omega t) + A_2 \cos 2(ka - \omega t) \tag{8}$$

where A_1 and A_2 are the amplitudes of the fundamental and second harmonic waves, respectively. The acoustic nonlinearity parameter is related to these amplitudes as

$$\beta = \frac{8}{k^2 a} \frac{A_2}{A_1^2} \tag{9}$$

where ω is the fundamental frequency, k is the propagation constant and a is the distance measured from the generating transducer to the instantaneous position of the fundamental wave in the solid. Its magnitude determines the extend of the distortion of the fundamental wave. If one considers a longitudinal wave mode in an isotropic solid, the acoustic nonlinearity parameter is related to the Lamé and the Murnaghan constants by

$$-\beta = 3 + \frac{2l + 4m}{\lambda + 2\mu} \tag{10}$$

Using this relationship the acoustic nonlinearity parameter can be calculated when the third order elastic constants are known.

EXPERIMENTAL

In this study, two different sets of specimens were used. The matrix was an Al - 8091 alloy in one case and in the other case an Al - 7064 alloy. The chemical compositions of both alloys are shown in table 1. As reinforcement material these composites contain SiC - particles. The particles had a more or less globular shape, ranging from 1 - 5 μm in size. The material has finally been extruded to rods. Micrographs taken for different cuts of the specimens revealed a planar random distribution of the reinforcement in the plane normal to the extrusion direction and a particle alignment along the extrusion direction.

A block diagram of the experimental set up for the determination of the nonlinearity parameter is shown in Fig.1 . A lithium niobate transducer attached to the specimen by a solid bond is used to generate ultrasonic pulses. These pulses have typically a center frequency of 10 MHz and a bandwidth of 200 kHz. The ultrasonic signal propagates along the extrusion direction of the specimen whose surfaces are made parallel to each other and are lapped optically flat. The 10 MHz fundamental as well as the 20 MHz harmonic signal cause a distortion of the free surface of the specimen. The displacement amplitudes carried by the two frequencies are measured in order to determine the nonlinearity parameter using eq.(9).

Table 1: Chemical compositions of the aluminum alloys in weight percent .

	Alloying Elements									
Alloy	Si	Fe	Cu	Mg	Zr	Li	Zn	Cr	Co	Al
8091	0.02	0.01	1.90	0.80	0.11	2.70	----	----	----	rem
7064	0.05	0.10	2.00	2.30	0.20	----	7.10	0.12	0.22	rem

For measurements of the absolute amplitudes, the capacitive detector technique described in [8] has been used. This technique allows the detection of displacement amplitudes of a free surface with a sensitivity of 10^{-3} Å.

In order to verify the behavior predicted by eq.(9), the amplitudes of the fundamental and second harmonic have been measured as a function of increasing source voltage. A plot of the harmonic amplitude A_2 vs. the square of the fundamental amplitude A_1 yields a linear relationship over the whole range of the driving voltages used, as shown in Fig.2 . The slope of a linear fit through these data is used to calculate the nonlinearity parameter. In many of the engineering materials the attenuation of ultrasonic waves depends on their frequencies. Unless the attenuation of the second harmonic is twice that of the fundamental, a correction has to be made according to relationship [9]

$$\beta = \beta_{meas.} \frac{\alpha_2 - 2\alpha_1}{1 - \exp[(2\alpha_1 - \alpha_2)\, a]} \qquad (11)$$

where α_1 and α_2 are the attenuation coefficients of the fundamental and the second harmonic waves respectively. The attenuation coefficients for 10 and 20 MHz longitudinal waves in the MMC-specimens have been used to perform this correction. Another correction due to diffraction effects has been neglected because of the large lateral dimensions of the specimens.

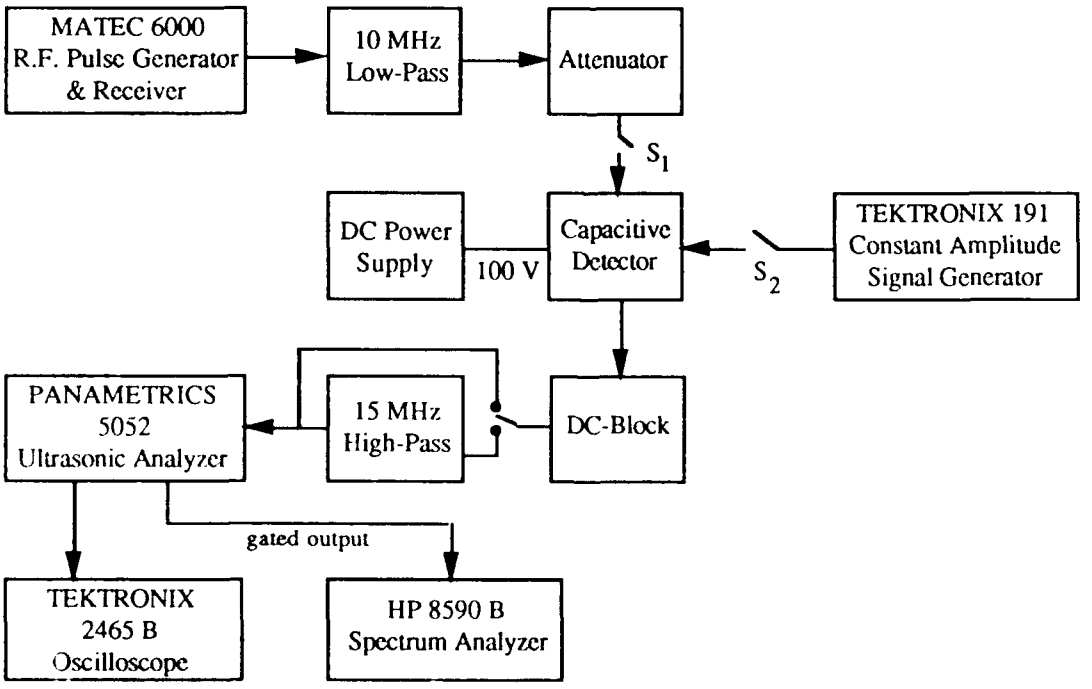

Fig. 1. Block diagram of the capacitive detector system.

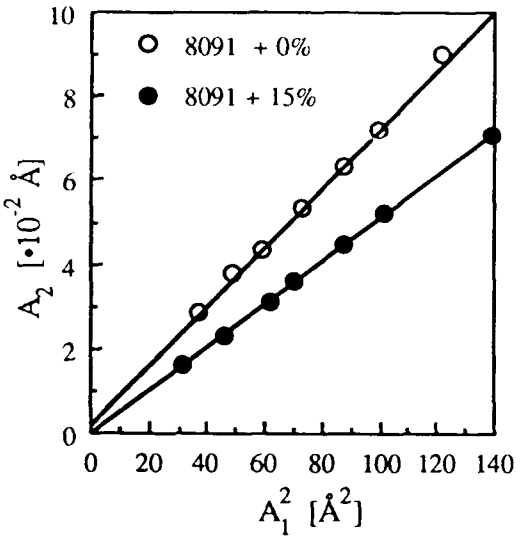

Fig. 2. Measured displacement amplitudes for fundamental and second harmonic signals.

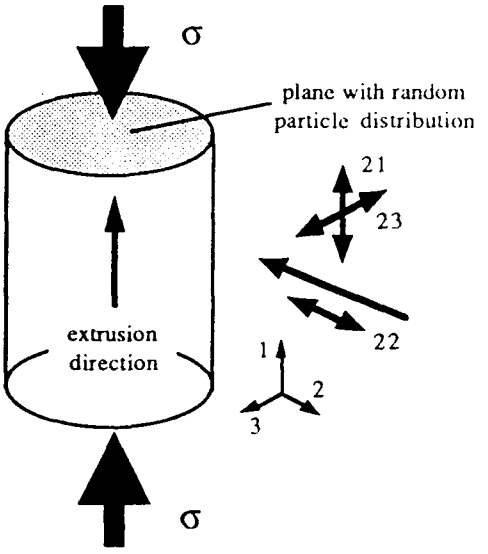

Fig. 3. Velocity designations and direction of applied stress

Acoustoelastic constants are determined by applying a uniaxial compressive stress while ultrasonic waves are propagating transversely to the load direction. The relative changes in velocity for three different wave modes (Fig.3) are measured using the pulse echo overlap technique. This technique is described in detail in [10] and can resolve velocity changes up to one part in 10^6. The changes caused by the acoustoelastic effect are typically in the order of one part in 10^4 and depend on the polarization of the wave. The slope of the velocity data vs. the elastic strain is used to determine the acoustoelastic constants and then, with eqs.(6), to calculate the third order elastic constants. The average values resulting from measurements in two different propagation directions within the quasi-isotropic plane are used to represent the material parameters.

RESULTS AND DISCUSSION

From measurements of densities and of ultrasonic velocities the second order elastic constants of the metal matrix composites have been evaluated by Lee et al. [13] using eq.(5). Their results are listed in Tab.3 . From this table it is seen that both, the Young's and shear moduli increase linearly with the SiC content. The Young's modulus follows closely the isostress condition represented by

$$E_{comp} = [E_{Al} \cdot E_{SiC}]/[E_{SiC} \cdot f_{Al} + E_{Al} \cdot f_{SiC}] \qquad (12)$$

where f is the volume fraction of the indicated phase.

The values of the acoustoelastic constants of the metal-matrix composites, determined from the relative changes in the ultrasonic velocity as a function of elastic strain, are the average values of the data obtained by Lee et al. [13] and are listed in Tab.2 . The AECs are reproducible within 2%. From the table, one can see that the values of the AECs of the 7064 alloy are larger than those of the 8091 alloy. Also the AECs for both sets of MMCs decrease as the content of SiC increases. Smaller absolute values of AECs indicate a smaller change in the ultrasonic velocity as a function of elastic strain which means a smaller deviation from the ideal Hookean behavior of the material.

Table 2 : Averaged acoustoelastic constants of the examined MMCs.

Material	Acoustoelastic Constants					
	AEC 22	Δ%	AEC 21	Δ%	AEC 23	Δ%
Al - 8091	1.12	0	-2.59	0	0.87	0
+10% SiC	1.08	-3.7	-2.17	-19.4	0.82	-5.7
+15% SiC	0.92	-17.9	-1.91	-35.6	0.74	-14.9
Al - 7064	1.44	0	-3.10	0	1.93	0
+15% SiC	1.20	-16.7	-2.35	-24.2	1.27	-34.2
+20% SiC	0.88	-38.9	-1.85	-40.3	0.92	-52.3

From the acoustoelastic constants and the second order elastic constants, the third order elastic constants were determined using eq.(6). From an analysis of error propagation the inaccuracy is found to be highest in the Murnaghan constant l and is equal to 15%. The inaccuracies of the constants m and n are 5% and 3% respectively. In general, the values of the Murnaghan constants m and n are not significantly influenced by the content of SiC within the experimental error. The constant m, however, has a tendency towards less negative values, whereas the constant n is showing no trend at all. The Murnaghan constant l changes considerably and even becomes positive when SiC is added. Compared to the elastic moduli μ and E, the third order elastic constants do not show a clear relationship with the content of reinforcement, whereas those of the elastic moduli increase in a predictable manner.

The Murnaghan constants l and m are used to calculate the nonlinearity parameter according to eq.(8) . The values of the calculated nonlinearity parameter are listed in Tab.4 as $\beta_{calc.}$ Also included in Tab.4 are the values of the directly measured nonlinearity parameter as $\beta_{meas.}$ The experimental error is 10% for the calculated and 15% for the measured nonlinearity parameter. For both $\beta_{calc.}$ as well as $\beta_{meas.}$ the values decrease considerably with increasing volume percentages of SiC.

As can be seen from Fig.4, the values of the calculated nonlinearity parameter for the 8091 as well as for the 7064 alloys change linearly as a function of second phase content. The values of the composites with the Al - 8091 matrix appear to be smaller than those of the composites with the Al - 7064 matrix.

Table 3 : Second and third order elastic constants of MMCs.

Material	SOEC [GPa]			TOEC [GPa]		
	λ	μ	E	l	m	n
Al - 8091	42.0	30.1	77.7	-34	-320	-438
+10% SiC	42.8	35.4	91.0	34	-313	-466
+15% SiC	42.4	37.6	95.7	33	-288	-454
Al - 7064	54.1	26.9	71.4	-33	-359	-515
+15% SiC	57.4	35.1	91.5	43	-343	-516
+20% SiC	54.3	38.0	99.2	24	-309	-486

Table 4 : Calculated and directly determined nonlinearity parameter.

Material	βcalc.	Δ%	βmeas.	Δ%
Al - 8091	10.2	0	10.6	0
+10% SiC	7.4	-27.5	8.5	-19.8
+15% SiC	6.2	-39.2	6.9	-34.9
Al - 7064	10.9	0	8.7	0
+15% SiC	7.1	-34.9	6.6	-24.1
+20% SiC	6.2	-43.1	5.8	-33.3

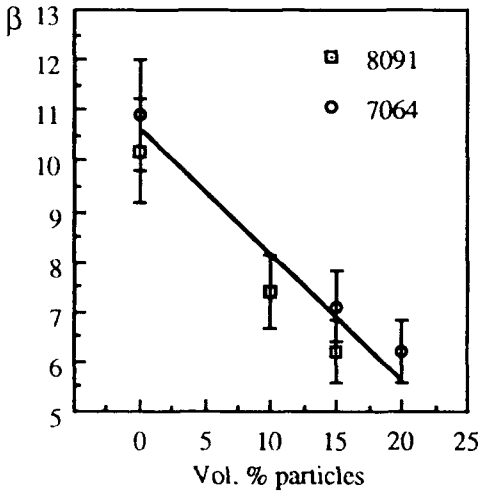

Fig. 4. Calculated nonlinearity parameter as a funtion of particle content

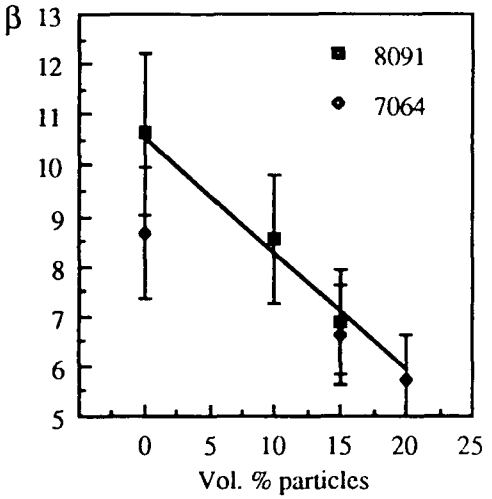

Fig. 5. Measured nonlinearity parameter as a funtion of particle content

A plot of $\beta_{meas.}$ vs. the volume fraction of reinforcement is displayed in Fig.5 . The values of both composites are close to a linear relationship between $\beta_{meas.}$ and the volume fraction of SiC. One value, namely that of the unreinforced 7064 specimen, is clearly deviating from this behavior. Interferences in the backwall echo sequence obtained on this specimen indicate a strong texture in the extrusion direction. Since the nonlinearity parameter varies significantly in different lattice directions of single crystalline materials, a texture is likely to change the value of the nonlinearity parameter.

The lower values for the nonlinearity parameter of SiC reinforced aluminum alloys can be understood from the fact, that ceramic materials with low nonlinearity will lower the nonlinearity parameter of aluminum alloys when a composite is formed. This does not mean that a law of mixture is applicable to model the bulk nonlinearity of a metal-matrix composite. Influences from the interfacial region between matrix and reinforcement are expected to contribute to the nonlinearity of the composite.

Because there is no significant difference between the calculated nonlinearity parameter determined in the isotropic plane and the one directly measured along the extrusion direction, it can be assumed that the nonlinearity parameter depends primarily on the overall content of reinforcement. Influences from the particle alignment in the extrusion direction could not be detected within the accuracy of the measurements.

Theoretical investigations by Cantrell [12] have shown that the nonlinearity parameter is related to the coefficient of thermal expansion (CTE) which is also a nonlinear

quantity. In previous studies [11, 14], the coefficient of thermal expansion in MMCs has been found to decrease with increasing amounts of reinforcement. Measurements of the CTEs of the composites investigated in this paper are in progress.

CONCLUSIONS

The results of this study show that the acoustoelastic constants and the acoustic nonlinearity parameter are influenced by the amount of reinforcement in metal-matrix composites. Therefore, they are promising candidates to characterize the mechanical behavior of MMCs nondestructively. Also, the two quantities clearly indicate a decreasing elastic nonlinearity of the composite with the increasing content of SiC. The nonlinearity parameter changes linearly as a function of second phase content.

The absolute values of the calculated as well as of the directly measured acoustic nonlinearity parameter are in good agreement within the accuracy of the measurements. This shows that both techniques, measurements of absolute amplitudes using the capacitive gap receiver and measurements of the acoustoelastic effect, are suitable methods for the determination of the nonlinearity parameter.

The direct measurement of the nonlinearity parameter using the capacitive gap receiver requires a careful preparation of the specimen surfaces. The measurement of the acoustoelastic effect is restricted to simple specimen geometries since it requires the application of external stresses. The selection between the two methods depends on the geometry condition of the sample.

ACKNOWLEDGEMENT

This work is financially supported by the Army Research Office under contract No. DAAL03-88-K-0096.

REFERENCES

1. Y. Pao, W. Sachse and H. Fukuoka in Physical Acoustics Vol. XVII, Academic Press, 1984
2. J.S. Heyman, S.G. Allison, K. Salama, and S.L. Chu, Symposium on NDE, Applications to Materials Processing, edited by O. Buck and S. Wolf, p. 177, 1983
3. J.H. Cantrell, W.T. Yost, S. Razvi, P. Li and K. Salama, Proc. IEEE Ultrasonics Symposium 1986, p. 1075.
4. K. Brugger, Physical Review, 133 A, p. 1611, 1964
5. J.H. Cantrell, Physical Review, B21, p. 4191, 1980
6. D.M. Egle and D.E. Bray, J. Acoust. Soc. Am. 60, p. 741, 1976
7. M.A. Breazeale and J. Philip in Physical Acoustics Vol. XVII, Academic Press,1984
8. W.B Gauster and M.A. Breazeale, Rev. Sci. Instrum. 37, p. 1544, 1966
9. A.L. Thuras, R.T. Jenkins and H.T. O'Neil, J. Acoust. Soc. Am. 6, p. 173, 1935
10. E.P. Papadakis, J. Acoust. Soc. Am. 52, p. 845 (1972).
11. M.S. Misra and P.D. Lagreca, 6th Annual Discontinuous Reinforced Aluminum Materials Workshop, Park City, Utah, 1984
12. J.H. Cantrell, J. Acoust. Soc. Am. 77, p.47, 1985
13. D.F. Lee, K. Salama and E. Schneider, Proccedings of the 3rd Int. Symp. on Nondestructive Characterization of Materials, 1988
14. B.J. MacLean and M.S. Misra, Mechanical Behavior of Metal Matrix Composites, Conference Proceedings, edited by J.E. Hack and M.F. Amateau, 1983

Acoustoelastic characterisation of materials

J. H. Cantrell and K. Salama

The increasing demand for new, more reliable materials, which are often used in hostile environments, has led to the necessity of establishing equally reliable, quantitative techniques for the non-destructive evaluation (NDE) and characterisation of such materials. Non-destructive evaluation methods are commonly used in applications ranging from materials processing and control to monitoring the effects of environmental degradation and the estimation of remaining useful life of materials. Although linear ultrasonic methods have long been among the most popular and useful of NDE methodologies, this review is concerned with the considerable effort that has been expended recently on understanding, developing, and applying non-linear acoustoelastic techniques. Although applications to complex materials are usually correlative, recent progress in the quantitative modelling of the acoustoelastic properties of multiphase alloys in terms of material composition is also reviewed. Considerable emphasis is placed on understanding the relationship between non-linear acoustoelastic properties and the fundamental atomic structure of simple materials. Such considerations lead to an enhanced understanding of the effect of residual and applied stresses on the acoustoelastic and thermoelastic measurements of metallic alloys. Similar considerations of magnetic domain structure provide an explanation of the effect of stress on the magnetoelastic properties of ferromagnetic materials. Implications of these advances to the non-destructive characterisation and evaluation of materials are discussed. IMR/223

Dr J. H. Cantrell is with NASA Langley Research Center, Hampton, VA, USA and Professor K. Salama is in the Department of Mechanical Engineering, University of Houston, Houston, TX, USA.

List of symbols

a_i	Lagrangian (material) coordinates
A_{ijkl}	Huang coefficients
b	crack half length
B_{ij}	components of Boussinesq stress tensor
C_{ijkl}	Brugger elastic constants
e_i	depletion constants
f	volume fraction of spherical inclusions
f_p	total volume fraction of second phase components
F	inverse of wave propagation time
H, H_i	acoustoelastic constants
H	magnetic field strength
I_s	effective stress intensity factor
k	bulk modulus
k_i	bulk modulus of inclusion
k_m	bulk modulus of matrix
K, K_{ij}	Salama–Ling proportionality constants
K_T	compressibility
l	wave propagation distance
l, m, n	Murnaghan constants
L_{ijkl}	propagation matrix
M_a	components of uniaxial stress direction
N_i	components of unit propagation direction
p	magnitude of uniaxial or hydrostatic stress
S	entropy
S_{ijkl}	compliance coefficients
t	time
t_{ij}	thermodynamic tension
T	temperature
T_{ij}	initial stress tensor
u_i	components of particle displacement vector
u_{ij}	displacement gradient
$\tilde{u}_{ij}$	displacement gradient referred to deformed state
$\langle u_i \rangle$	acoustic radiation induced static displacement
U	internal energy per unit mass
U_i	components of wave polarisation vector
v	true sound velocity
v_1	longitudinal wave true sound velocity
v_2, v_3	shear wave true sound velocity
W	natural sound velocity
W_0	natural sound velocity at zero stress
x_i	components of particle position vector
α_i	direction cosines
α_{ij}	transformation coefficients
α^T_{ij}	thermal strain tensor
α^T	thermal expansivity
β	acoustic non-linearity parameter
$\tilde{\beta}$	acoustic non-linearity parameter for solid s tion
δ_{ij}	Kronecker delta
γ_i	direction cosines
ε_{el}	linear elastic strain
ε_{me}	magnetoelastic strain
η_{ij}	Lagrangian strains
θ	dilatation
$\vec{\kappa}, \kappa_i$	wave propagation vector
λ, μ	Lamé constants
λ_{ij}	thermal stress tensor
λ^m_{abc}	saturation magnetostriction along [abc]
μ	shear modulus
μ_i	shear modulus of inclusion
μ_m	shear modulus of matrix
ν_m	Poisson's ratio of matrix
ξ_1, ξ_2	amplitudes of fundamental and second harmonic waves

ρ average mass density of matrix and inclusion
ρ_i mass density of inclusion
ρ_m mass density of matrix
ρ_0 mass density of material in unperturbed state
σ_{ij} stress tensor
ω angular frequency

Introduction

Ultrasonic methods have long been used to characterise various properties of materials ranging from the fundamental to the most practical applications. Ultrasonic measurements of fundamental material properties, for example, have provided some of the first experimental evidence of the double well interatomic potential in vitreous silica.[1] They have also been used to quantify the superconducting state of materials,[2] and have provided well established methods of testing lattice dynamical theories of the solid state.[3–5] Several recent review articles and monographs,[6–10] highlighting the practical applications of ultrasonic methods, are testimonials to the flexibility and utility of ultrasound in assessing properties of materials from simple crack detection to the characterisation of material microstructure and defect induced changes in elastic properties. Indeed, ultrasonic techniques have become an indispensable tool in the non-destructive characterisation, evaluation, and testing of materials.

The purpose of the present review is to summarise recent developments in non-linear acoustoelasticity that bear directly on the thermoelastic properties, and in appropriate cases on magnetoelastic properties, of multiphase materials. Nonlinear acoustoelasticity entails consideration of the variation in the sound velocity as a function of the state of stress in the material as well as the consideration of acoustic harmonic generation and radiation induced static stresses and strains in the material generated from an initially pure sinusoidal source. In order to emphasise the common basis of these related, but quite distinct, non-linear phenomena the theoretical treatment of each phenomenon is initiated from the same set of generalised wave equations. While it will become apparent that acoustoelastic measurements can be used to determine the effective second and higher order elastic constants as well as various mechanical moduli of materials, the emphasis here is on the parameters associated with and defined from the measurement process itself. These measurement defined acoustoelastic constants and non-linearity parameters offer the most direct route to the characterisation of many important material properties from interatomic potentials to stress fields and the state of fatigue. The connection with fundamental dynamical properties is emphasised throughout this review in an effort to underscore the role of material anharmonicity in acoustoelasticity and thus to provide some link between macroscopic acoustic measurements and the atomic properties of elemental or single phase material. The complexities introduced in measurements of multiphase materials are addressed from a consideration of models giving the effective parameters as a function of total volume fraction of second phase constituents.

A considerable portion of the review is also devoted to the effects of residual and applied stresses on ultrasonic measurements. Indeed, one of the most important problems in the non-destructive characterisation of materials is the determination of residual and applied stresses. Such stresses play a fundamental role, for example, in the corrosion or embrittlement of metals and in crack initiation. Acoustoelastic techniques as a means of characterising such fields have been extensively reviewed elsewhere,[6] and so will not be repeated here. Rather, in keeping with the spirit of this review, the role of stress fields as they affect the thermoelastic and, in ferromagnetic solids, magnetoelastic properties of materials is addressed. In doing so recent advances in stress field assessment not previously considered are presented. In order to clarify the meaning of the various elastic and mechanical moduli from a measurement perspective, the connection between static or low frequency dynamic moduli measurements generally performed in mechanical testing and the second order elastic constants obtained in bulk ultrasonic measurements is given in Appendix 1.

The microstructural variation in acoustic properties has been the key to the development in the past decade of a number of new microscopes which utilise acoustic waves in some fashion for obtaining the microscopic images.[11,12] The images so attained provide information quite different from that obtained in conventional light or electron microscopes. Different types of acoustic microscopes use different energy sources, such as electron beams, lasers, and piezoelectric transducers, for generating the acoustic images and are descriptively named, for example, the scanning electron acoustic microscope, the thermoacoustic microscope, and the scanning acoustic microscope. Although the image contrast and spatial resolution attainable in such microscopes are in large measure dictated by the details of energy source–material interactions, the dependency on the local variations in the material elastic or thermoelastic properties, including residual stresses, is a necessary consideration in such interactions. Indeed, in some cases features directly associated with the residual stress fields can be imaged,[13] revealing even the subtlest influence of thermoelasticity on the contrast mechanisms. The concepts summarised in this review, when combined with an appropriate model of the microscope under consideration, are pertinent to an understanding of many of the contrast mechanisms in the various acoustic microscopes, particularly those involving acoustic bulk wave propagation.

General equations of elastic wave motion

Consider first the adiabatic propagation of an elastic, bulk travelling wave in a lossless solid of

arbitrary crystalline symmetry. The equations of motion (Newton's law) in Lagrangian (material) coordinates a_j are[14] (Einstein summation of repeated indices assumed throughout text)

$$\rho_0 \frac{\partial^2 x_i}{\partial t^2} = \frac{\partial \sigma_{ij}}{\partial a_j} \quad \ldots \quad (1)$$

where x_i are the components of the particle position vector, σ_{ij} are components of the stress tensor, t is time, and ρ_0 is the mass density of the solid in the unperturbed (natural) state. If the stress tensor is defined in terms of Lagrangian strain derivatives of the internal energy per unit mass $U(a_k,\eta_{ks},S)$ where η_{ks} are the Lagrangian strains and S is the entropy, the stress tensor is commonly called the first Piola–Kirchhoff tensor. Formally, the first Piola–Kirchhoff tensor is defined by[15]

$$\sigma_{ij} = \rho_0 \alpha_{ik} \frac{\partial U}{\partial \eta_{jk}} \quad \ldots \quad (2)$$

where α_{ik} are the transformation coefficients defined by

$$\alpha_{ik} = \delta_{ik} + \frac{\partial u_i}{\partial a_k} \quad \ldots \quad (3)$$

In equation (3), δ_{ik} are Kronecker deltas and $u_i = x_i - a_i$ are components of the displacement vector. The Lagrangian strains η_{kl} are defined by[16]

$$\eta_{jk} = (\alpha_{ij}\alpha_{ik} - \delta_{jk})/2 \quad \ldots \quad (4)$$

Many researchers (Brillouin[17] and Born and Huang[18] among others) have preferred to use the Boussinesq stress tensor B_{ij}, which is defined in terms of derivatives of the internal energy per unit mass with respect to the displacement gradient, $(\partial u_i/\partial a_j) = u_{ij}$. Using equations (2)–(4), it is straightforward to show the equivalence of the two stress tensors by writing

$$B_{ij} = \rho_0 \frac{\partial U}{\partial u_{ij}} = \rho_0 \frac{\partial \eta_{kl}}{\partial u_{ij}} \frac{\partial U}{\partial \eta_{kl}} = \rho_0 \alpha_{ik} \frac{\partial U}{\partial \eta_{kj}} = \sigma_{ij} \quad \ldots \quad (5)$$

Another stress tensor of relevance here is the thermodynamic tensions t_{ij} defined by

$$t_{ij} = \rho_0 \frac{\partial U}{\partial \eta_{ij}} \quad \ldots \quad (6)$$

Huang[19] expanded the internal energy per unit mass in terms of the displacement gradients as

$$\rho_0 U = A_{ij} u_{ij} + \frac{1}{2} A_{ijkl} u_{ij} u_{kl} + \frac{1}{3!} A_{ijklmn} u_{ij} u_{ki} u_{mn} + \ldots \quad (7)$$

where $A_{ij}\ldots$ are referred to as the Huang (or propagation) coefficients. Equation (7) serves to define the nth order Huang coefficients as

$$A_{ijkl\ldots} = \rho_0 \left(\frac{\partial^n U}{\partial u_{ij} \partial u_{kl} \ldots} \right)_{\partial u/\partial a = 0} \quad \ldots \quad (8)$$

The relationship between the Huang coefficients and the elastic constants referred to the Lagrangian strain measure $C_{ijkl\ldots}$ was found by Wallace[14] to be

$$\begin{aligned} A_{ij} &= C_{ij} = T_{ij} \\ A_{ijkl} &= T_{jl}\delta_{ik} + C_{ijkl} \\ A_{ijklmn} &= C_{jlmn}\delta_{ik} + C_{jknl}\delta_{im} + C_{ijnl}\delta_{km} + C_{ijklmn} \end{aligned} \quad \ldots \quad (9)$$

The $C_{ijkl\ldots}$ are the nth order elastic coefficients of Brugger[20] defined for adiabatic conditions by the *nth order derivative of the internal energy* per unit mass with respect to the Lagrangian strains

$$C_{ijkl\ldots} = \rho_0 \left(\frac{\partial^n U}{\partial \eta_{ij} \partial \eta_{kl\ldots}} \right)_{\rho=0} \quad \ldots \quad (10)$$

It is clear from equations (6) and (10) that $C_{ij} = T_{ij}$ is the thermodynamic tension evaluated at $\eta = 0$. From equations (5) and (3) we find that $\sigma_{ij} = t_{ij} = C_{ij} = T_{ij}$ when $\partial u/\partial a$, hence η, is zero. The coefficient C_{ij} is thus identified as the initial stress T_{ij} in the solid.

Acoustoelasticity

Traditionally, acoustoelasticity has been viewed as that aspect of material anharmonicity giving rise to the variation in sound velocity as a function of the state of stress in the material. Although acoustoelastic measurements are a popular means of assessing stress fields, the emphasis here is to explore the relationships between acoustoelasticity and certain aspects of material microstructure. In particular, the use of a measurement defined acoustoelastic constant as a material characterisation parameter is considered. Applications of the concepts developed here to two phase materials are also emphasised.

General theory

It is necessary to obtain the elastic wave velocities as a function of applied or residual stress. It is expedient then to expand the stress σ_{ij} in equation (1) about the homogeneously deformed initial state X, i.e.

$$\begin{aligned} \sigma_{ij} &= (\sigma_{ij})_X + \left(\frac{\partial \sigma_{ij}}{\partial u_{kl}} \right)_X \left(\frac{\partial u_k}{\partial a_l} - \frac{\partial \bar{u}_k}{\partial a_l} \right) + \ldots \\ &= (\sigma_{ij})_X + \left(\frac{\partial \sigma_{ij}}{\partial u_{kl}} \right)_X \frac{\partial \tilde{u}_k}{\partial a_l} + \ldots \end{aligned} \quad \ldots \quad (11)$$

where $\tilde{u}_k = u_k - \bar{u}_k$, the overbar represents the value of the parameter referred to the deformed state, and the expansion coefficients are evaluated at the deformed state X. From equations (1), (5), (7), and (11) we thus obtain

$$\rho_0 \frac{\partial^2 x_i}{\partial t^2} = \rho_0 \frac{\partial^2 \tilde{u}_i}{\partial t^2} = \tilde{L}_{ijkl} \frac{\partial^2 \tilde{u}_k}{\partial a_l \partial a_j} \quad \ldots \quad (12)$$

where the propagation matrix

$$\tilde{L}_{ijkl} = \left(\frac{\partial \sigma_{ij}}{\partial u_{kl}} \right)_X = A_{ijkl} + A_{ijklmn}\bar{u}_{mn} + \ldots \quad (13)$$

Assuming wave propagation of the form

$$\tilde{u}_k = U_k \exp i(\omega t - \bar{\kappa} \cdot \bar{a}) \quad \ldots \quad (14)$$

where $\vec{N} = \vec{\kappa}/|\vec{\kappa}|$ is the unit propagation direction and $W = \omega/|\vec{\kappa}|$ is designated[21] as the natural velocity, since it is the velocity referred to the natural state. Substituting equation (14) into equation (12), the set of linear equations for the unit polarisation vector $\vec{U}$ is obtained

$$(\bar{L}_{ijkl}N_jN_l - \rho_0 W^2\delta_{ik})U_k = 0 \quad . \quad . \quad . \quad . \quad (15)$$

Equation (15) is the basic equation of acoustoelasticity. It provides the variation in the sound velocity (here the natural velocity) as a function of applied or residual strain and wave polarisation.

Consider now the rate of change of the square of the natural velocity with respect to the applied stress p (uniaxial or hydrostatic) evaluated at the natural configuration (i.e. where $p = 0$).

$$\left[\frac{\partial(\rho_0 W^2)}{\partial p}\right]_{p=0} = \left[\left(\frac{\partial \bar{t}_{ab}}{\partial p}\right)\left(\frac{\partial \bar{\eta}_{pq}}{\partial \bar{t}_{ab}}\right)\left(\frac{\partial \bar{u}_{rs}}{\partial \bar{\eta}_{pq}}\right) \times \left(\frac{\partial(\rho_0 W^2)}{\partial \bar{u}_{rs}}\right)\right]_{p=0}$$

$$= \left(\frac{\partial \bar{t}_{ab}}{\partial p}\right)_{p=0} S_{rsab}\left[\frac{\partial(\rho_0 W^2)}{\partial \bar{u}_{rs}}\right]_{p=0} \quad . \quad . \quad . \quad . \quad . \quad . \quad . \quad (16)$$

where $S_{rsab} = (\partial \eta_{rs}/\partial \bar{t}_{ab})_{p=0}$ are the isothermal compliance coefficients. For applied hydrostatic pressure or uniaxial compression of magnitude p in the direction $\vec{M}$

$$\left(\frac{\partial \bar{t}_{ab}}{\partial p}\right)_{p=0} = \left\{\begin{array}{l} -\delta_{ab} \text{ for hydrostatic pressure} \\ -M_aM_b \text{ for uniaxial compression} \end{array}\right\} \quad (17)$$

Substituting equations (9), (13), and (15) (for the natural state) into equation (16) gives the equations of Thurston and Brugger[21]

$$\left[\frac{\partial(\rho_0 W^2)}{\partial p}\right]_{p=0} = \left(\frac{\partial \bar{t}_{ab}}{\partial p}\right)_{p=0} \times [N_aN_b + U_jU_k(2\rho_0 W_0^2 S_{jkab} + N_rN_sS_{ipab}C_{jrksip})] \quad . \quad . \quad (18)$$

where

$$(\rho_0 W^2)_{p=0} = (\rho_0 W_0^2) = C_{mrns}N_rN_sU_mU_n \quad (19)$$

Equations (18) and (19), derived for solids of arbitrary crystalline symmetry, specifically show the dependence of the natural velocity and the change of natural velocity with stress in terms of the second and third order elastic constants of the solid. From the experimental measurements of natural velocity as a function of stress the equations suggest that one can determine the second and third order elastic constants of the material. Indeed, calculation of the elastic constants from such measurements have become quite well established.[3,8,21] There are, in general, 81 second order elastic constants and 729 third order elastic constants. For solids of lowest crystalline symmetry (triclinic crystal system) this number reduces to 21 independent second order elastic constants and 56 independent third order elastic constants. For higher symmetries the number of independent constants are even further reduced. For example, the independent elastic constants reduce to 3 second order and 6 third order constants for cubic crystals of highest symmetry and for isotropic solids (the highest attainable symmetry) the numbers are 2 second order and 3 third order elastic constants.

For isotropic solids the second order constants often used in the literature are the Lamé constants λ and μ and the third order constants are often the Murnaghan constants l, m, and n. These constants are related to the Brugger elastic constants $C_{ijkl...}$ for isotropic solids as[8]

$$\begin{aligned} \lambda + 2\mu &= C_{11} = C_{22} = C_{33} \\ \lambda &= C_{12} = C_{13} = C_{23} = C_{21} = C_{31} = C_{32} \\ \mu &= C_{44} = C_{55} = C_{66} \\ 2l + 4m &= C_{111} \\ 2l - 2m + n &= C_{123} \\ m - n/2 &= C_{144} \\ l &= C_{112}/2 \\ m &= C_{155} \\ n &= 4C_{456} \end{aligned} \quad . \quad . \quad . \quad . \quad . \quad . \quad . \quad . \quad . \quad . \quad (20)$$

where all other second and third order elastic constants are zero. Voigt notation is used in the above equations for the Brugger elastic constants whereby the single subscript k replaces the subscripted pair (i,j) according to the following scheme:

$i, j =$	11	22	33	32 or 23	31 or 13	21 or 12
$k =$	1	2	3	4	5	6

In a typical ultrasonic experiment, one generally measures as a function of applied stress the variation in time required for a generated plane wave front to propagate between parallel sample surfaces. An inverse measure of that propagation time is the parameter F defined by

$$F = l^{-1}v \quad . \quad . \quad . \quad . \quad . \quad . \quad . \quad . \quad . \quad . \quad (21)$$

where v is the true sound velocity and l is the propagation distance in the sample in the homogeneously deformed state. Thurston and Brugger[21] have shown that the true velocity is related to the velocity referred to the natural state W by

$$v = l_0^{-1}lW \quad . \quad . \quad . \quad . \quad . \quad . \quad . \quad . \quad . \quad . \quad (22)$$

where l_0 is the propagation distance in the undeformed sample. From equations (18) and (22) and an expansion of $(l_0^{-1}l)$ in terms of the Lagrangian strains,[22] one can obtain the expressions of Hughes and Kelly[23] derived from isotropic solids which relate the true sound velocity to the applied stress σ. Their expressions, for example, for axial stress applied in a direction perpendicular to the wave

propagation direction are

$$\rho_0 v_1^2 = \lambda + 2\mu - \frac{\sigma}{3k_0}\left[2l - \frac{2\lambda}{\mu}(m + \lambda + 2\mu)\right]$$

$$\rho_0 v_2^2 = \mu - \frac{\sigma}{3k_0}\left[m + \frac{\lambda n}{4\mu} + \lambda + 2\mu\right]$$

$$\rho_0 v_3^2 = \mu - \frac{\sigma}{3k_0}\left[m - \frac{\lambda + \mu}{2\mu}n - 2\lambda\right] \quad . \quad . \quad (23)$$

where v_1 is the longitudinal velocity and v_2 and v_3 are the velocities of shear waves when the polarisation direction is parallel to and perpendicular to that of stress, respectively.

There is advantage, however, in measuring changes in the natural velocity as a function of applied stress, since such measurements are obtained from time measurements in the deformed state but the length measurements are referred to the undeformed length of the solid. This is seen by substituting equation (21) into equation (22) to get

$$F = l_0^{-1} W \quad . \quad . \quad . \quad . \quad . \quad . \quad . \quad . \quad . \quad . \quad (24)$$

From equation (24)

$$H = \frac{1}{F}\frac{\partial F}{\partial p} = \frac{1}{W}\frac{\partial W}{\partial p} = \frac{1}{2\rho_0 W^2}\frac{\partial(\rho W^2)}{\partial p} \quad (25)$$

When evaluated at $p = 0$, it has become popular to refer to H as the 'stress acoustic constant' or the 'acoustoelastic' constant. It is clearly a material parameter, since it depends on the second and third order elastic constants of the material. Cantrell[22] has determined the general relationship between the fractional change in the natural velocity with respect to stress for a wave of polarisation $\bar{U}$ propagating along $\bar{N}$, i.e. the generalised acoustoelastic constant $H_{uv}(\bar{U},\bar{N})$, and the fractional change in the true velocity v to be

$$H_{uv}(\bar{U},\bar{N}) = \left(\frac{1}{v}\frac{\partial v}{\partial \eta_{rs}} - N_r V_s\right) S_{rsuv} \quad . \quad . \quad (26)$$

where η_{rs} are the Lagrangian strains resulting from the imposed stress, and S_{rsuv} are the compliance coefficients. For acoustic wave propagation perpendicular to the direction of applied stress in isotropic solids, equation (26) shows that acoustoelastic constants are also equal to the fractional change in the true velocity with respect to the applied stress. For acoustic longitudinal wave propagation along the direction of applied stress in such solids, the fractional variations in the true and natural velocities differ by an additive constant.

The exact meaning of the experimental parameter F in equation (25) depends on the particular experimental technique. For example, if one uses a resonance or resonance derived technique, then F is the acoustic standing-wave resonance frequency f. If one uses a pulse coincidence technique, then F is the inverse pulse repetition rate. It is important to emphasise that all the above equations specifically refer to acoustic bulk wave propagation in materials. The elastic moduli or constants used to quantify this wave propagation are constants referred to unbounded or bulk solids and accurately represent acoustic wave propagation when the dimensions of the sample are generally large compared with an acoustic wavelength. Such elastic constants, however, are quantitatively related to the elastic or mechanical moduli typically obtained from static engineering measurements or low frequency dynamic measurements as shown in Appendix 1.

In general, for a given combination of stress, propagation, and polarisation directions, the relationship between the natural sound velocity and stress may be obtained by integrating equation (25) to get

$$\bar{W}(\sigma) = W_0 + W_0 H\sigma \quad . \quad . \quad . \quad . \quad . \quad . \quad . \quad (27)$$

where $W_0 = \bar{W}(0)$, the natural velocity at zero stress. As suggested by equation (27) unknown stresses can be determined when both the natural velocity in the absence of stress and the acoustoelastic constant are known independently. This approach was first used by Crecraft,[24] who showed that acoustoelasticity could be used as a practical method for determining applied and residual stresses in engineering materials. Theoretically, one could calculate the acoustoelastic constants from equations (18), (19), and (25) if the second and third order elastic constants are known. Unfortunately, measurements of the third order elastic constants have been performed mostly on pure materials and some simple alloys. Indeed, the technique mostly used for such measurements have been that of determining the stress dependence of the natural velocity, i.e. the acoustoelastic constant of the material. It is important to point out here that the measured velocity and stress dependent velocity changes in engineering materials depend strongly on microstructural features which make it necessary to perform a calibration between velocity and stress (i.e. determine the acoustoelastic constant) for each material in order for the method to be used in the determination of unknown stresses. Microhomogeneity, texture, and weak anisotropy of the material, which are usually neglected in engineering applications of the theory of elasticity, cannot be neglected in the applications of acoustoelasticity. Results by Smith *et al.*[25] show that third order elastic constants for polycrystalline materials can differ widely, even for alloys having the same composition. For structural aluminium of slightly different composition differences as large as 50% are observed.

Models of two phase systems

Most experimental measurements of the acoustoelastic constants have been performed either on simple, single phase materials or on complex, multiphase materials that have been treated as single phase materials. It is important to recognise that in quantitatively characterising complex materials one must also understand the effects of material composition on the measured acoustic parameters. In order to calculate the acoustoelastic constant in a two phase alloy, Salama *et al.*[26]

assume that the precipitates in the alloy can be represented by a dilute suspension of spherical particles in an infinite solid solution matrix. The physical meaning of this idealisation is that the precipitates are so small and so far apart that all the interactions between them can be neglected, no matter what the size of the representative volume may be. The effective elastic constants of such materials have been calculated by Christensen[27] using the energy methods approach and Eshelby's formula[28] for the calculation of strain energy in systems containing inhomogeneities. For a dilute concentration of inclusion i, Christensen found that the effective shear and bulk moduli μ and k are related to those of the matrix as

$$\frac{\mu}{\mu_m} = 1 - \frac{15(1-\nu_m)[1-(\mu_i/\mu_m)]f}{(7-5\nu_m)+2(4-5\nu_m)(\mu_i/\mu_m)} \qquad (28)$$

and

$$\frac{k}{k_m} = 1 - \frac{[1-(k_i/k_m)]f}{1+[(k_i-k_m)/(k_m+4\mu_m/3)} \qquad (29)$$

where the subscripts m and i, respectively, denote matrix and inclusion, f is the volume fraction of the spherical inclusions under dilute conditions, and ν_m is Poisson's ratio of the matrix. The ultrasonic longitudinal velocity v_l is related to the elastic moduli μ and k as[9]

$$\rho v_l^2 = k + 4\mu/3 \qquad (30)$$

where ρ is the average mass density of the medium (matrix plus inclusions).

Case 1

For an inclusion with elastic moduli not too different from those of the matrix, such that $\mu_i \approx \mu_m$ and $k_i \approx k_m$, but $\mu_i - \mu_m \neq 0$ and $k_i - k_m \neq 0$, equations (28) and (29), respectively, become

$$\mu_i = \mu_m + (\mu_i - \mu_m)f \qquad (31)$$

and

$$k = k_m + (k_i - k_m)f \qquad (32)$$

Equations (31) and (32) indicate that the elastic moduli of a two phase material is a function of the inclusion concentration as well as the difference between the corresponding constants of the inclusion and matrix. Substituting equations (31) and (32) into equation (30) gives for the longitudinal velocities

$$\rho v_l^2 = \rho_m(v_l^2)_m - f[\rho_m(v_l^2)_m - \rho_i(v_l^2)_i] \qquad (33)$$

For alloys containing dilute concentrations of precipitates, $\rho = \rho_m$ and equation (33) can be written as

$$v_l^2 = (v_l^2)_m - f\left[(v_l^2)_m - \frac{\rho_i}{\rho}(v_l^2)_i\right] \qquad (34)$$

Equation (34) indicates that the longitudinal velocity in the two phase alloy increases or decreases from that of the solid solution phase according to whether the density of the precipitates is respectively higher or lower than that of the solid solution phase, since the difference between the longitudinal velocities in the precipitates and the solid solution is usually small.

Consider the application of a uniaxial stress in a direction perpendicular to that of the longitudinal wave propagation direction. Differentiating equation (34) with respect to stress σ and assuming that in the dilute approximation $(v_l)_m = v_l$ and that, tenuously, the densities of the two phases present remain roughly unchanged with stress variations, the fractional change in ultrasonic velocity in the two phase material is estimated as

$$\frac{1}{W_l}\left(\frac{dW_l}{d\sigma}\right) = \frac{1}{v_l}\left(\frac{dv_l}{d\sigma}\right)$$
$$= (1-f)\left[\left(\frac{1}{v_l}\right)_m\left(\frac{d(v_l)_m}{d\sigma}\right)\right]$$
$$+ f\left(\frac{\rho_i(v_l^2)_i}{\rho_m(v_l^2)_m}\right)_m\left[\left(\frac{1}{v_l}\right)_i\left(\frac{d(v_l)_i}{d\sigma}\right)\right] \qquad (35)$$

From the definition of the acoustoelastic constant, equation (25), it is concluded from equation (35) that the change in the effective longitudinal wave acoustoelastic constant for the two phase system caused by the presence of precipitates is linearly proportional to the volume concentration of the inclusion and depends on the elastic moduli of the precipitates and the solid solution phases, as well as their stress dependences. These latter quantities are generally unavailable and make the calculations of the effective acoustoelastic constants rather difficult.

Case 2

When the elastic moduli of the precipitate are much greater than those of the matrix, i.e. $\mu_i \gg \mu_m$ and $k_i \gg k_m$, equations (28) and (29) become, respectively

$$\mu = \mu_m + \mu_m\frac{15(1-\nu_m)f}{2(4-5\nu_m)} \qquad (36)$$

and

$$k = k_m + (k_m + 4\mu_m/3)f \qquad (37)$$

These equations indicate that the effective shear and bulk moduli of the two phase alloy system do not depend on those of the precipitates; however, they vary linearly with their concentrations. Substituting equations (36) and (37) into equation (30) and considering $v_l = v_2[2(1-\nu)]^{1/2}$, where v_2 is the shear wave velocity, we obtain in the dilute approximation that

$$(1-f)v_l^2 = (v_l^2)_m + \frac{3(3-5\nu_m)}{(4-5\nu_m)}f(v_l^2)_m \qquad (38)$$

Again in order to obtain an expression for the effective acoustoelastic constant in alloys containing precipitates with elastic moduli much higher than those of the solid solution, equation (38) is differentiated with respect to the stress σ, again under the condition that the stress is applied in a direction perpendicular to the wave propagation direction.

Under such conditions and considering the relationship between the longitudinal and shear wave velocities, $v_l^2 = v_s^2[2(1-\nu)/(1-2\nu)]$, the relative change in the effective longitudinal wave acoustoelastic constants H_l is given as

$$\frac{(H_l)_m - H_l}{H_l} = fB_m\left[\frac{(H_l)_m - (H_2)_m}{(H^2)}\right] \quad \ldots \quad (39)$$

where

$$B_m = \frac{15(1-\nu_m)(1-2\nu_m)}{(4-5\nu_m)^2} \quad \ldots \quad (40)$$

and where $(H_2)_m$ is the shear wave acoustoelastic constant and $(H_l)_m$ is the longitudinal wave acoustoelastic constant of the matrix material. Equation (39) indicates that the relative change in the effective longitudinal acoustoelastic constant H_l of a two phase material is linearly proportional to the volume fraction of the dilute second phase. The constant of proportionality depends on the Poisson's ratio of the solid solution phase and the relative difference between longitudinal and shear wave acoustoelastic constants. Comparison of the theoretical models with experimental results is presented in the section on 'Experimental results' below, but first techniques for measuring the acoustoelastic constants are briefly discussed.

Measurement techniques

The ultrasonic measurement techniques generally used in the determination of acoustoelastic constants are based on the propagation of continuous waves (CW), radiofrequency (rf) bursts (tonebursts), or broadband pulses in the medium of interest. Comprehensive descriptions of these techniques have been given in several review articles and monographs, e.g. McSkimin,[29] Truell *et al.*,[30] Papadakis,[31] Breazeale *et al.*,[32] and Ratcliff.[33] In view of the extensive review literature on acoustoelastic measurement methodology details are not given here, but it is pointed out that the techniques generally are based on measured parameters that are ultimately referred to a time standard. The specific technique may utilise a standing-wave pattern, a pulse coincidence or pulse overlap scheme in which a certain phase relationship among the pulses is maintained, or even a hybrid of the above. In any case the measurement parameter of interest is generally a frequency or the inverse of a pulse repetition rate which is measured as a function of the impressed strain or stress in the material.

Experimental results

In order to study the sensitivity of acoustoelastic constants to changes in microstructure, Heyman *et al.*[34] measured the acoustoelastic constants in the four carbon steels AISI 1020, AISI 1045, AISI 1095, and ASTM 533B. In steel alloys, carbon in excess of the solubility limit (0·02 wt-%) forms a second phase, namely iron carbide (cementite), which precipitates from the solid α-ferrite. Compared with ferrite, cementite is very hard and its presence within the ferrite increases the strength of the steel. Table 1 lists the values of the acoustoelastic constants and the longitudinal wave velocities obtained for these steels. Also included in the table are the volume fraction of second phase precipitates in these alloys and the percentage changes in the acoustoelastic constants with respect to those of the 100% solid solution. The latter are obtained by extrapolating the experimental values of the acoustoelastic constants to 100% solid solution. The relative variations in the acoustoelastic constants as a function of volume fraction of precipitates are plotted in Fig. 1, which shows that the acoustoelastic constant decreases linearly as the amount of carbide (cementite) phase is increased in the alloy. In this study the amount of carbide phase is calculated using the lever rule and the nominal carbon content in the alloy. These results were also confirmed by Allison *et al.*[35] where the acoustoelastic constants in the four steels AISI 1016, AISI 1045, AISI 1095, and AISI 8620 are found to decrease linearly with the increase of the carbide phase.

More recently Schneider *et al.*[36] studied the relationship between the acoustoelastic constants and percentage of precipitates in the five aluminium alloys 1100, 3003, 5052, 6061, and 2024. Aluminium alloys that contain small percentages of other elements such as copper, magnesium, and silicon

Table 1 Variations of acoustoelastic constants and longitudinal ultrasonic velocities with volume fraction of compound precipitates in carbon steels and heat treatable aluminium alloys

Alloy	Volume fraction of precipitates, %	Velocity, m s^{-1}	Acoustoelastic constant, GPa	Change in ascoustoelastic constant, %
Steel				
100% ferrite	0	...	440*	0
AISI 1020	3·1	5889	418	5·0
ASTM 533B	3·9	5880	410	6·8
AISI 1045	7·3	5883	375	14·8
AISI 1095	14·7	5910	325	26·1
Aluminium				
100% solid solution	0	...	83*	0
6061–T6 (Al–Mg–Si)	3·0	6112	79	4·8
2024–T351 (Al–Cu)	5·9	6153	74·7	10·0

* From extrapolation of acoustoelastic constants *v.* volume fraction

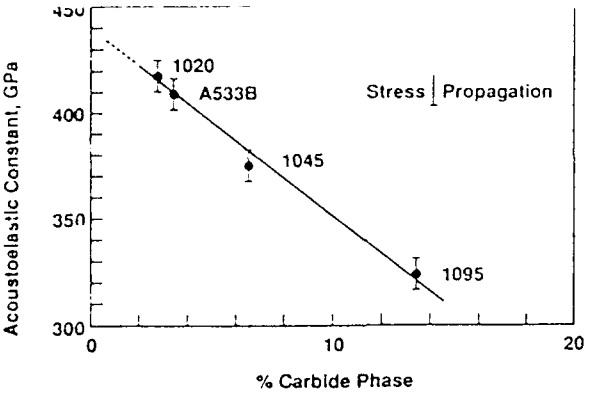

1 Graph of acoustoelastic constant of carbon steel as function of volume percent carbide (cementite) phase

form intermetallic precipitates such as $CuAl_2$, $CuMgAl_2$, and Mg_2Si. These precipitates are very hard and cause the strengthening of the aluminium alloy. Some values of the acoustoelastic constants and the longitudinal wave velocities are also given in Table 1. The results of this study, shown in Fig. 2, reveal that the acoustoelastic constants in the heat treatable alloys 6061 and 2024 decrease as a function of the second phase precipitates. The behaviour in the work hardenable alloys 1100, 3003, and 5052, however, is opposite, i.e. the acoustoelastic constants increase with the increase of percentage of precipitates.

A plot of the acoustoelastic constant as function of aging time in aluminium alloys is shown in Fig. 3. The results indicate that the acoustoelastic constant does not change significantly with aging time, although the average size of the precipitate particles are expected to change.[37] It is thus inferred that the acoustoelastic constant is not significantly influenced by changes in the size and distribution of second phase precipitate particles, at least of the size represented in the figure.

Equations (35) and (39) obtained above represent the changes in the acoustoelastic constants when a second phase precipitate is in equilibrium with a solid phase. By considering that the changes

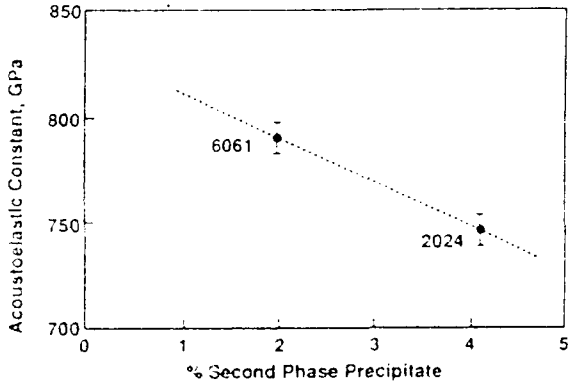

2 Graph of acoustoelastic constant of heat treatable Al alloy 6061 (Al–Mg–Si) and 2024 (Al–Cu) as function of volume fraction of second phase precipitates

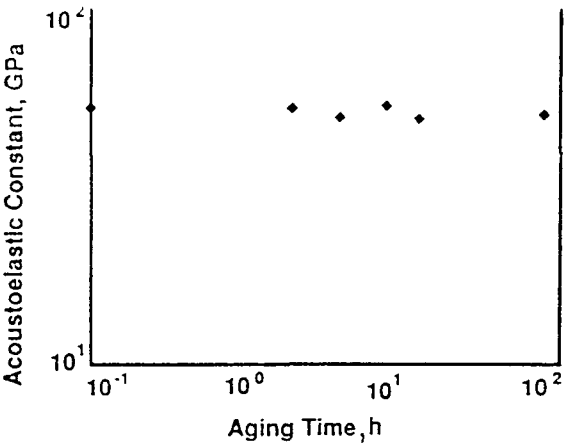

3 Graph of acoustoelastic constant of aluminium alloys as function of aging time

in the acoustoelastic constants of carbon steels measured by Heyman *et al.*[34] and by Allison *et al.*,[35] and of the aluminium alloys 6061–T6 and 2024–T351 measured by Schneider *et al.*[36] are due only to the presence of precipitates in the solid solution phase, a comparison between theory and experiment can be made. Further, since the precipitates in both systems investigated are of higher rigidity than those of the solid solution phase, equation (39) is considered to be a better representation of the experimental data.

Figures 1 and 2 indicate that the relative changes in the acoustoelastic constants for the longitudinal waves vary linearly with the volume fraction of second phase, as predicted by equation (39). The figures also show that the constant of proportionality between the relative changes of the acoustoelastic constants and the volume fraction of second phase in the steel and aluminium systems are the same and approximately equal to 1·8. This means that the acoustoelastic constants in these alloys can be calculated empirically using the values of this quantity in the 100% solid solution material and the volume fraction of second phase in the alloy. This acoustoelastic constant is the proper value to be used in the residual stress determination of the alloy.

Considerable research effort has been devoted in recent years to the development of metal matrix composites. The non-destructive characterisation of the elastic and anelastic behaviour of such materials is essential to their manufacturing processes. The effects on the measured elastic properties of variations in the volume fraction of second phase SiC particles in a number of aluminium alloy matrices have been reported.[38–40] Of particular interest here are the measured values of the acoustoelastic constants as a function of the volume percent SiC in the matrix. A typical data set is shown in Fig. 4 for SiC particles in a 7064 aluminium alloy matrix. The relationship between the acoustoelastic constant and the percent SiC is seen to be approximately linear up to roughly 10% volume fraction. This behaviour is a nominal agreement with equation (39) and thus indicates

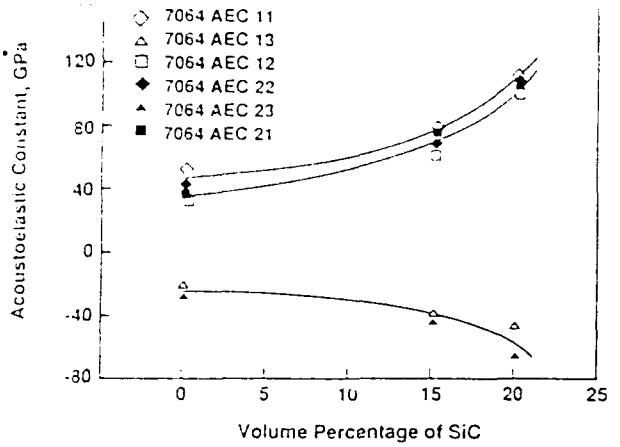

4 Graph of acoustoelastic constant as function of volume percent SiC particles in 7064 (Al–Zn–Mg)

that up to 10% volume fraction, the SiC particles are considered to be of dilute concentration in the aluminium matrix. Thereafter, the curve rapidly becomes non-linear.

Non-linear wave propagation

A further aspect of acoustoelasticity is the distortion of an acoustic waveform as it propagates through a material. Such distortion is another manifestation of the same material interatomic anharmonicity that governs the stress dependence of the sound velocity, but it results from a rather different mechanism involving self-induced stress fields. The quantitative measure of such non-linear wave propagation is the acoustic non-linearity parameter β. It, like the acoustoelastic constant, is found to be a very useful parameter for assessing material properties.

General theory

Consider the solid to be in the natural state, i.e. $T_{ij} = 0$. Substituting equations (5) and (7), into equation (1) and retaining first order non-linear terms gives

$$\rho_0 \frac{\partial^2 u_i}{\partial t^2} = \left[A_{ijkl} + A_{ijklmn} \frac{\partial u_m}{\partial a_n} \right] \frac{\partial^2 u_k}{\partial a_j \partial a_l} \qquad (41)$$

The self-resonant or mutual resonant solution to equation (41) assuming the boundary condition

$$u_i = \xi U_i \cos\omega t \quad \text{at } a = 0 \qquad (42)$$

is to a first order in the non-linearity[14]

$$u_i = \langle u_i \rangle + \xi_1 U_i \cos(\omega t - \vec{\kappa} \cdot \vec{a}) + \beta \xi_1^2 \kappa^2 l U_i \cos(2\omega t - 2\vec{\kappa} \cdot \vec{a})/8 + \ldots \qquad (43)$$

where l is the distance of wave propagation and β is the non-linearity parameter defined by[41]

$$\beta = -\frac{A_{ijklpq} N_i N_j N_l U_i U_k U_p}{A_{ijkl} N_j N_l U_i U_k} \qquad (44)$$

Just as in the case of the acoustoelastic coefficient, the non-linearity parameter is seen from equations (9) and (44) to depend on the second and third order elastic constants of the material, and the directions of wave propagation and polarisation.

The term $\langle u_i \rangle$ in equation (43) is a constant that represents a static or dc displacement arising from the non-linearity of the material. The magnitude of the static displacement has been the source of some controversy which has been recently resolved by Cantrell *et al.*[42,43] They showed that the static displacement is intrinsically linked with the existence of a non-zero acoustic radiation stress in the solid which when properly included in the perturbation solution to equation (41) yields the value

$$\langle u_i \rangle = \beta \xi_1^2 \kappa^2 l U_i / 8 \qquad (45)$$

The sign of the static displacement is governed by the sign of the non-linearity parameter. For pure mode acoustic wave propagation directions the sign of the non-linearity parameter is typically positive and according to equation (45) leads to a radiation induced static dilation in the solid within the spatial extent of the acoustic wave. A negative non-linearity parameter, on the other hand, gives rise to a radiation induced static contraction. This phenomenon has been confirmed in single crystal silicon,[43,44] germanium,[45] and vitreous silica.[44]

Measurement technique

Equation (43) indicates that the acoustic non-linearity parameters may be obtained either from measurements of the absolute amplitudes of the fundamental acoustic wave and generated second harmonic wave or from measurements of the fundamental and static displacement signals. Specifically, if ξ_1 and ξ_2 are the measured amplitudes of the fundamental and second harmonic signals, then the non-linearity parameter β is determined by

$$\beta = 8 \frac{\xi_2}{\kappa^2 \xi_1^2 l} \qquad (46)$$

A block diagram of the equipment arrangement typically used in non-linearity parameter measurements is shown in Fig. 5. The diagram shows the setup for both the harmonic generation and the static displacement techniques. A rf signal (typically in the range 5–30 MHz) from a CW oscillator is combined in a mixer with a gating pulse from a logic and timing generator. The rf pulse is amplified by a broadband linear rf power amplifier and is used to drive a narrow band lithium niobate transducer bonded to one end of a cylindrical sample. The transducer generates a gated ultrasonic signal or toneburst which propagates through the sample. The toneburst is received by a broadband air-gap capacitive transducer at the opposite end of the sample.

The capacitive transducer is a parallel plate arrangement in which the sample end surface functions as the ground plate. The other plate is an optically flat electrode which is recessed approximately 7 μm from the sample surface. A dc bias (typically 50–150 V) is applied through a 1 MΩ resistor to the electrode. Gauster and Breazeale[46]

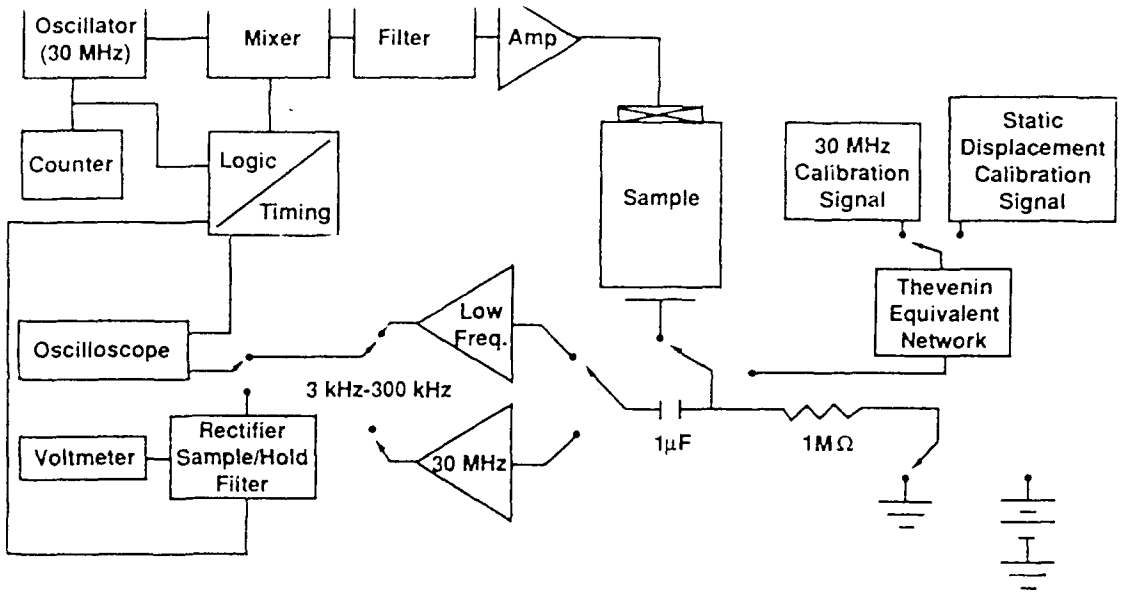

5 Block diagram of typical equipment arrangement for measurements of acoustic non-linearity parameters

have shown that the measurement of the output voltage from such a capacitive arrangement may be converted to a displacement measurement of the sample surface using the relation

$$V_d = V_b(u/s) \quad \ldots\ldots\ldots\ldots \quad (47)$$

where V_d is the output voltage, V_b the dc bias voltage, u the displacement of the sample surface, and s the gap spacing between the capacitor plates. Yost and Breazeale[47] have shown that the capacitive transducer is capable of measuring displacement amplitudes of the order 10^{-16} m, which is quite adequate for measurements in the range 10^{-13}–10^{-10} m representing typical amplitudes of second harmonic and static displacement signals.

The displacement amplitudes of the fundamental and harmonically generated toneburst are obtained by switching the output of the capacitive transducer into the appropriate (preferably narrow band if) preamplifier. The output of the preamplifier is sent into a rectifier and filter assembly which converts the toneburst into a detected signal. The output of the sample and hold is measured by a voltmeter and recorded. The capacitive transducer is now switched out and a Thevenin equivalent network is switched into the circuit. A substitutional calibration signal corresponding to either the fundamental or harmonically generated signal, as the case may be, is now switched into the Thevenin equivalent network and adjusted in amplitude until the voltmeter connected to the sample and hold reads the same value as that of the ultrasonic toneburst measurement. Since the amplitude of the calibration signal is measured at the input to the Thevenin equivalent network, the measured value is equal to the signal produced by the capacitive transducer.

In order to display the acoustic radiation induced static displacement pulse the output of the capacitive transducer is connected to a low frequency (of order 3–300 kHz) preamplifier by a short, low capacitance lead. The output of the preamplifier is sent to an oscilloscope where the static displacement signal is displayed. A template is placed over the screen to record the static displacement shape. The shape of the static displacement signal is that of a right angled triangle whose slope is equal to the right-hand side of equation (45) with $l = 1$. Calculation of the non-linearity parameter is obtained from measurements of the slope and the fundamental amplitude ξ_1.

Acoustic non-linearity parameters and material properties

The acoustic non-linearity parameters β play a central role in determining the thermoelastic properties of crystalline solids, since they directly quantify the anharmonic character of the lattice modes. Cantrell[48] has shown that if one considers a crystalline solid to consist of a large number of incoherent non-linear acoustic radiation sources identified with the vibrating particles of the lattice, then randomisation of the resulting acoustic field together with the assumption of a stochastically independent, fluctuating radiation field at the absolute zero of temperature leads to an expression of the temperature dependent radiation field in terms of the zero point field. This leads directly to expressions of the thermodynamic state functions that intrinsically include the non-linearity parameters as a direct measure of structure dependent modal anharmonicity. These 'non-linear' state functions in turn lead to calculations of the temperature dependence of elastic moduli[49] as well as to calculations of the thermal expansion coefficients[48] directly in terms of the non-linearity parameters.

The relationship between the non-linearity

Table 2 Comparison of structure, bonding, and acoustic non-linearity parameters along [100] direction of cubic crystals

Structure	Bonding	β_{av}	Range of β
NaCl	Ionic	14·6	14·0–15·4
bcc	Metallic	8·2	7·4–8·8
fcc (inert gas)	van der Waals	6·4	5·8–7·0
fcc	Metallic	5·6	4·0–7·0
Fluorite	Ionic	3·8	3·4–4·6
Zinc blende	Covalent	2·2	1·8–3·0

parameters and fundamental lattice properties is intrinsic. Cantrell[50] has shown from a survey of crystals of cubic symmetry that for a given acoustic mode (i.e. direction of acoustic wave propagation and polarisation) the non-linearity parameters are found to be ordered according to the crystalline structure. Results for wave propagation along the [100] direction in cubic crystals are given in Table 2. Listed in the table are the structure of the crystal, the type of atomic bonding, the range of values of β for all crystals having a given structure, and the average values of the βs in that range. The acoustic non-linearity parameters are seen to be strongly ordered according to the type of crystalline structure. The range of values of β for a given structure is distinct; overlap of ranges occurs only slightly for fcc and fluorite structures. The influence of the type of atomic bonding may be inferred from a comparison of the fcc structured crystals. The βs for the fcc metallic bonded crystals and the fcc van der Waals bonded crystals are approximately equal even though the difference in strength of these bonds is very large. It is inferred that the influence of the bonding on the value of the non-linearity parameter is small compared with that of the geometrical arrangement of atoms defining the structure.

In order to explain these results Cantrell,[51] following an approach suggested by Ghate[52] and by Hiki and Granato,[53] proposed a model based in first approximation on a short range, two body, central force potential of the Born–Mayer type. He showed that the non-linearity parameters depend only on the atomic arrangement of the crystal and the 'hardness' parameter of the Born–Mayer potential. He also found that the hardness parameter together with the atomic nearest neighbour separation distance determines the shape or curvature of the potential curve. The dependence on the shape, rather than the magnitude, of the potential curve provides a general explanation of the results of Table 2 including the insensitivity of the acoustic non-linearity parameters to the bond strength.

While the model successfully explains the results of Table 2 for crystalline solids, it does not readily predict the sign and magnitude of the non-linearity parameter for vitreous silica, an amorphous solid. The β parameter for vitreous silica is negative[54] in contrast to the positive values of the parameter typically measured for the pure mode propagation directions in crystalline solids. In addition, Yost and Cantrell[54] have observed what they believe to be the degeneration of an acoustic radiation induced static displacement pulse, $\langle u_i \rangle$ in equation (43), into a series of bulk solitons in samples of vitreous silica. The large negative non-linearity parameter gives rise to a contractive static pulse in the material which when combined with the large velocity dispersion in the medium provides conditions suitable for the generation of solitary waves or solitons. The observations of bulk solitons and acoustic radiation induced static contraction in vitreous silica may be of some significance in the statistical mechanical treatment of amorphous structures,[55] a subject of considerable current interest. Vitreous silica is known to have a negative thermal expansion coefficient at low temperatures where long wavelength vibrational modes dominate the dynamical properties. At higher temperatures, where the expansivity is positive, the short wavelength vibrational modes become more populated and the lattice dynamics is dominated by a local quartz-like structure having positive non-linearity parameters along the pure mode propagation directions. The sign of the thermal expansivity at high and low temperatures is thus reflected in the sign of the non-linearity parameters appropriate to the atomic structure 'seen' by the dominate lattice vibrational mode at that temperature.

The significance of atomic structure and its effect on the non-linearity parameter is not diminished in considerations of complex materials. Material microstructure is governed fundamentally by even more complicated arrangements of atoms, including random or amorphous-like configurations in many cases, which also affect the non-linearity parameter. Of particular concern here, however, is the fact that the mechanical properties of many engineering materials are derived, at least in part, from the presence of secondary phases in the solid solution matrix. The presence of the second phase, for example, raises the flow stress; and the extent of strengthening depends to first order on the volume fraction, size, and characteristics of the second phase precipitates which form during the manufacturing process. A mathematical model has been proposed by Cantrell *et al.*[56] giving the effective non-linearity parameter of an alloy as a function of total volume fraction of second phase precipitates. Although the relationship is in general non-linear (*see* Appendix 2 for derivation) the equation is approximated to within experimental error for volume fractions of second phase up to ~10% by the linear expression

$$\beta = \tilde{\beta}(1 + Rf_p) \qquad (48)$$

where

$$R = \sum_i \left[\frac{\tilde{C}_{11}}{(C^c_{11})_i} \left(2 - \frac{\beta_i C_{11}}{\tilde{\beta}(C^c_{11})_i} \right) e_i \right] - \frac{\tilde{C}_{11}}{(C^c_{11})_p} \left(2 - \frac{\beta_p C_{11}}{\tilde{\beta}(C^c_{11})_p} \right) \qquad (49)$$

In these equations f_p denotes the total volume fraction of second phase precipitates; the C_{11}s are 'quasi-isotropic' second order elastic constants

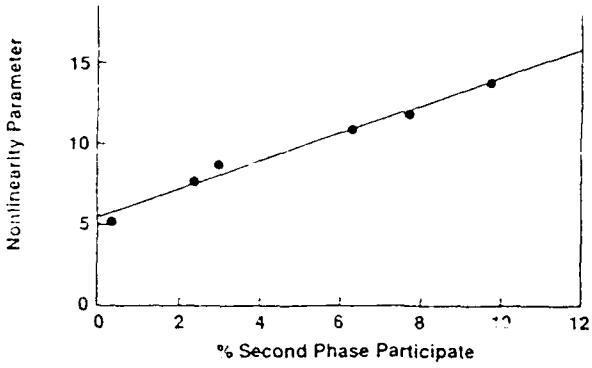

6 Graph of acoustic non-linearity parameter of 7075 (Al–Zn–Mg) as function of volume fraction of second phase precipitates

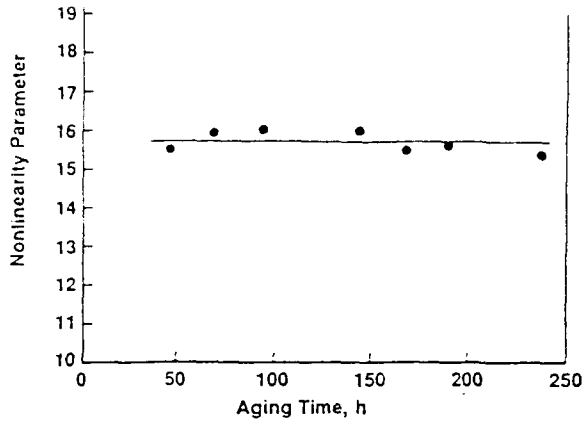

7 Graph of acoustic non-linearity parameter of 7075 (Al–Zn–Mg) as function of aging time

(Voigt notation). The overbar denotes the values of the parameters for which $f_p = 0$, i.e. pure solid solution; the subscript p refer to values for the total second phase precipitates taken collectively; the subscript i refers to the individual constituents of the solid solution; the superscript c refers to solid state constituents; and e_i is the 'depletion constant' for constituent i formed from solid solution.

Razvi *et al.*[37] provided experimental confirmation of equation (49) for measurements of β in the heat treatable aluminium alloy 7075 (Al–Zn–Mg). The results of their measurements of the effective non-linearity parameter β as a function of volume fraction of second phase precipitates f_p are shown in Fig. 6. A least squares fit to the data results in a linear curve with a 1·0 correlation coefficient given by the solid line in the figure. The lack of experimental measurements of the non-linearity parameters and the elastic constants of individual second phases of Al 7075 prevents an exact calculation of the effective non-linearity parameter of the material directly from equation (48). None the less, the agreement between the linear form of equation (48) and the linearity of the experimental data is evident. Measurements of the intercept and slope of the curve yield a value of 6·29 for the non-linearity parameter of pure solid solution of Al 7075 and a value of 0·12 for R.

It was assumed in the mathematical model that the number of randomly oriented grains contained within a pathlength of the propagating sound wave is sufficiently large that a good statistical sampling of quasi-isotropic behaviour is achieved. It was thus expected that the 5 cm pathlength in the specimens allows a wide variation of average grain size without violating the quasi-isotropic assumption. A manifestation of proper statistical sampling would be the invariance of the non-linearity parameter as a function of grain size. Figure 7 shows the measured non-linearity parameters in Al 7075, corrected for attenuation, as a function of aging up to 237 h. No significant variation in the effective β occurs although the average grain size is expected to change. It is inferred from these results and from Fig. 6 that the mathematical model qualitatively predicts the correct variation in the effective non-linearity parameter of Al 7075 as a function of volume fraction of second phase precipitates.

The dependence of the non-linearity parameter on the second phase precipitates for alloys and the dependence on the hardness parameter of the Born–Mayer potential for single crystals suggest a possible relationship between the non-linearity parameter and the engineering hardness number even though engineering hardness is measured by a plastically deforming test and the pertinent atomic mechanisms are complicated by microstructural details. None the less, measurements of the non-linearity parameters on aluminium alloys as a function of Rockwell F hardness were reported by Li *et al.*[57] Their results are shown in Fig. 8. Similar measurements on 18%Ni maraging steel as a function of Rockwell C hardness were reported by Yang *et al.*[58] and are shown in Fig. 9. In both cases there is a strong correlation between the non-linearity parameters and the hardness number.

Finally, Elber[59] reported the discovery of a crack closure phenomenon that occurs with metal fatigue. He noted that closure of the crack planes near the crack tip can occur while the applied stress is still tensile. The existence of a crack closure stress

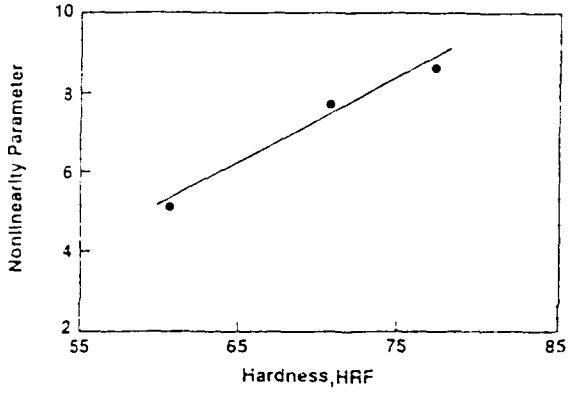

8 Plot of acoustic non-linearity parameter of Al alloys *v.* Rockwell F hardness

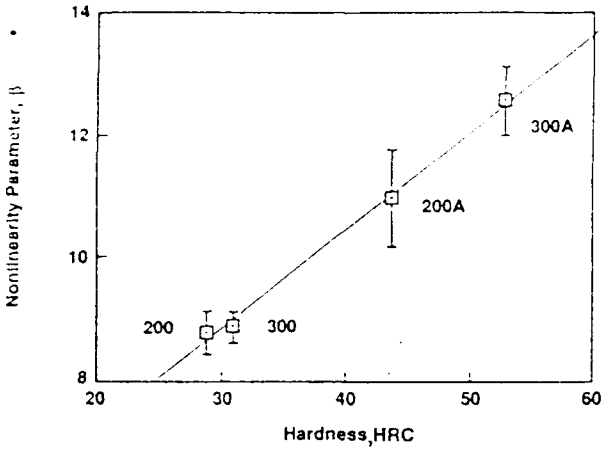

9 Plot of acoustic non-linearity parameter of 18% Ni maraging steel *v.* Rockwell C hardness

opens the way for defining an effective stress intensity factor I_σ, given by

$$I_\sigma = (\sigma - \sigma_{closure})(\pi b)^{1/2} \quad . \quad . \quad . \quad . \quad . \quad (50)$$

where σ is the applied tensile stress, $\sigma_{closure}$ the crack closure stress, and b the crack half length. The precision of I_σ depends on how well one can determine $\sigma_{closure}$. It is generally difficult to determine $\sigma_{closure}$ experimentally, since conventional crack opening determination is imprecise. However, Yost *et al.*[59] have resolved this difficulty by developing a technique based on the fact that as a crack in a compact tension specimen is opened acoustic second harmonics are generated at the (unbounded) surfaces of the crack interface. A typical data set is shown in Fig. 10 where the

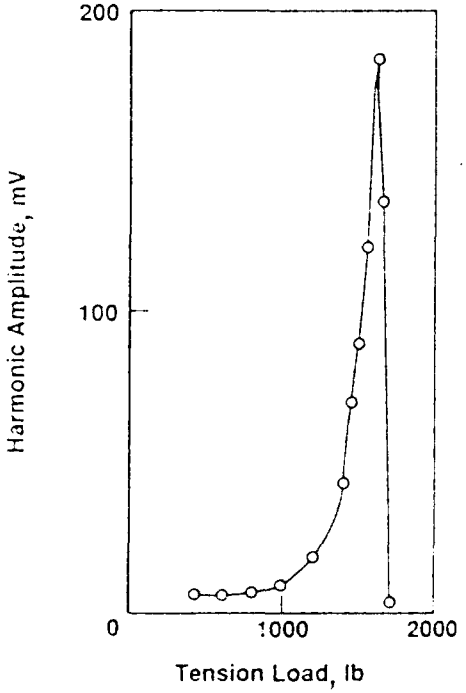

10 Graph of acoustic second harmonic amplitude generated at unbounded surface of crack interface in compact tension specimen as function of tensile load (1 lb ≡ 0·454 kg)

second harmonic generated at constant fundamental amplitude is plotted as a function of tension load. Crack opening occurs at a load corresponding to the peak of the generated harmonic amplitude.

Stress–temperature dependence of sound velocity

The variation in the temperature dependence of the sound velocity as a function of stress is the basis of a new method of characterising residual or applied stress fields in materials. Consider the thermodynamic tensions (equation (6)) to be a function of the Lagrangian strains η_{ij} and temperature T, i.e. $t_{ij} = t_{ij}(\eta, T)$. The differential can be written

$$dt_{ij} = -\lambda_{ij}dT + C_{ijkl}d\eta_{kl} \quad . \quad . \quad . \quad . \quad . \quad (51)$$

where $\lambda_{ij} = -(\partial t_{ij}/\partial T)_\eta$ is defined as the thermal stress tensor. For constant stress (i.e. $dt_{ij} = 0$) from equation (51)

$$\lambda_{ij} = C_{ijkl}\left(\frac{d\eta_{kl}}{dT}\right)_t = C_{ijkl}\alpha_{kl} \quad . \quad . \quad . \quad . \quad (52)$$

where

$$\alpha_{ij}^T = \left(\frac{d\eta_{kl}}{dT}\right)_t \quad . \quad . \quad . \quad . \quad . \quad . \quad . \quad . \quad (53)$$

is defined as the thermal strain tensor. For isotropic solids and cubic crystals

$$\eta_{ij} = \eta\delta_{ij} \quad . \quad . \quad . \quad . \quad . \quad . \quad . \quad . \quad (54)$$

where η is a scalar strain parameter. For this case

$$t_{ij} = -p\delta_{ij} \quad . \quad . \quad . \quad . \quad . \quad . \quad . \quad . \quad (55)$$

where p is a hydrostatic pressure. Thus from equations (52)–(55)

$$\frac{\partial p}{\partial T} = \frac{\alpha^T}{K_T} \quad . \quad . \quad . \quad . \quad . \quad . \quad . \quad . \quad (56)$$

where K_T is the compressibility and α^T is the thermal expansion coefficient. From equation (56) it can be inferred that a temperature dependent stress is induced in the material through the thermal expansion coefficient. For relatively small changes in the temperature, the stress p is linearly dependent on temperature and from equation (18) is seen to give rise to a linear variation of sound velocity with temperature.

Salama and Ling[61] considered the effect of stress on the temperature dependence of the ultrasonic velocity of aluminium and copper alloys by experimentally determining the relative change in the temperature derivative of the natural velocity $(\partial W/\partial T)$ as a function of applied stress σ. A graphical representation of their results is shown in Fig. 11. They find that the linear curves of Fig. 11 are represented quite well by the empirical equation

$$\left[\left(\frac{\partial W}{\partial T}\right)_\sigma - \left(\frac{\partial W}{\partial T}\right)_0\right]\left[\left(\frac{\partial W}{\partial T}\right)_0\right]^{-1} = -K\sigma \quad (57)$$

where $(\partial W/\partial T)_0$ is the temperature derivative of sound velocity at zero stress, $(\partial W/\partial T)_\sigma$ is that at

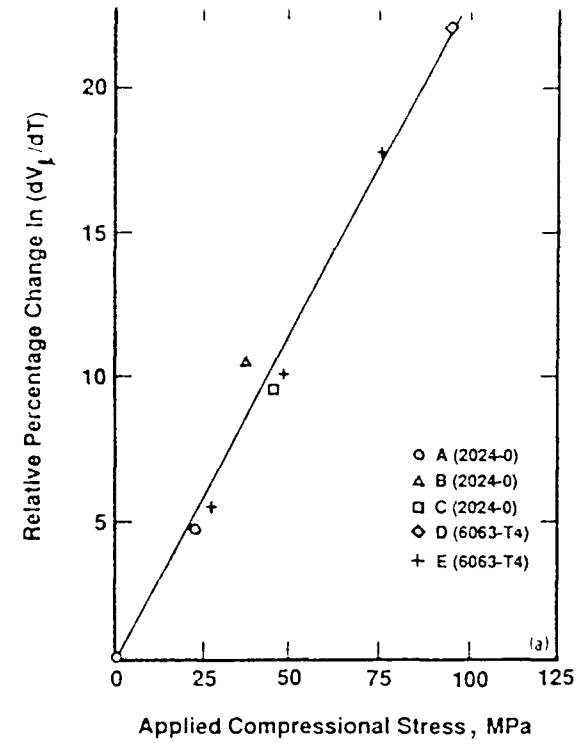

a Al alloys; *b* Cu alloys

11 Plot of temperature dependence of acoustic natural velocity as function of applied stress

applied stress, σ is the applied stress (compressional in their experiments), and K is a proportionality constant equal to $2{\cdot}4 \times 10^{-3}$ MPa^{-1} for aluminium alloys and $2{\cdot}5 \times 10^{-4}$ MPa^{-1} for copper alloys. These results were confirmed in steel and other aluminium alloys by Salama *et al.*[62–65]

A preliminary calculation of the temperature dependence of the sound velocity at zero initial stress was reported by Salama.[66] He also obtained a comparison between the calculated stress derivative of the temperature dependence at zero initial stress and experimental values of the stress derivative. The results yielded reasonable values for the stress dependences and led to the conclusion that the temperature dependence of ultrasonic velocity in metallic alloys varies linearly with stress as observed experimentally. A similar calculation and conclusion were obtained independently by Chern *et al.*[67]

More recently, Cantrell[68] obtained an analytical expression for the constant K by considering the explicit temperature dependence of the elastic moduli via the quasiharmonic-anisotropic-continuum model of crystals.[69] The effect of applied or residual stress was made explicit by expanding the elastic moduli about the state of zero stress in a manner analogous to that leading to equation (18). The generalised proportionality constant K_{pq}, analogous to K in equation (57), for arbitrary applied stress σ_{pq} is found to be

$$K_{pq} = \left(\frac{\partial C_{ijkl}}{\partial T}N_jN_lU_iU_k\right)^{-1}\left[2C_{klmn}\left(\frac{\partial S_{ijpq}}{\partial T}\right)\right.$$
$$\times N_lN_nU_kU_mU_iU_j + C_{ijklmn}\left(\frac{\partial S_{mnpq}}{\partial T}\right)N_jN_lU_iU_k$$
$$+ \left(\frac{\partial C_{ijklmn}}{\partial T}\right)S_{mnpq}N_jN_lU_iU_k - \frac{1}{2\rho_0\bar{W}^2}$$
$$\left.\times \frac{\partial(\rho_0\bar{W}^2)}{\partial T}(N_pN_q - C_{ijklmn}S_{mnpq}N_jN_lU_iU_k)\right] \quad \ldots\ldots\ (58)$$

where

$$\frac{\partial C_{\alpha\beta\gamma\delta}}{\partial T} = -k_B\rho_0\sum_{i=0}^{3n}\frac{\partial\gamma_i^{\alpha\beta}}{\partial\eta_{\gamma\delta}} \quad \ldots\ldots\ (59)$$

and

$$\frac{\partial C_{\alpha\beta\gamma\delta\rho\sigma}}{\partial T} = -k_B\rho_0\sum_{i=0}^{3n}\left[2\frac{\partial\gamma_i^{\alpha\beta}}{\partial\eta_{\gamma\delta}}\gamma_i^{\gamma\delta}\right.$$
$$+ 2\frac{\partial\gamma_i^{\alpha\beta}}{\partial\eta_{\rho\sigma}}\gamma_i^{\gamma\delta} + 2\frac{\partial\gamma_i^{\gamma\delta}}{\partial\eta_{\rho\sigma}}\gamma_i^{\alpha\beta} - 4\gamma_i^{\alpha\beta}\gamma_i^{\gamma\delta}\gamma_i^{\rho\sigma}$$
$$- \frac{1}{\rho_0W^2}(C_{\alpha\beta\gamma\delta\rho\sigma mn} + C_{\alpha\beta\gamma\delta\sigma mun}$$
$$\left.\times U_uU_v + 6C_{\alpha\beta\rho\sigma mun\delta}U_uU_v)N_mN_n\right] \quad \ldots\ldots\ (60)$$

where k_B is Boltzmann's constant, with

$$\gamma_i^{\alpha\beta} = -\frac{1}{2\rho_0W^2}[2\rho_0W^2U_\alpha U_\beta$$
$$+ (C_{\alpha\beta mn} + C_{\alpha\beta munv}U_uU_v)N_mN_n] \quad (61)$$

and

$$\frac{\partial\gamma_i^{\alpha\beta}}{\partial\eta_{\gamma\delta}} = 2\gamma_i^{\alpha\beta}\gamma_i^{\gamma\delta} - \frac{1}{2\rho_0W^2}(C_{\alpha\beta\gamma\delta mn}$$
$$+ C_{\alpha\beta\gamma\delta munv}U_uU_v + 4C_{\alpha\beta mun\gamma}U_uU_\delta)N_mN_n$$
$$\ldots\ldots\ (62)$$

The experimental measurements of Salama and Ling used a longitudinal ultrasonic wave propagating

in a direction perpendicular to a uniformly applied compressional static stress. Their work was performed on quasi-isotropic polycrystalline solids. For such an experiment situation the generalised expression for K_{pq}, equation (58), reduces to[68]

$$K = \left(\frac{\partial C_{11}}{\partial T}\right)^{-1}\left[(2C_{11} + C_{111} + C_{112})\left(\frac{\partial S_{12}}{\partial T}\right)\right.$$
$$+C_{112}\left(\frac{\partial S_{11}}{\partial T}\right) + \left(\frac{\partial C_{112}}{\partial T}\right)S_{11}$$
$$+\left(\frac{\partial C_{111}}{\partial T} + \frac{\partial C_{112}}{\partial T}\right)S_{12} - \left(\frac{1}{2C_{11}}\right)$$
$$\left.\times\left(\frac{\partial C_{11}}{\partial T}\right)(C_{111}S_{12} + C_{112}S_{12} + C_{112}S_{11})\right] \quad \ldots\ldots\ldots (63)$$

Note that equations (58) and (60) involve the temperature derivatives of third order elastic constants. From equations (61) and (62) it can be seen that such derivatives may be written explicitly in terms of fourth and fifth order elastic constants when the quasiharmonic-anisotropic-continuum model is used. Conversely, the experimental measurements of K provide a method of determining the fifth order elastic constants of the material in this approximation provided the fourth order constants can be determined from other methods. For pure aluminium and copper single crystals the K constants calculated for uniaxial stress applied along [001] and compressional wave propagation along [100] in these materials are $1{\cdot}8 \times 10^{-3}$ MPa^{-1} for aluminium and $3{\cdot}0 \times 10^{-4}$ MPa^{-1} for copper. These theoretical values are in very good agreement with the experimental values obtained by Salama and Ling for corresponding alloys of these elemental metals and suggest that the base metal of a given alloy system dominates the stress–temperature of the sound velocity in the alloys.

Low field magnetoacoustics

A novel technique for assessing stresses in ferromagnetic materials has been developed by Namkung *et al.*[70] The technique is based on the variation of the sound velocity measured as a function of low field magnetisation of the material. The normal crystalline structure of a solid is generally altered when the solid is ferromagnetically ordered. For solids such as iron the cubic unit cells are spontaneously deformed into tetragonal structures with the longer edges aligned along the magnetisation vector. The magnetisation vectors in turn are oriented along one of the six equivalent crystallographic ⟨100⟩ directions. A two dimensional representation of the net domain structure for the case of zero net magnetisation and zero initial stress is shown at the left in Fig. 12*a*. The effect of a residual or applied stress σ on the ferromagnetic state is to alter the energy density of a given

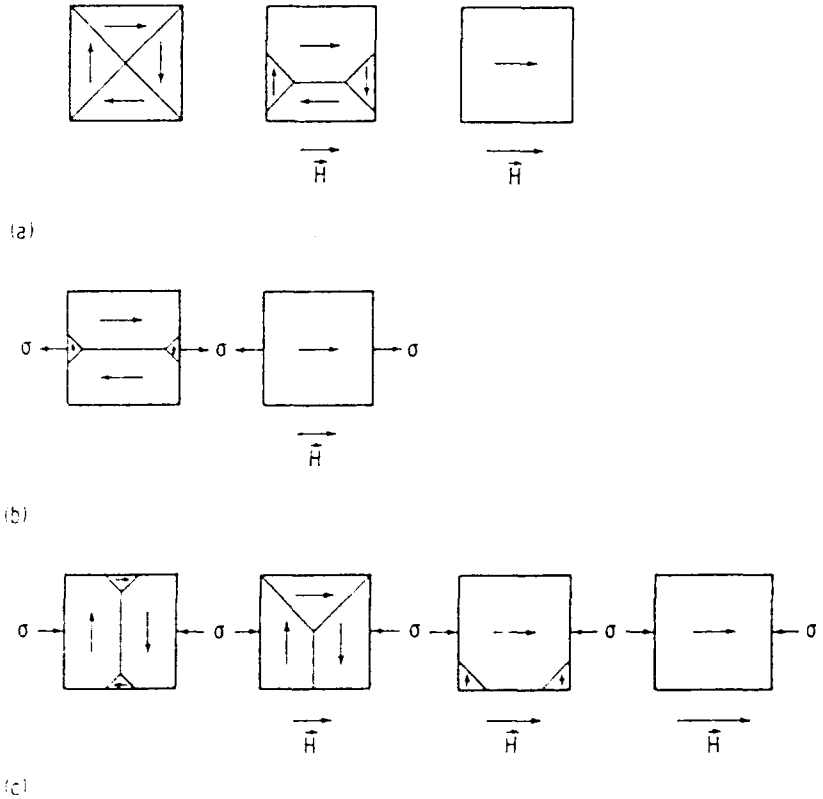

a effect of zero initial stress, *b* effect of tensile initial stress; *c* effect of compressive initial stress

12 Two dimensional representation of net magnetic domain structure

domain by the amount[71]

$$E_{k,me} = K_1^M(\alpha_1^2\alpha_2^2 + \alpha_2^2\alpha_3^2 + \alpha_3^2\alpha_1^2) - 3\lambda_{100}^m\sigma(\alpha_1^2\gamma_1^2 + \alpha_2^2\gamma_2^2 + \alpha_3^2\gamma_3^2)/2 - 3\lambda_{111}^m\sigma(\alpha_1\alpha_2\gamma_1\gamma_2 + \alpha_2\alpha_3\gamma_2\gamma_3 + \alpha_3\alpha_1\gamma_3\gamma_1) \quad . \quad . \quad . \quad . \quad . \quad . \quad . \quad (64)$$

where K_1^M is the first anisotropy constant, λ_{100}^m the saturation magnetostriction along the ⟨100⟩ axis, λ_{111}^m that along the ⟨111⟩ axis, and the α_is and γ_is are direction cosines of the magnetisation vector and uniaxial stress axis, respectively, with respect to the cube axes.

For transdomain stresses the magnetoelastic energy densities are generally different for adjacent domains and give rise to a net pressure acting on the domain walls separating them. From equation (64) the net pressure (i.e. energy density) is non-zero only for those adjacent domains whose magnetisation vectors are at right angles to each other (i.e. 90° domain walls). Under tension the 90° domain wall motion is such that the net volume of domains oriented along the uniaxial stress axis is increased as indicated by the domain representation at the left of Fig. 12*b*. Under compression the domains orient close to a plane perpendicular to the stress axis as shown at the left of Fig. 12*c*. In both cases the effect of stress is to decrease the area of 90° walls. The stress induced 90° wall motion, however, is generally restricted by the interaction between the walls and various lattice defects. Hence, complete domain alignment under stress does not generally occur in the case of impure ferromagnetic materials like steels.

When an external magnetic field is applied to the ferromagnetic solid, domains with low Zeeman energy become seed domains and their volume begins to expand. In this case both 180° and 90° wall motion occurs such that as the applied field increases more domains become oriented along the applied field direction. The case for zero initial stress in the material is illustrated in Fig. 12*a*. The relative change in net domain structure as a function of applied magnetic field is dependent on the domain structure initially induced by the stress at zero magnetic field conditions as illustrated in Fig. 12*b* and *c*. The applied magnetic field strength is shown to increase from zero at the left to some maximum value indicated at the right in the figure.

The effect of net domain orientation on the sound velocity in the ferromagnetic material is governed by the relative amount of 90° domain walls available in the material at the time of the velocity measurement. The elastic modulus E of ferromagnetic materials is given by

$$E = \frac{\sigma}{\varepsilon_{el} + \varepsilon_{me}} \quad . \quad . \quad . \quad . \quad . \quad . \quad . \quad . \quad . \quad . \quad (65)$$

where σ is the applied stress, σ_{el} the linear elastic strain, and ε_{me} the magnetoelastic strain. The magnetoelastic strain is generally assumed to be proportional to the total area of 90° domain walls. From equation (65) and Fig. 12, the expected functional change in sound velocity as a function of applied magnetic field strength H for various states of initial stress is qualitatively shown in Fig. 13. It is of interest to note that tensile and compressive stresses give rise to initial slopes of opposite polarity and thus provide a means of testing the sign of the initial stress.

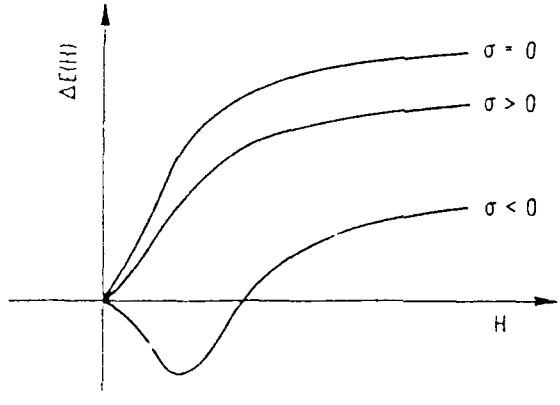

13 **Predicted changes in sound velocity as function of magnetic field strength for various states of initial stress**

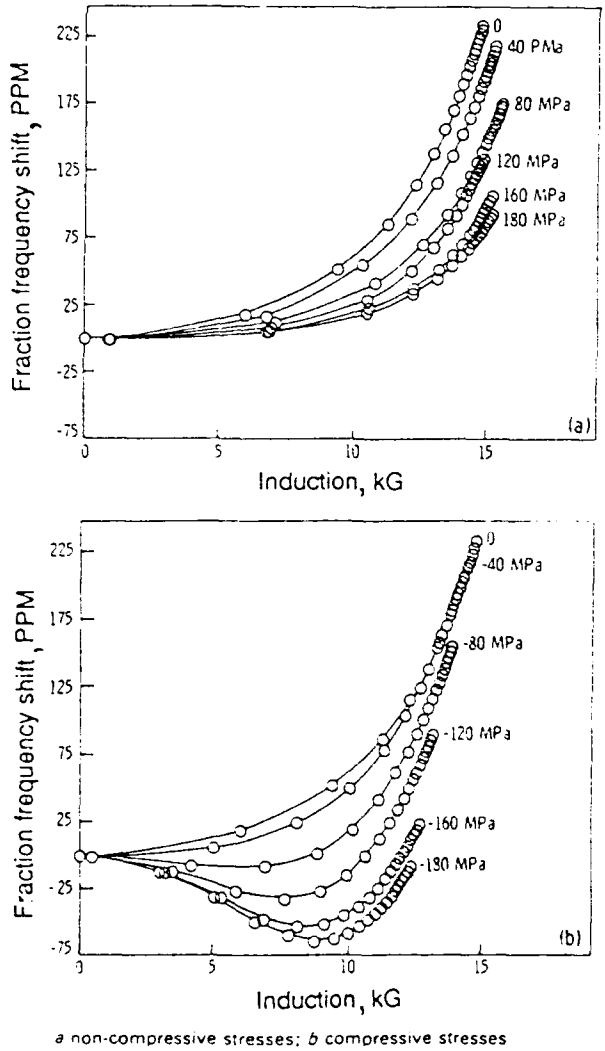

a non-compressive stresses; *b* compressive stresses

14 **Changes in sound velocity in AISI 1020 steel as function of magnetic field strength for various states of initial stress; PPM parts per million**

Namkung *et al.*[70,72,73] have performed an extensive series of natural velocity measurements in various steel samples using the pulsed phase-locked loop technique.[34] Their results[73] for AISI 1020 steel are shown in Fig. 14. The curves are in nominal agreement with the model curves in Fig. 13. Their results[70,72] for railroad steel, however, show some deviation from the model. Specifically, the curves at tension indicate a greater modulus or velocity change than the curve at zero stress. In addition, the unstressed curve is relatively flat until a rather large magnetisation is induced in the sample. Namkung *et al.*[73] explain that the deviation results from the high degree of local lattice strain that significantly impedes the motion of 90° walls but has little influence on the 180° wall motion. While the 180° wall motion contributes to the magnetisation of the material, only the 90° wall motion affects the elastic modulus and velocity changes. The unstressed curve is thus expected to remain relatively flat until high field strengths are achieved. The velocity increase at higher fields is caused mainly by domain rotation and in part by 90° wall motion. The effect of initial tension is to aid the magnetic field in moving 90° walls at a somewhat reduced field strength. This results in an increasingly upward shift of the tension curves as the initial tension increases.

Conclusions

It is clear that non-linear acoustic methods can be used to obtain useful and in some cases unique information about materials. Although the same basic experimental acoustic techniques are applicable to most materials, the meaning and interpretation of the experimental results are limited by the validity of the acoustic models used to describe the material. Most measurements of non-linear thermoelastic properties have been performed on materials having a relatively simple, well defined, single phase structure in which elastic wave behaviour is understood from the generalised wave equations for solids of arbitrary crystalline symmetry. Indeed, elastic constant data (particularly the higher order elastic constants) have been reported mostly on relatively defect free single crystals. Multiphase and composite materials, although more complex structurally, have generally been treated acoustically as quasi-isotropic or at best mildly textured materials without regard to their microstructural composition. Although acoustic wave propagation can in principle be treated as taking place in such materials with effective elastic moduli that reflect whatever degree of symmetry the researcher feels necessary to consider, the compositional character of complex materials in itself is important and deserves specific consideration.

An attempt has been made in this review to redress the general lack of compositional consideration by emphasising the interrelationship of material composition, material properties, and acoustic measurements. Although the acoustic models presented here in terms of volume fraction of material constituents are in some cases simplistic, the essential features predicted by the models are borne out in experiment. The models, indeed, do provide a more comprehensive understanding of the influence of material composition on acoustic properties and, hopefully, will serve as catalysts for the development of better, more comprehensive, models of compositional influence on wave behaviour. The success of many non-destructive evaluation efforts and the evolution of new non-destructive methodologies rests in large part on the ability to model comprehensively such microstructural influences on acoustic properties. The consideration of compositional influence, including magnetic or other domain effects where appropriate, and the linking of acoustic non-linearity to the basic lattice dynamical behaviour of materials are necessary to provide the proper science base for advancement and innovation in non-destructively assessing, characterising, and testing the thermoelastic and mechanical properties of materials.

Acknowledgments

The authors would like to thank Drs J. H. Heyman, W. T. Yost, and M. Namkung for helpful discussions. K. Salama would like to acknowledge the support of the Army Research Office under contract No. DAAL03–88–K–0096.

References

1. S. HUNKLINGER, W. ARNOLD, S. STEIN, R. NAVA, and K. DRANSFELD: *Phys. Lett.*, 1972, A42, 253.
2. R. T. BEYER and S. V. LETCHER: 'Physical ultrasonics'; 1967, New York, Academic Press.
3. D. C. WALLACE: 'Thermodynamics of crystals'; 1972, New York, Wiley.
4. P. BRUESCH: 'Phonons: Theory and experiments'; 1982, Berlin, Springer-Verlag.
5. M. A. BREAZEALE and J. PHILIP: in 'Physical acoustics', Vol. 17, (ed. W. P. Mason and R. N. Thurston), 1–60; 1984, New York, Academic Press.
6. Y.-H. PAO, W. SACHSE, and H. FUKUOKA: in 'Physical acoustics', Vol. 17, (ed. W. P. Mason and R. N. Thurston), 61–143; 1984, New York, Academic Press.
7. D. R. ALLEN, W. H. B. COOPER, C. M. SAYERS, and M. G. SILK: in 'Research techniques in nondestructive testing', Vol. 6, (ed. R. S. Sharpe), 151–209; 1982, New York, Academic Press.
8. R. E. GREEN: 'Treatise on materials science and technology', Vol. 3, 1973, New York, Academic Press.
9. H. F. POLLARD: 'Sound waves in solids'; 1977, London, Pion Ltd.
10. M. R. JAMES and O. BUCK: *Crit. Rev. Solid State Mater. Sci.*, 1980, 9, 61–105.
11. G. S. CARGILL, III: in 'Physical acoustics', Vol. 16, (ed. W. P. Mason and R. N. Thurston) 125–195; 1988, New York, Academic Press.
12. D. G. P. FATKIN, C. B. SCRUBY, and G. A. D. BRIGGS: *J. Mater. Sci.*, 1989, 24, 23.
13. J. H. CANTRELL, M. QIAN, M. V. RAVICHANDRAN, and K. M. KNOWLES: *Appl. Phys. Lett.*, 1990, 57, 1870.
14. D. C. WALLACE: in 'Solid state physics', Vol. 25, (ed. H. Ehrenreich *et al.*), 301–404; 1970, New York, Academic Press.
15. R. N. THURSTON: in 'Physical acoustics', Vol. 1A, (ed. W. P. Mason), 2–109; 1964, New York, Academic Press.
16. F. D. MURNAGHAN: 'Finite deformation of an elastic solid'; 1951, New York, Wiley.
17. L. BRILLOUIN: 'Tensors in mechanics and elasticity'; 1964, New York, Academic Press. (English translation of 'Les tenseurs en mechanique et en elasticite'; 1938 Paris, Masson)
18. M. BORN and K. HUANG: 'Dynamical theory of crystal lattices', 1954, Oxford University Press.

19. K. HUANG: *Proc. R. Soc.*, 1950, **A203**, 178.
20. K. BRUGGER: *Phys. Rev.*, 1964, **133**, A1611.
21. R. N. THURSTON and K. BRUGGER: *Phys. Rev.*, 1964, **133**, A1604.
22. J. H. CANTRELL: *J. Test. Eval.*, 1982, **10**, 223.
23. D. S. HUGHES and J. L. KELLY: *Phys. Rev.*, 1953, **92**, 1145.
24. D. I. CRECRAFT: *J. Sound Vibr.*, 1967, **5**, 173.
25. R. T. SMITH, R. STERN, and R. W. B. STEPHENS: *J. Acoust. Soc. Am.*, 1966, **40**, 1002.
26. K. SALAMA, E. SCHNEIDER, and S. L. CHU: in 'Review of progress in quantitative nondestructive evaluation', Vol. 5B, (ed. D. O. Thompson and D. E. Chimenti), 1431–1438; 1986, New York, Plenum Press.
27. R. M. CHRISTENSEN: 'Mechanics of composite materials'; 1979, New York, Wiley.
28. J. D. ESHELBY: in 'Progress in solid state physics', Vol. 3, (ed. F. Seitz and D. Turnbull), 79; 1956, New York, Academic Press.
29. H. J. McSKIMIN: in 'Physical acoustics', Vol. 1A, (ed. W. P. Mason), 271–417; 1964, New York, Academic Press.
30. R. TRUELL, C. ELBAUM, and B. B. CHICK: 'Ultrasonic methods in solid state physics'; 1969, New York, Academic Press.
31. E. P. PAPADAKIS: in 'Physical acoustics', Vol. 17, (ed. W. P. Mason and R. N. Thurston), 277–374; 1976, New York, Academic Press.
32. M. A. BREAZEALE, J. H. CANTRELL, and J. S. HEYMAN: in 'Methods of experimental physics', Vol. 19, (ed. F. D. Edmonds), 67–135; 1981, New York, Academic Press.
33. B. J. RATCLIFFE: *J. Nondestr. Test.*, 1969, **11**, 48.
34. J. S. HEYMAN, S. G. ALLISON, K. SALAMA, and S. I. CHU: in 'Symp. on NDE, Applications to materials processing', (ed. O. Buck and S. Wolf), 177–184; 1983, Metals Park, OH, American Society for Metals.
35. S. G. ALLISON, J. S. HEYMAN, and K. SALAMA: in Proc. IEEE Ultrasonic Symp., Cat. No. 84CH2112–1, 997; 1984, New Tork, Institute of Electrical and Electronic Engineers.
36. E. SCHNEIDER, S. K. CHU, and K. SALAMA: in Proc. IEEE Ultrasonic Symp., Cat. No. 84CH2112–1, 944; 1984, New York, Institute of Electrical and Electronic Engineers.
37. S. RAZVI, P. LI, K. SALAMA, J. H. CANTRELL, and W. T. YOST: in 'Review of progress in quantitative nondestructive evaluation', Vol. 6B, (ed. D. O. Thompson and D. E. Chimenti), 1403; 1987, New York, Plenum Press.
38. D. F. LEE, S. RAZVI, K. SALAMA, and E. SCHNEIDER: in Proc. 16th Symp. on NDE, San Antonio, TX, 1987, NTIAC, Southwest Research Institute, 153.
39. D. F. LEE, K. SALAMA, and E. SCHNEIDER: in Proc. 3rd Int. Symp. on Nondestructive Characterization of Materials, (ed. P. Holler), 173; 1988, Berlin, Springer-Verlag.
40. B. GRELSSON AND K. SALAMA: in 'Review of progress in quantitative nondestructive evaluation', Vol. 9B, (ed. D. O. Thompson and D. E. Chimenti), 1441–1447; 1989, New York, Plenum Press.
41. J. H. CANTRELL: *Phys. Rev. B*, 1980, **21**, 4191.
42. J. H. CANTRELL: *Phys. Rev. B*, 1984, **30**, 3214.
43. J. H. CANTRELL, W. T. YOST, and P. LI: *Phys. Rev. B*, 1987, **35**, 9780.
44. W. T. YOST and J. H. CANTRELL: *Phys. Rev. B*, 1984, **30**, 3221.
45. J. H. CANTRELL and W. P. WINFREE: *Appl. Phys. Lett.*, 1980, **37**, 785.
46. W. B. GAUSTER and M. A. BREAZEALE: *Rev. Sci. Instrum.*, 1966, **37**, 1544.
47. W. T. YOST and M. A. BREAZEALE: *Phys. Rev. B*, 1974, **9**, 510.
48. J. H. CANTRELL: in 'Ultrasonics International '85 Conf. Proc.', (ed. Z. Novak), 551; 1985, Guildford, Surrey, IPC Science and Technology Press.
49. J. H. CANTRELL: Proc. IEEE Ultrasonics Symp., Cat. No. 86CH2375–4, 1079; 1986, New York, Institute of Electrical and Electronics Engineers.
50. J. H. CANTRELL: in Proc. IEEE Ultrasonics Symp., Cat. No. 87CH2492–7, 425; 1987, New York, Institute of Electrical and Electronics Engineers.
51. J. H. CANTRELL: *Proc. Inst. Acoustics*, 1989, **11**, (5), 445.
52. P. B. GHATE: *Phys. Rev.*, 1965, **139**, A1666.
53. Y. HIKI and A. V. GRANATO: *Phys. Rev.*, 1966, **144**, 411.
54. J. H. CANTRELL and M. A. BREAZEALE: *Phys. Rev. B*, 1978, **17**, 4864.
55. J. F. CURRIE, J. A. KRUMHANSL, A. R. BISHOP, and S. E. TRULLINGER: *Phys. Rev. B*, 1980, **22**, 477.
56. J. H. CANTRELL, W. T. YOST, S. RAZVI, P. LI, and K. SALAMA: in Proc. IEEE Ultrasonics Symp., Cat. No. 86CH2375–4, 1075; 1986, New York, Institute of Electrical and Electronics Engineers.
57. P. LI, W. T. YOST, J. H. CANTRELL, and K. SALAMA: in Proc. IEEE Ultrasonics Symp., Cat. No. 85CH2209–5 SU, 1113; 1985, New York, Institute of Electrical and Electronics Engineers.
58. H. YANG, W. T. YOST, and J. H. CANTRELL: in Proc. IEEE Ultrasonics Symp., Cat. No. 87CH2492–7, 1131; 1987, New York, Institute of Electrical and Electronics Engineers.
59. W. ELBER: 'The significance of fatigue crack closure: Damage tolerance in aircraft structures', STP 486, 230; 1971, Philadelphia, PA, American Society for Testing and Materials.
60. W. T. YOST, M. NAMKUNG, and S. G. ALLISON: in 'Review of progress in quantitative nondestructive evaluation', Vol. 7B, (ed. D. O. Thompson and D. E. Chimenti), 1525; 1987, New York, Plenum Press.
61. K. SALAMA and C. K. LING: *J. Appl. Phys.*, 1980, **51**, 1505.
62. K. SALAMA, A. L. W. COLLINS, and J. J. WANG: in 'Proc. of DARPA/AF review of progress in quantitative nondestructive evaluation', Report AFWAL-TR-81-4080, (ed. D. O Thompson and R. B. Thompson), 265, Air Force Wright Aeronautical Laboratories, Dayton, OH, 1981.
63. K. SALAMA, C. K. LING, and J. J. WANG: *Exp. Tech.*, 1981, **5**, 14.
64. K. SALAMA, J. J. WANG, and G. C. BARBER: in 'Review of progress in quantitative nondestructive evaluation', Vol. 2B, (ed. D. O. Thompson and D. E. Chimenti), 1355; 1983, New York, Plenum Press.
65. K. SALAMA and J. J. WANG: in 'Proc. of German–US workshop on research and development to new procedures in NDT', (ed. P. Holler), 539; 1983, Berlin, Springer Verlag.
66. K. SALAMA: in 'Review of progress in quantitative nondestructive evaluation', Vol. 4B, (ed. D. O. Thompson and D. E. Chimenti), 1109; 1985, New York, Plenum Press.
67. E. J. CHERN, J. S. HEYMAN, and J. H. CANTRELL: in Proc. IEEE Ultrasonics Symp., Cat. No. 81CH1689–9, 960; 1981, New York, Institute of Electrical and Electronic Engineers.
68. J. H. CANTRELL: in 'Ultrasonics International '89 Conf. Proc.', 977; 1989, Guildford, Surrey, Butterworth.
69. J. A. GARBER and A. V. GRANATO: *Phys. Rev. B*, 1975, **11**, 3998.
70. M. NAMKUNG, D. UTRATA, S. G. ALLISON, and J. S. HEYMAN: in 'Review of progress in quantitative nondestructive evaluation', Vol. 5B, (ed. D. O. Thompson and D. E. Chimenti), 1481; 1985, New York, Plenum Press.
71. B. D. CULLITY: 'Introduction to magnetic materials'; 1972, Menlo Park, CA, Addison-Wesley.
72. M. NAMKUNG, D. UTRATA, S. G. ALLISON, and J. S. HEYMAN: in Proc. IEEE Ultrasonics Symp., Cat. No. 85CH2209–5 SU, 1022; 1985, New York, Institute of Electrical and Electronics Engineers.
73. M. NAMKUNG, D. UTRATA, P. LANGLOIS, P. W. KUSHNICK, and J. L. GRANGER: in 'Review of progress in quantitative nondestructive evaluation', Vol. 8B, (ed. D. O. Thompson and D. E. Chimenti), 2067; 1988, New York, Plenum Press.
74. R. E. APFEL: *J. Acoust. Soc. Am.*, 1983, **74**, 1866.

APPENDIX 1

Dynamic moduli and elastic constants

The mechanical properties of isotropic solids are usually obtained from static or low frequency dynamic testing of specimens having a specified geometrical shape. Here the relationships between the elastic moduli measured in such tests and the elastic constants (specifically Lamé constants) obtained from ultrasonic measurements of the same material are summarised. The relationship between the Lamé constants and the Brugger second order elastic constants, generally used in the text, is given in equation (20).

The linear stress–strain relationship (Hooke's law) for an isotropic solid in terms of the Lamé constants λ and μ can be written in the form

$$\sigma_{ij} = 2\mu\varepsilon_{ij} + \lambda\theta\delta_{ij} \quad \ldots\ldots\ldots \quad (66)$$

where θ is the dilation or change in material volume defined by

$$\theta = \varepsilon_{11} + \varepsilon_{22} + \varepsilon_{33} \quad \ldots\ldots\ldots \quad (67)$$

and ε_{ij} are the linear strains defined in terms of the displacement gradients $(\partial u_i/\partial a_j)$ as

$$\varepsilon_{ij} = \frac{1}{2}\left(\frac{\partial u_j}{\partial a_j} + \frac{\partial u_j}{\partial a_i}\right) \quad \ldots\ldots\ldots \quad (68)$$

Equation (66) is obtained directly from equations (5), (7), and (20) where only the linear terms are retained in the final expression. The μ constant is often referred to as the shear or rigidity modulus and is given the symbol G by many authors. The Lamé constants can be obtained from measurements of the compressional and shear bulk wave velocities of the unstressed (i.e. $\sigma = 0$) sample as indicated by equations (23).

The bulk modulus k is an important engineering modulus defined from a static measurement of the change in the material volume resulting from an applied hydrostatic pressure p as

$$k = -\frac{\Delta p}{\Delta\theta} = \lambda + 2\mu/3 \quad \ldots\ldots\ldots \quad (69)$$

The right-hand side of equation (69) is obtained by writing $\sigma_{ij} = -p\delta_{ij}$ for the hydrostatic pressure and using this expression in equation (66). As indicated in equation (69), the bulk modulus can also be calculated from knowledge of the Lamé constants determined from ultrasonic bulk wave measurements.

Consider now a cylindrical, isotropic solid and deform the solid statically along the cylindrical axis, which is defined as the x or 1-axis. The surface of the cylinder is stress free and so from equation (66)

$$\begin{aligned} \sigma_{11} &= 2\mu\varepsilon_{11} + \lambda\theta \\ 0 &= 2\mu\varepsilon_{22} + \lambda\theta \quad \ldots\ldots\ldots \quad (70) \\ 0 &= 2\mu\varepsilon_{33} + \lambda\theta \end{aligned}$$

Young's modulus E is defined as the ratio of the applied axial stress σ_{11} to the longitudinal strain ε_{11} and from equation (70)

$$E = \frac{\sigma_{11}}{\varepsilon_{11}} = \frac{\mu(3\lambda + 2\mu)}{\lambda + \mu} \quad \ldots\ldots\ldots \quad (71)$$

Although equation (71) is defined from static conditions, Young's modulus can be obtained from measurements of the velocity v_E of low frequency longitudinal waves propagating along the cylinder axis as

$$E = \rho_0 v_E^2 \quad \ldots\ldots\ldots \quad (72)$$

It is important to emphasise that the velocity v_E measured under the above conditions is not equal to the velocities measured in unbounded media, as given in equation (23). The propagation medium can be considered effectively unbounded when the ultrasonic frequencies are sufficiently large that the acoustic wavelength is small compared with the dimensions of the sample.

Poisson's ratio ν is also defined from static conditions as the ratio of the lateral strain to the longitudinal strain and is obtained from equation (70) as

$$\nu = -\frac{\varepsilon_{22}}{\varepsilon_{11}} = \frac{\lambda}{2(\lambda + \mu)} \quad \ldots\ldots\ldots \quad (73)$$

It is clear from the above relationships that the various moduli are intrinsically related. For example, it is easily shown that

$$\lambda = \frac{E\nu}{(1 + \nu)(1 - 2\nu)} = \frac{2\nu\mu}{1 - 2\nu} \quad \ldots\ldots \quad (74)$$

and

$$\mu = \frac{E}{2(1 + \nu)} \quad \ldots\ldots\ldots\ldots \quad (75)$$

APPENDIX 2

Non-linearity parameters of multiphase alloys

A mathematical model was developed by Cantrell *et al.*[56] to describe the effective non-linearity parameters of multiphase alloys. The model is based on the law of mixtures for the non-linearity parameter and is reproduced here to underscore the essential features and assumptions not brought out in the text.

Consider a rotation of the Cartesian reference frame such that the direction of acoustic wave propagation is always along the x or 1-axis of the rotated coordinate system. Then perform a second orthogonal transformation on the system which diagonalises the non-linear equations of motion, equation (41), such that the equations are decoupled into three independent equations corresponding to the three wave polarisation directions. Performing these same transformations on the general stress–strain relationship of equation (5) and keeping only terms to first order in the non-linearity lead to the relationship between the transformed stress σ_{pq} and the transformed displacement gradients $(\partial u_j/\partial a_1)$ given by[41] (no sum on j)

$$\sigma_{pq} = \mu_j^{pq}\frac{\partial u_j}{\partial a_1} + \frac{1}{2}\nu_{jj}^{pq}\left(\frac{\partial u_j}{\partial a_1}\right)^2 \quad \ldots\ldots \quad (76)$$

where μ_j^{pq} and ν_{jj}^{pq} are linear combinations of second and third order elastic constants, a_1 is the Lagrangian coordinate along the x or 1-axis, and $j = 1,2,3$ is a mode index representing the appropriate polarisation direction. Consideration is restricted to longitudinal waves ($j = 1$) in quasi-isotropic solids (i.e. solids consisting of randomly oriented grains). Thus the superscripts and subscripts are dropped and the longitudinal stresses σ

written

$$\sigma = C_{11}\left(\frac{\partial u}{\partial a}\right) - \frac{1}{2}C_{11}\beta\left(\frac{\partial u}{\partial a}\right)^2 \quad \ldots \quad (77)$$

where C_{11} is the longitudinal second order elastic constant written in Voigt notation and β is the acoustic non-linearity parameter. Solving for $(\partial u/\partial a)$ in terms of σ we obtain

$$\left(\frac{\partial u}{\partial a}\right) = \frac{1}{C_{11}}\sigma + \frac{1}{2}\frac{\beta}{C_{11}^2}\sigma^2 \quad \ldots \quad (78)$$

Consider now the solid to consist of any number of phases N. Assume that for a given phase i, the grain orientations are perfectly random (no texture) and that the number such grains contained within a path length of sound is sufficiently large to provide a good statistical sampling. To the extent that such conditions are maintained the value of the effective non-linearity parameter is expected to be independent of grain size.

In order to obtain the appropriate mixing law for β define V_0 and ρ_0 to be the initial (unperturbed) volume and mass density, respectively, of the solid. The local transformation from the initial state to the deformed state V or ρ is defined through the Jacobian

$$J = \frac{V}{V_0} = \frac{\rho_0}{\rho} \quad \ldots \quad (79)$$

The volume at any time is considered to consist of a number N of constituent phases i such that

$$V = \sum_{i=1}^{N} V^i \quad \ldots \quad (80)$$

Then from equations (79) and (80)

$$J = \frac{1}{V_0}\sum_i V^i = \frac{1}{V_0}\sum_i J_i V_0^i = \sum_i J_i f_i \quad \ldots \quad (81)$$

where $J_i = (V^i/V_0^i)$ is the Jacobian for phase i and $f_i = (V_0^i/V_0)$ is the volume fraction of phase i. Expanding the Jacobian in terms of the displacement gradients $(\partial u_i/\partial a_j) = u_{ij}$ and keeping the linear terms (small strains), then (Einstein summation)

$$J = 1 + u_{kk} \quad \ldots \quad (82)$$

Substituting equation (82) into equation (81) gives

$$u_{kk} = \sum_i u_{mm}^i f_i \quad \ldots \quad (83)$$

Consider now the quasi-isotropic solid and assume that for a given phase i the grain orientations are sufficiently random and of sufficiently large number that each phase responds individually as an isotropic structure. Under such conditions, equation (83) may be written

$$\left(\frac{\partial u}{\partial a}\right) = \sum_i \left(\frac{\partial u}{\partial a}\right)_i f_i \quad \ldots \quad (84)$$

in the notation of equation (77). From equations (78) and (79), together with the assumption of local equality of stresses, we obtain

$$\frac{1}{C_{11}}\sigma + \frac{1}{2}\frac{\beta}{C_{11}^2}\sigma^2 = \left(\sum_i \frac{1}{C_{11}^i} f_i\right)\sigma + \left(\sum_i \frac{\beta_i}{2(C_{11}^i)^2} f_i\right)\sigma^2 \quad (85)$$

Equating like powers of σ, we obtain

$$\frac{1}{C_{11}} = \sum_i \frac{1}{C_{11}^i} f_i \quad \ldots \quad (86)$$

and

$$\beta = C_{11}^2 \sum_i \frac{\beta_i}{2(C_{11}^i)^2} f_i \quad \ldots \quad (87)$$

In general, a non-linear relationship is found between the effective non-linearity parameter β and the volume fraction f_i of individual phases because of the appearance of C_{11}^2 in equation (87). It is of interest to point out that for liquid media the second order elastic constants $C_{44} = 0$ and $C_{11} = C_{12}$. In this case $(C_{11}^i)^{-1}$ can be identified with the liquid state compressibilities and equation (87) becomes identical to the results of Apfel[74] for immiscible liquid mixtures.

Assume now that the solid consists of any number of distinct second phase precipitates and that the relative volume fractions of constituent second phase precipitates for a given alloy are constant – only the total volume fraction of second phase precipitates is considered to change. Hence, the effective non-linearity parameter β_p and the effective $(C_{11})_p$ of the second phase precipitates taken collectively remain unchanged. The invariance of the relative volume fractions of second phase precipitates must necessarily come at the expense of the solid solution constituents. It is assumed that the depletion of the constituents of solid solution occurs linearly as

$$f_i^c = \bar{f}_i^c - e_i f_p \quad \ldots \quad (88)$$

where f_i^c is the present volume fraction of solid solution constituent i, f_p is the total volume fraction of second phase precipitates, $\bar{f}_i^c$ is the volume fraction of constituent i in pure solid solution (i.e. when $f_p = 0$), and e_i is the 'depletion' constant for constituent i.

From the above considerations equation (86) can be written

$$\frac{1}{C_{11}} = \sum_i \frac{1}{(C_{11}^i)_i} f_i^c + \frac{1}{(C_{11})_p} f_p \quad \ldots \quad (89)$$

where in equation (89) and in all following equations the summation is taken over solid solution constituents only, the superscript c refers to solid solution constituents, and the subscript p refers to the second phase constituents taken collectively. It has been assumed, somewhat tenuously, in writing equation (89) that the solid solution constituents behave as an immiscible mixture. While this assumption is not strictly true, the summation term in the equation is, none the less, representative of

an effective linear dependence on f_p. From equations (88) and (89)

$$\frac{1}{C_{11}} = \frac{1}{\bar{C}_{11}} + f_p\left[\frac{1}{(C_{11})_p} - \sum_i \frac{1}{(C_{11}^s)_i} e_i\right] \quad . \quad . \quad (90)$$

where

$$\frac{1}{\bar{C}_{11}} = \sum_i \frac{1}{(C_{11}^s)_i} f_i^s \quad . \quad . \quad . \quad . \quad . \quad (91)$$

is the solid solution contribution.

Similarly, from equations (87), (88), and (90) it is found that the effective non-linearity parameter β of the solid in terms of total volume fraction of second phase precipitates f_p is given by

$$\beta = \left[1 + f_p\left(\frac{\bar{C}_{11}}{(C_{11})_p} - \sum_i \frac{\bar{C}_{11}}{(C_{11}^s)_i} e_i\right)\right]^{-2} \times \left\{\bar{\beta} + f_p\left[\left(\frac{\bar{C}_{11}}{(C_{11})_p}\right)^2 \beta_p - \sum_i \left(\frac{\bar{C}_{11}}{(C_{11}^s)_i}\right)^2 \beta_i e_i\right]\right\} \quad . \quad . \quad . \quad . \quad . \quad (92)$$

where

$$\bar{\beta} = (\bar{C}_{11})^2 \sum_i \left(\frac{1}{(C_{11}^s)_i}\right)^2 \beta_i f_i^s \quad . \quad . \quad . \quad . \quad . \quad (93)$$

is the non-linearity parameter for pure solid solution. For typical values of the C_{11}s and βs the coefficients of the terms containing f_p in equation (92) are estimated to be of order unity. Expanding equation (92) in a power series for small values of f_p and keeping only the linear terms, gives

$$\beta = \bar{\beta}(1 + Rf_p) \quad . \quad . \quad . \quad . \quad . \quad . \quad . \quad . \quad . \quad (94)$$

where the constant

$$R = \sum_i \left[\frac{\bar{C}_{11}}{(C_{11}^s)_i}\left(2 - \frac{\beta_i \bar{C}_{11}}{\bar{\beta}(C_{11}^s)_i}\right) e_i\right] - \frac{\bar{C}_{11}}{(C_{11}^s)_p}\left(2 - \frac{\beta_p \bar{C}_{11}}{\bar{\beta}(C_{11}^s)_p}\right) \quad . \quad . \quad . \quad . \quad (95)$$

Equation (95) is a linear approximation to equation (92). A survey of typical values of $(C_{11})_i$ and β_i indicates that equation (95) should be accurate for most materials to within typical experimental uncertainty for volume fractions as high as approximately 10%.

Proceedings ICM-6, July 1991

ELASTIC STRENGTH OF PARTICLE AND FIBER REINFORCED METAL-MATRIX COMPOSITES

B. GRELSSON and K. SALAMA

Department of Mechanical Engineering, University of Houston
Houston, Texas 77004

ABSTRACT

Conventionally, metal matrix composites (MMC) are reinforced with either particles or fibers. Recently, a new class of composites where a mixture of particles and fibers is used as reinforcement has emerged. The particles improve the isotropic mechanical and thermal properties, whereas the fibers introduce directionally favorable properties for specific applications of the material. The elastic properties of three different matrix alloys containing 6% alumina fibers and varying alumina particle volume fractions of 9, 13, and 17% have been determined using ultrasonic velocity measurements. The results show that the elastic moduli increase with the particle content and the composites have the highest elastic stiffness in the directions of the fiber plane. A model is developed to explain the observed elastic moduli of this type of composites. The model uses results of the theories by Ledbetter and Datta for spherical inclusions and Hashin and Rosen for aligned fibers. Furthermore, it includes an averaging procedure suggested by Christensen and Waals. The agreement between measured and calculated elastic moduli is found to be good. In a second series of measurements, the elastic moduli in two sets of extruded MMCs and one set of pressed MMCs are determined. These composites are reinforced with silicon carbide particles. Their elastic moduli as well as their elastic anisotropies are explained using the theories discussed earlier.

INTRODUCTION

In order to increase structural efficiencies in modern design, materials possessing high stiffness and high strength are required. One class of engineering materials fulfilling these requirements are metal-matrix composites (MMCs). In these composites, properties of the material can be tailored by the appropriate selection of matrix and reinforcement materials and by their mutual arrangement in order to meet specific needs of the designed component. The matrix and the reinforcement are to be selected so that they combine their different mechanical and elastic properties in a synergistic way. Also, microstructures resulting from different fabrication processes are found to influence properties of these composites and provide valuable information for their further development.

Many models have been developed to determine the effective elastic moduli of composite materials. Most of these models deal with reinforcement in the form of spherical particles (Ledbetter and Datta, 1986, Budiansky, 1965), ellipsoidal inclusions (Eshelby, 1957, Chow, 1977) or infinitely long fibers (Hashin and Rosen, 1964, Hill, 1964). Ledbetter and Datta used

a multiple scattering theory to predict the elastic behavior of composites with a nonhomogeneous particle distribution. In the model they assume that the particles together with the matrix form an enriched "sea" that surrounds "islands" of pure matrix material. These non-spherical islands are aligned and produce anisotropy. On the other hand, in order to determine the effective elastic properties of fiber reinforced materials, Hashin and Rosen introduced the composite cylinders model. In this model, the composite is considered to be comprised of infinitely long circular cylinders embedded in a continuous matrix phase. Each fiber has a radius, a, which is surrounded by an annulus of matrix material of radius b, and the ratio a/b is considered to be constant for all composite cylinders. In order to obtain a volume filling configuration, the absolute size of the cylinders must vary considerably.

In some industrial applications composites used are of a more complex nature, where a mixture of particles and fibers is used as a second phase. To our knowledge no models that describe the elastic properties of these composites are available. The present study is concerned with composites reinforced with low values of both particles and fibers, and hence, no interaction between fibers and particles is assumed. In modeling these composites, we first consider the matrix material and the particles to form an effective matrix. Since the particles are homogeneously distributed in the metal, the effective matrix is considered to be homogeneous (Ledbetter and Datta, 1986). The effective matrix is then considered to be reinforced with fibers which are randomly oriented in one plane. The influence of the fibers on the elastic moduli of the composites is then determined first by using the composite cylinders model for an aligned fiber system (Hashin and Rosen, 1964) and second by preforming a geometric average procedure (Christensen and Waals, 1972) which takes care of the 2-dimensionally random orientation of the fibers. The results obtained show a good agreement between calculations and measurements where details are given elsewhere (Grelsson and Salama, 1990).

EXPERIMENTAL

The metal matrix composites used in this investigation consist of aluminum alloys as the matrix material and either SiC-particles or alumina fibers and particles as the reinforcement. The composites based on Al 7064 and Al 8091 were obtained as extruded rods of 25 mm in diameter. The specimens based on Al 6061 were received as pressed plates of the dimension 6 x 25 x 60 mm. The alumina reinforced specimens were manufactured by squeeze casting and received as bars of the dimension 12 x 12 x 50 mm. The volume percentage of reinforcement in the different sets of MMCs is shown in Table 1. Specimens are cut from the as-received

Table 1. Manufacturing method, matrix alloy and volume fraction of reinforcement of the MMCs investigated.

Manufacturing method	Matrix alloy and volume fraction of reinforcement
Extruded rods	Al 7064 + 0% SiC
	Al 7064 + 15% SiC
	Al 7064 + 20% SiC
	Al 8091 + 0% SiC
	Al 8091 + 10% SiC
	Al 8091 + 15% SiC
Pressed plates	Al 6061 + 0% SiC
	Al 6061 + 25% SiC
	Al 6061 + 40% SiC
Squeeze cast bars	A132 + 23% Al_2O_3
	A13 + 19% Al_2O_3
	A1100 + 15% Al_2O_3

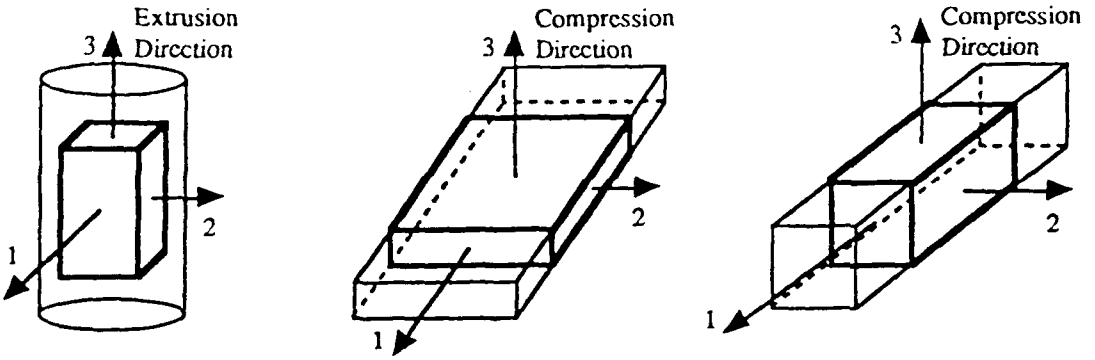

Extruded Al 7064 and Al 8091 MMC rods

Pressed Al 6061 MMC plates

Squeeze cast MMC bars

Fig. 1. Specimen geometry and designated coordinate systems.

composites and the faces of each specimen are machined flat and parallel to within ±25 μm. The coordinate systems are chosen such that in extruded samples the X_1- and X_2-axes are perpendicular to the extrusion direction. In the pressed specimens the X_1- and X_2-axes are in the plate perpendicular to each other and the X_3-axis is oriented parallel to the compression direction. In the squeeze cast samples the X_1- and X_2-directions are in the fiber rich plane at right angles to each other and the X_3-direction is normal to the fiber rich plane. Fig. 1 displays schematically the cut of the specimens, the manufacturing parameters, and the orientation of the coordinate systems. For all specimens the microstructure is examined in the three orthogonal planes in terms of particle size distribution and area fraction covered by the reinforcement. Measurements of ultrasonic velocities were performed using the pulse-echo-overlap method with is described in details elsewhere (Salama and Ling, 1980). X- and Y-cut transducers of 10 and 2.25 MHz were used for the generation of the longitudinal and transverse waves, respectively. The elastic constant are calculated using the relationship $C_{ij} = \rho V_{ij}^2$ where ρ is the mass density.

RESULTS AND DISCUSSIONS

Extruded MMCs

The measured Young's and shear moduli along the three principal axes in the Al 7064 MMCs are listed in Table 2 as a function of the volume fraction of SiC. The same moduli for the Al 8091 MMCs are shown in Table 3. Also included in these tables are the elastic moduli predicted using a model in which the composites are assumed to consist of an aluminum matrix and

Table 2. Calculated and measured Young's and shear moduli of the Al 7064 MMC specimens. Moduli are shown in units of [GPa].

MMC	Al 7064 + 15% SiC		Al 7064 + 15% SiC	
Modulus	calc.	meas.	calc.	meas.
E_{11}	90.0	90.3	96.8	99.9
E_{22}	90.0	90.5	96.8	97.2
E_{33}	90.9	91.4	98.1	100.5
G_{12}	34.0	34.9	36.6	38.0
G_{13}	34.1	35.6	36.8	39.6
G_{23}	34.1	35.3	36.8	38.4

Table 3. Calculated and measured Young's and shear moduli of the Al 8091 MMC specimens. Moduli are shown in units of [GPa].

MMC	Al 8091 + 10% SiC		Al 8091 + 15% SiC	
Modulus	calc.	meas.	calc.	meas.
E_{11}	92.6	91.3	99.3	96.8
E_{22}	92.6	91.8	99.3	96.7
E_{33}	93.2	92.6	100.2	98.3
G_{12}	35.7	35.8	38.4	38.1
G_{13}	35.8	36.2	38.5	38.7
G_{23}	35.8	36.1	38.5	38.5

homogeneously distributed particles of spherical shape. The particles, however, are arranged so that they form unidirectional fibers of particle-rich and particle-free aluminum. This arrangement is chosen to model the microstructure observed in the extruded composites containing spherical particles where the particles cluster together and form areas with high particle concentration and islands of pure matrix material. Due to the extrusion, these areas align in a rod-like shape along the extrusion direction.

From Table 2 and Table 3 one can see that the anisotropy for predicted Young's moduli between the extrusion direction and the two transverse directions is of the same order (~ 1%) as that of the measured moduli. The anisotropy predicted for the shear moduli is negligible and the measured shear moduli is within the experimental error. However, there is a tendency in all measurements indicating that the shear stiffness is lower in the X_1X_2-plane than in the other two planes. This agrees with the difference observed in the calculations of Young's moduli where the extrusion direction is found to be stiffer than the two other directions.

Pressed MMCs

The measured Young's and shear moduli along the principal axes in the Al 6061 MMCs together with the elastic moduli predicted by the model assuming dilute concentrations of homogeneously distributed particles of spherical shape are plotted in Figs. 2 and 3 as a function of the volume fraction of SiC-particles. The plots clearly shows that the model predicts the overall increase of the elastic moduli relatively well for specimens containing 25% SiC. However, it fails for the 40% SiC-reinforced specimen. In this specimen, the values predicted by the model are much smaller than the measured ones. The disagreement between predicted and measured moduli is due to the fact that the model assumes a dilute concentration of particles. The plots in Figs. 2 and 3 also indicate that the increase of the moduli deviates from a linear relationship towards higher values of volume fractions of reinforcement. This behavior may be attributed to particle interactions when the mean-free-pathlength between them is reduced as their volume fraction is increased.

The measured elastic anisotropies found between the directions in the plate and that normal to the plate can be explained by the metallurgical investigations where it is observed that the area of the particles in the compression direction is slightly larger in the compression direction than that in the plane of the plate. This suggests that the particles have the shape of spheroids and that they tend to align during the compression such that their c-axes coincide with the compression direction. The alignment of the particles results in a higher elastic stiffness in the plane of the plate which agrees with the measured elastic properties. The metallurgical investigations also show that the aspect ratio is only slightly less than one. According to calculations by Ledbetter and Datta, such a low aspect ratio does not result in elastic anisotropies as large as they are found in the investigated MMCs which are approximately 5%. Calculations assuming an aspect ratio of 0.8 predict an anisotropy of the order of 1% for the Al 6061 matrix reinforced with 25% SiC.

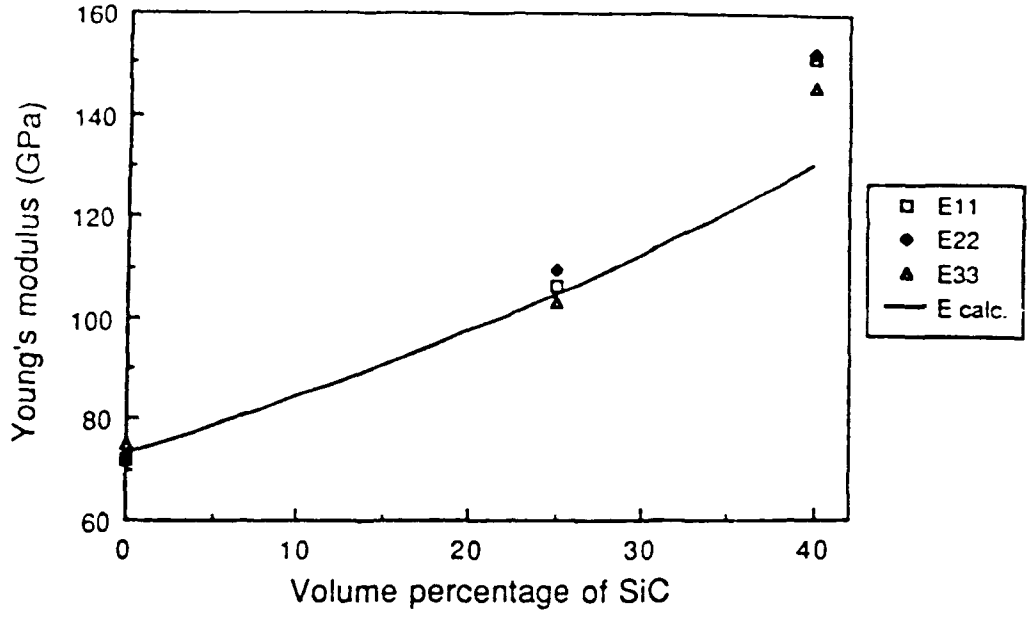

Fig. 2. Measured and calculated Young's moduli in the Al 6061 MMC specimens as a function of volume percentage SiC.

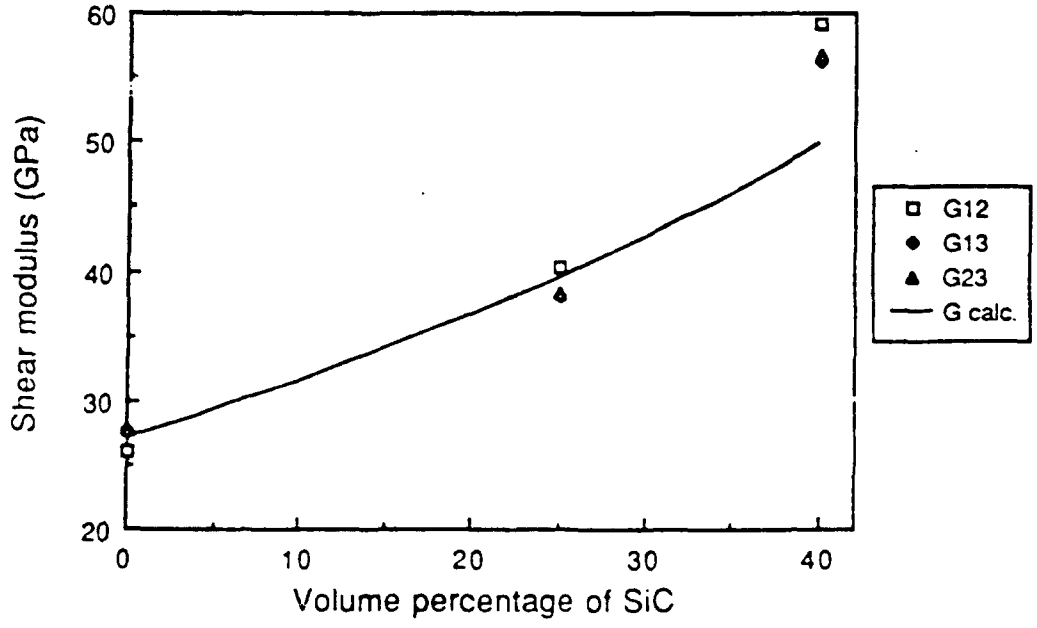

Fig. 3. Measured and calculated shear moduli in the Al 6061 MMC specimens as a function of volume percentage SiC.

Table 4. Calculated and measured Young's and shear moduli of the squeeze cast MMC specimens. Moduli are shown in units of [GPa].

MMC	Al 123 + 23% Al_2O_3		Al 13 + 19% Al_2O_3		Al 1100 + 15% Al_2O_3	
Modulus	calc.	meas.	calc.	meas.	calc.	meas.
E_{11}	102.2	101.9	94.9	97.1	88.0	86.4
E_{22}	102.2	102.0	94.9	97.2	88.0	88.2
E_{33}	99.6	100.7	92.1	94.3	85.0	83.9
G_{12}	38.8	38.4	35.9	36.9	33.5	32.8
G_{13}	37.4	37.8	34.4	35.2	31.9	31.0
G_{23}	37.4	38.2	34.4	35.8	31.9	31.1

Measurements in the unreinforced material have shown that the texture present influences the elastic properties significantly. Here, the texture accounts for a 4% higher Young's modulus in the compression direction. Thus, it seems reasonable to consider that the texture is responsible for the major part of the anisotropy observed in the reinforced specimens.

Squeeze Cast MMCs

In the squeeze cast specimens, the alumina fibers are randomly oriented in one plane whereas the alumina particles are also homogeneously distributed. The elastic moduli along the principal axes of the composites are predicted using a model which assumes the composites to be comprised of an effective matrix consisting of the pure aluminum and the homogeneously particles. The effective matrix is then considered to be reinforced with planar-randomly distributed fibers. The predicted as well as the measured elastic moduli are listed in Table 4. The results show that the increase in the elastic moduli due to the reinforcement is reasonably well predicted by the model. A more crucial test of the applicability of this model is its ability to predict the elastic anisotropy between the directions in the fiber-rich plane and the direction normal to the plane. Since the fiber content is the same for all three specimens, the anisotropy is expected to be more pronounced the lower the stiffness of the effective matrix i.e. the lower the concentration of alumina particles is. This behavior is experimentally observed as shown by the values of the Young's and shear moduli in Table 4. The difference in the moduli between the in-plane directions and the normal direction is less pronounced the higher the stiffness of the effective matrix becomes. Quantitatively, the measured anisotropies are well predicted by the model.The model, however, assumes that there is no interaction between particles and fibers and therefore it is more suitable for composites with low particle content.

ACKNOWLEDGEMENT

This work is sponsored by the Army Research Office under contract No. DAAL03-88-K-0096.

REFERENCES

Budiansky, B. (1965), *J. Mech. Phys. Solids*, 13, 223.
Chow, T.S. (1977), *J. Appl. Phys.*, 48, 4072.
Christensen, R.M. and Waals, F.M. (1972), *J. Comp. Mater.*, 6, 518.
Eshelby, J.D. (1957), *Proc. Roy. Soc. (London)*, 241A, 376.
Grelsson, B. and Salama, K. (1990), *Res. Nondestructive Evaluation*, 2, 83.
Hashin, Z. and Rosen, B.W., (1964), *J. Appl. Mech.*, 31, 223.
Hill, R. (1964), *J. Mech. Phys. Solids*, 12, 199.
Ledbetter, H.M. and Datta, S.K. (1986), *J. Acoust. Soc. Am.*, 79, 239.
Salama, K. and Ling, C.K. (1980), *J. Appl. Phys.*, 51, 1505.

Res Nondestr Eval (1991) 3:159–170

Elastic Nonlinearity in Metal-Matrix Composites

H. Mohrbacher* and K. Salama

Department of Mechanical Engineering, University of Houston, Houston, TX 77204, USA

Abstract. Parameters characterizing the elastic nonlinearity in metal-matrix composites are studied. The composites consist of the aluminum alloys 8091 or 7064 containing silicon carbide particles up to 20% volume fraction. Two different ultrasonic measurements, namely the acoustoelastic effect and the harmonic generation, are used for the determination of acoustic nonlinearity parameters. Their dependence on the content of SiC in the composite is investigated. The values of the nonlinearity parameter are found to decrease with increasing volume fraction of SiC-particles. The changes are explained in terms of the effects of SiC-particles on the second and third order elastic constants of the composites.

Introduction

Elastic nonlinearity is responsible for the deviation of a material's stress-strain response from the linear relationship represented by the isothermal form of the generalized Hooke's law. This law can be written as

$$\sigma_{ij} = C_{ijkl}\varepsilon_{kl}, \tag{1}$$

where σ_{ij} and ε_{kl} are the stress and strain tensors respectively, and C_{ijkl} is the fourth order tensor which represents the second order elastic constants. The nonlinear elastic behavior of materials can be determined from measurements of the stress dependance of ultrasonic velocities as well as the distortion of ultrasonic waves by the generation of higher harmonics. Consequently, these effects can be used to characterize a material's elastic nonlinearity nondestructively.

In recent studies, the influence of microstructure on the acoustic nonlinearity parameter has been investigated in aluminum alloys. Razvi et al. [1] found a linear correlation between the acoustic nonlinearity parameter and the volume fraction of second phase precipitates in some heat treatable aluminum alloys. Another correlation was found by Yost et al. [2] between the hardness and the

* *Permanent address*: Fraunhofer Institut für zerstörungsfreie Prüfverfahren (IzfP), Universitätsgeb. 37, W-6600 Saarbrücken, Federal Republic of Germany

acoustic nonlinearity parameter in maraging steel. These studies directed the attention to similar investigations of the nonlinearity parameter in two phase materials such as metal-matrix composites (MMC). These composites consist of a metallic matrix and a metallic or ceramic reinforcement which can be presented in the form of particles, short or long fibers. The properties of the composite depend on those of the constituent phases as well as on the interaction between the phases in the composite. The interaction is determined by the geometrical arrangement of the reinforcement as well as the bond strength between the two phases. In order to verify the desired bulk properties, the nondestructive characterization of linear and nonlinear elastic behavior of such composites is essential.

In this investigation, nonlinear elastic effects were determined as a function of the SiC-particle content in the aluminum alloys 8091 and 7064 by measuring the stress dependance of the ultrasonic velocity and the harmonic distortion of ultrasonic waves. These measurements yield the effective second and third order elastic constants as well as the effective acoustic nonlinearity parameter of the composite.

Elastic Nonlinearity in Solids

All elastic properties of a solid can be derived from the elastic energy representation of that solid. In general, the strain energy of deformation per unit volume, Φ, can be expanded as a power series in the elastic strain, ε, as

$$\Phi(\varepsilon) = \Phi_0 + C_{ij}\varepsilon_{ij} + \frac{1}{2} C_{ijkl}\varepsilon_{ij}\varepsilon_{kl} + \frac{1}{6} C_{ijklmn}\varepsilon_{ij}\varepsilon_{kl}\varepsilon_{mn} - \ldots . \qquad (2)$$

According to Brugger [3], Φ_0 is the strain energy per unit volume in the undeformed state and the coefficients $C_{ij\ldots}$ in the expansion are the elastic constants. In a linear elastic solid there are no contributions to the elastic energy from terms higher than the power two in ε. All materials, however, have anharmonic elastic potential which is determined by the ratio of the third and the second order contributions to the elastic energy.

In an isotropic solid, the strain energy density depends only on the invariants I_1, I_2, and I_3 of the strain tensor since the elastic constants are invariant under arbitrary rotations. Murnaghan [4] writes Φ for an isotropic material as

$$\Phi = \Phi_0 + \sigma I_1 + \frac{\lambda + 2\mu}{2} I_1^2 - 2\mu I_2 + \frac{l + 2m}{3} I_1^3 - 2mI_1I_2 + nI_3, \qquad (3)$$

where σ is the stress, λ and μ are the second order Lamé constants, and l, m, and n are the third order elastic constants in Murnaghan notation. The second and third order elastic constants can be conveniently obtained from ultrasonic measurements. The second order Lamé constants are directly related to ultrasonic velocities as

$$\mu = \rho V_S^2 \quad \text{and} \quad \lambda = \rho(V_L^2 - 2V_S^2), \qquad (4)$$

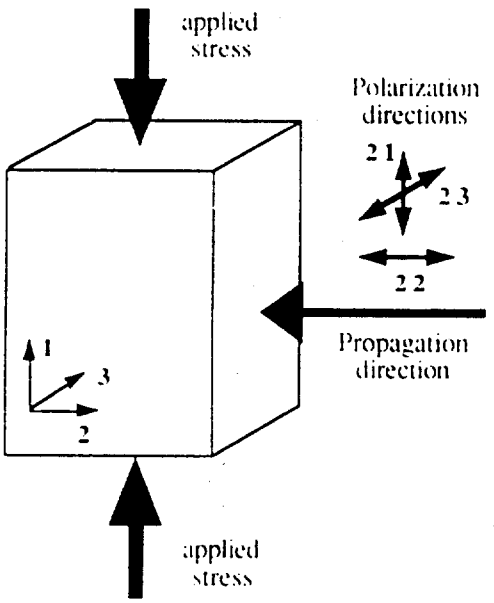

Fig. 1. Designation of wave modes and direction of applied stress

where ρ is the density and V_S and V_L are the shear and the longitudinal wave velocities, respectively.

A formalism which allows the evaluation of the third order elastic constants l, m, and n from the strain dependance of the ultrasonic velocity was developed by Hughes and Kelly [5]. In an uniaxially strained specimen, the velocities of ultrasonic waves depend linearly on the elastic strain. Commonly, three wave modes are used: the two linearly polarized shear waves and the longitudinal wave, having polarization and propagation directions as indicated in Fig. 1. The slopes of these linear relationships normalized with respect to the velocities in the strain-free specimen are called acoustoelastic constants and related to the third order elastic constants l, m, and n as

$$l = \frac{\lambda}{1-2\upsilon}\left[\frac{1-\upsilon}{\upsilon}\frac{dV_{22}/V_{22}^0}{d\varepsilon} + \frac{2}{1+\upsilon}\left(\frac{dV_{21}/V_{21}^0}{d\varepsilon} + \upsilon\frac{dV_{23}/V_{23}^0}{d\varepsilon}\right) + 2\upsilon\right], \quad (5a)$$

$$m = 2(\lambda+\mu)\left(\frac{\upsilon}{1+\upsilon}\frac{dV_{23}/V_{23}^0}{d\varepsilon} + \frac{1}{1+\upsilon}\frac{dV_{21}/V_{21}^0}{d\varepsilon} + 2\upsilon - 1\right), \quad (5b)$$

$$n = \frac{4\upsilon}{1+\upsilon}\left(\frac{dV_{21}/V_{21}^0}{d\varepsilon} - \frac{dV_{23}/V_{23}^0}{d\varepsilon} - 1 - \upsilon\right), \quad (5c)$$

where V_{ij} are the ultrasonic velocities with propagation and polarization directions as indicated in Fig. 1, the superscript 0 denotes the velocity at zero strain, and υ is the Poisson's ratio.

Another method for the determination of the nonlinear elastic effect is the generation of higher harmonics. An originally sinusoidal sound wave gets distorted while propagating through a nonlinear material. The anharmonicity of

the interatomic potential function leads to the nonlinear wave equation which can be written for a longitudinal wave propagating in an isotropic solid as [6]

$$\rho \frac{\partial^2 u}{\partial t^2} - (\lambda + 2\mu) \frac{\partial^2 u}{\partial x^2} = \left[3 + \frac{2l + 4m}{\lambda + 2\mu}\right] \frac{\partial u}{\partial x} (\lambda + 2\mu) \frac{\partial^2 u}{\partial x^2}, \tag{6}$$

where u is the displacement and t and x are the time and space variables, respectively. This nonlinear wave equation differs from the linear wave equation by the perturbation term on the right hand side which is determined by the ratio of the third- and second-order elastic constants. The term in brackets in Eq. 6 is called the acoustic nonlinearity parameter β, and is related to these elastic constants as

$$-\beta = 3 + (2l + 4m)/(\lambda + 2\mu). \tag{7}$$

It is interesting to see from Eq. 6 that the condition for linear longitudinal wave equation is not the third-order elastic constants to be equal to zero, but the ratio $(2l + 4m)/(\lambda + 2\mu)$ is equal to -3.

According to Thurston and Shapiro [6], the solution of this equation for u can be obtained, using a perturbation technique, as

$$u = A_1 \sin(\omega t - kx) + A_2 \cos(2\omega t - 2kx) + \ldots . \tag{8}$$

Here, ω is the frequency of the ultrasonic wave, k is the wave number, and A_1 is the amplitude of the fundamental wave. The generated second harmonic will have an amplitude A_2 and twice the fundamental frequency. The amplitude of the second harmonic is related to the square of the fundamental amplitude as

$$A_2 = \frac{1}{8} \beta A_1^2 k^2 x, \tag{9}$$

where x is the propagation distance of the wave.

In multi phase materials such as metal-matrix composites, the constituents may have very different elastic and mechanical properties which result in the effective macroscopic properties of the composite. In general, these effective properties are not expected to follow a linear law of mixture. Cantrell et al. [7] showed that the effective nonlinearity parameter of multi phase materials is a nonlinear function of the volume fraction of the participating phases. Furthermore, different phases interact with each other at the interfaces where very high residual stresses are likely to be present. These are either compatibility stresses due to differences in the elastic-plastic properties of the constituent phases or thermal stresses arising from differences in the coefficients of thermal expansion. The lattice distortion in these phases, due to the presence of residual stresses, will additionally contribute to the effective acoustic nonlinearity parameter of the composite.

Table 1. Chemical composition of the investigated aluminum alloys in wt. %

	Alloying elements								
Alloy	Si	Fe	Cu	Mg	Zr	Li	Zn	Cr	Co
Al-7064	0.05	0.10	2.60	2.30	0.20	—	7.10	0.12	0.22
Al-8091	0.02	0.01	1.90	0.80	0.20	2.70	—	—	—

Experimental

Specimens

In the present investigation, two metal-matrix composites with matrices of the heat treatable aluminum alloys Al-8091 and Al-7064 are examined. Their chemical compositions are shown in Table 1. The aluminum matrices are reinforced with globular silicon carbide (SiC) particles up to 20% volume fraction of sizes ranging between 1 and 5 μm. The specimens were received as extruded rods of 1 inch in diameter. Due to the manufacturing process, the particles are aligned along the extrusion direction, while in the plane perpendicular to the extrusion direction the particles are randomly distributed. Micrographs of these two planes are shown in Fig. 2 for the composite consisting of Al-8091 and 10% SiC-particles. For harmonic generation measurements, the specimens are cut to a length of two inches. Opposite faces are machined parallel and then polished to optical flatness. After measuring the acoustic nonlinearity parameter, the sides of the specimens were milled to a square shaped cross section in order to measure acoustoelastic constants.

Ultrasonic Velocity Measurements

In order to determine the third order elastic constants, the strain dependance of the ultrasonic velocity needs to be measured. This effect is typically in the order of one part in 10^4 and requires very precise time of flight measurements. The system used in this investigation utilizes the pulse-echo overlap method for the determination of the time of flight as described in [8]. In Fig. 3, a block diagram of the system components is shown. Using this system, an absolute time resolution of ± 200 ps can be measured. During the time of flight measurements, compressive strains are applied to the specimen along the extrusion direction and are varied systematically in the elastic regime. The time of flight data are acquired by a computer and ultrasonic velocities are calculated as a function of the applied strain. Corrections are made for the change in the lateral dimension of the strained specimen which is due to the Poisson's expansion. The linear relationship between the ultrasonic velocity and the elastic strain is then evaluated by a least squares fit algorithm. The slope of the curve is normalized with respect to the velocity of the unstrained specimen and is called the acoustoelastic constant. The acoustoelastic constants of the three wave modes shown in Fig. 1 are used in the calculation of the third order elastic constants using Eqs. 5.

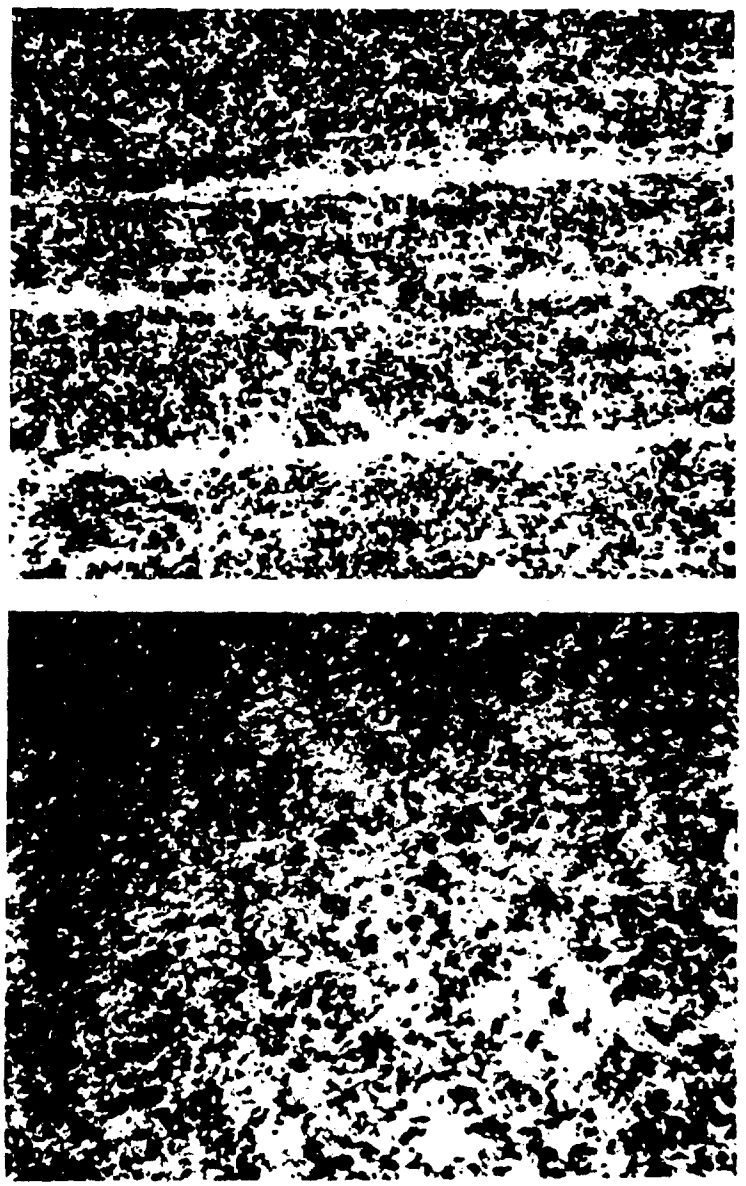

Fig. 2. Particle distribution in extruded MMC specimens: **a** extrusion direction, **b** transverse direction

Absolute Amplitude Measurements

For the direct measurements of the acoustic nonlinearity parameter the absolute amplitudes of the fundamental and the second harmonic waves are determined. This is achieved using a capacitive detector system which is described in detail elsewhere [9]. The block diagram in Fig. 4 shows the experimental setup schematically. For the excitation of the fundamental longitudinal wave,

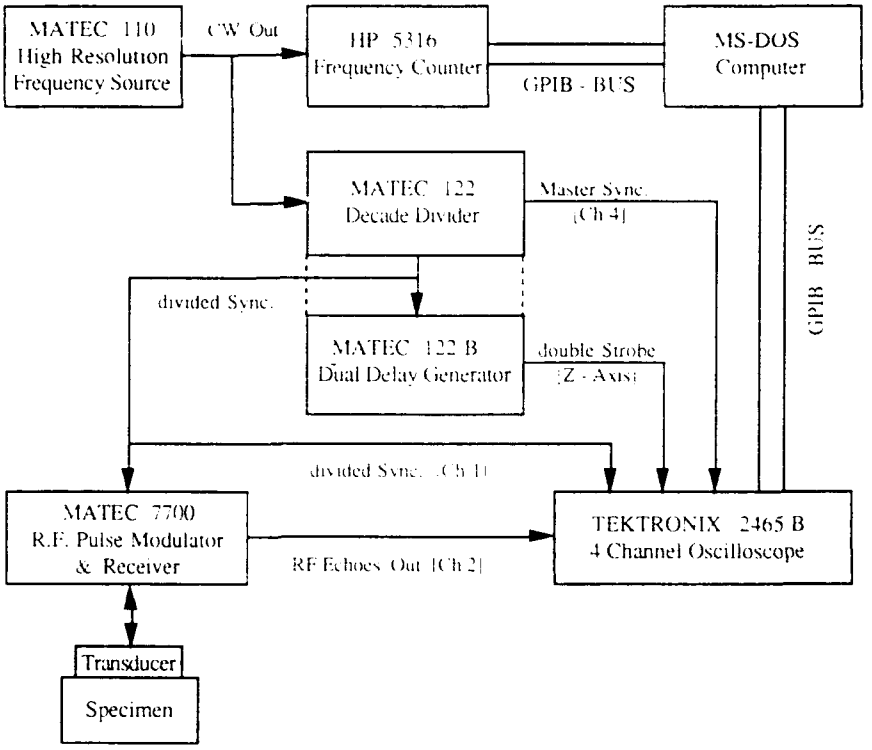

Fig. 3. Block diagram of the ultrasonic time of flight measurement setup

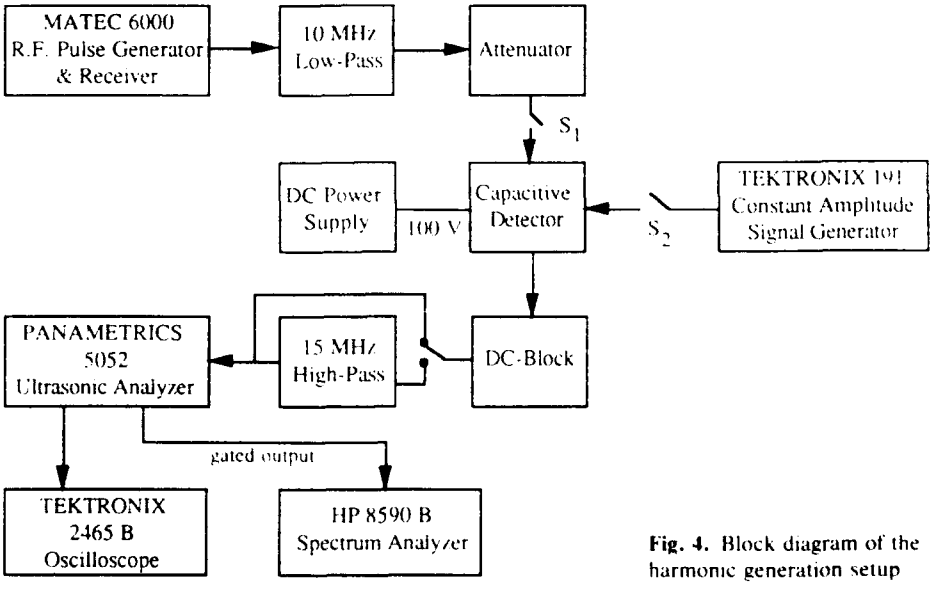

Fig. 4. Block diagram of the harmonic generation setup

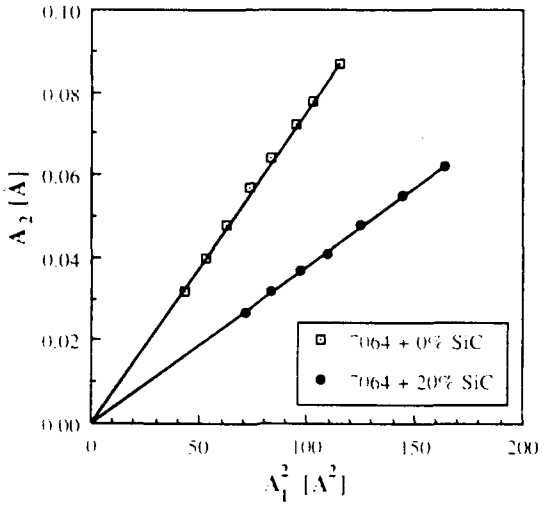

Fig. 5. Correlation between fundamental and second harmonic amplitude

an electric 10 MHz signal is applied to a narrow band undamped lithium niobate transducer which is bonded to the surface of the specimen. The longitudinal wave which has a bandwidth of 200 kHz and a duration of 5 μs is propagated along the extrusion direction. The superposition of the fundamental wave and its second harmonic is picked up by the capacitive transducer on the opposite surface. During the measurements, the received signal is amplified and the amplitudes of its frequency components are analyzed. These measurements are repeated for different driving amplitudes. The amplitude of the second harmonic is plotted vs. the square of the fundamental amplitude in Fig. 5 for two of the specimens examined in this investigation. The linear relationship between the two quantities is predicted by Eq. 9. The slope of a linear least squares fit through the measured points is then used to evaluate the acoustic nonlinearity parameter β.

Results and Discussion

For both sets of composites, the second and third order elastic constants are calculated using measured ultrasonic velocities and their strain derivatives, respectively. Their values are listed in Table 2. It has to be noted that the third

Table 2. Second and third order elastic constants of MMCs

	SOEC [GPa]				TOEC [GPa]		
	λ	μ	E	ν	l	m	n
Al-8091	44.9	31.0	80.2	0.30	−218	−378	−435
+10% SiC	46.3	35.8	91.7	0.28	−185	−365	−454
+15% SiC	46.0	38.1	96.9	0.27	−162	−360	−423
Al-7064	59.3	27.4	73.4	0.34	−324	−397	−403
+15% SiC	57.0	34.7	91.0	0.31	−215	−397	−454
+20% SiC	57.6	38.1	99.1	0.30	−214	−397	−461

Table 3. Nonlinearity parameters of metal-matrix composites as calculated from elastic constants and measured from harmonic generation

	β (Eq. 12)	Rel. change	β (meas.)	Rel. change
Al-8091	15.2	0%	10.2	0%
+10% SiC	12.6	−17%	8.5	−17%
+15% SiC	11.5	−24%	7.5	−26%
Al-7064	16.6	0%	8.6	0%
+15% SiC	13.0	−22%	6.9	−20%
+20% SiC	12.1	−27%	5.9	−31%

order elastic constants of the composites are determined using formulas which were derived for isotropic materials, although the micrographs reveal some anisotropic particle distribution. This may affect the absolute value of the third order elastic constants determined in these composites. It is assumed, however, that changes in these values due to different particle content is not affected.

The data in Table 2 indicate a considerable increase in the magnitudes of the Young's modulus E and the shear modulus μ with the SiC-particle content. At the same time, the Poisson's ratio υ is reduced. The experimental error in these constants is estimated to be within 2%. One can also see from Table 2 that the changes in the third order elastic constants are less pronounced. The inaccuracy in these values is 15% for l, 5% for m and 3% for n. Only in the case of the constant l, a clear influence of reinforcement is observed. Its magnitude decreases when SiC-particles are added to the matrix. The value of the constant l, however, saturates at higher particle content in the composite. For the constants m and n, no significant trend can be observed.

The values of the second and third order elastic constants are used to calculate the nonlinearity parameters according to Eq. 7 and their values are listed in Table 3. The inaccuracy in the calculated nonlinearity parameter is estimated to be 10%. Also included in Table 3 are the values of the nonlinearity parameter determined directly from the harmonic generation experiments. Here, the inaccuracy is estimated to be of the order of 15%. From the data in Table 3, one can see that both calculated and experimentally measured nonlinearity parameters decrease considerably with increasing particle content.

Table 3 also indicates that the experimentally measured values of the acoustic nonlinearity parameter are about 50% smaller than those calculated. This difference may be caused by the anisotropy in the elastic properties due to the particle alignment as well as the texture in the aluminum matrix [10]. The values of the directly measured nonlinearity parameter are obtained using longitudinal waves which propagate along the extrusion direction while those calculated are obtained using second and third order elastic constants measured in the transverse direction. Because of the strong dependence of the nonlinearity parameter on the crystallographic orientation of single crystals, texture is likely to introduce significant anisotropy in this parameter. Furthermore, inaccurate absolute values of the third order elastic constants, due to the use of formulas which are only valid for isotropic materials, may contribute to

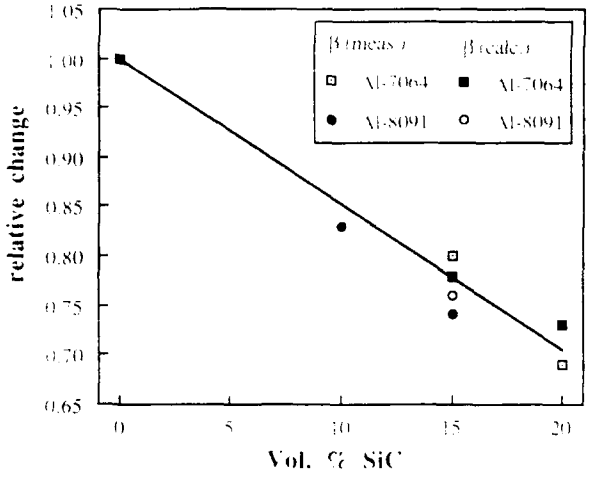

Fig. 6. Relative change of measured and calculated nonlinearity parameters as a function of SiC-particle content

the observed difference. Good agreement, however, is found in the relative changes of the measured and calculated nonlinearity parameters. As can be seen from Fig. 6, the relative change in the nonlinearity parameter with the SiC content indicates a linear relationship between the two quantities. The relative change is in the order of 30% over the range of 20% volume fraction of SiC-particles added to the Al-alloys.

An explanation for the decreasing values of the nonlinearity parameter in MMCs may be found by separately analyzing the contributions of the second and the third order elastic constants shown in Eq. 7. The second order elastic constants appear in the denominator of Eq. 7 and, accordingly, their increase with particle content will yield a decrease in the nonlinearity parameter. The increase in these constants is determined by the elastic moduli of the constituents of the composite as well as the interface between reinforcement and matrix. Theoretically, the upper and lower limits for the elastic moduli of two phase materials are determined by the isostrain and isostress conditions [11]. The third order constants in the numerator of Eq. 7 decrease in magnitude as a function of particle content and, thus, their contributions also lower the values of the nonlinearity parameter in the composites. However, it appears that the contributions of the second order elastic constants dominate the magnitude of the effective nonlinearity parameter in the composite, especially at higher amounts of reinforcement.

This analysis can also be applied to the results obtained by Razvi et al. on Al-7075 alloys containing different amounts of second phase precipitates which are shown in Fig. 7. Here, the nonlinearity parameter was measured using harmonic generation and found to increase with the volume fraction of second phase. Also included in Fig. 7 are the results obtained on the Al-7064 metal-matrix composites. Unlike the SiC-particle reinforced Al-7064 MMCs, the change in the second order elastic constants of Al-7075, due to the presence of precipitates, is found to be very small [1]. On the other hand, the presence of the second phase precipitates is responsible for a high degree of distortion in

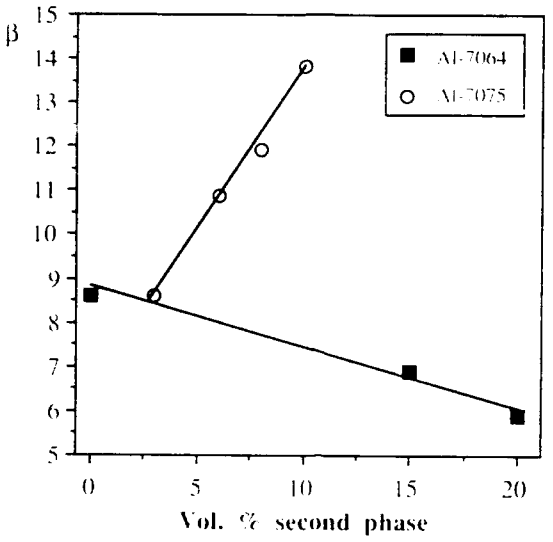

Fig. 7. Comparison of measured nonlinearity parameters in precipitation hardened Al-7075 and Al-7064 based MMC specimens

the matrix, which is the effective hardening mechanism in such alloys. Consequently, the denominator of Eq. 9 remains approximately constant. Unfortunately, the effect of second phase precipitates on the third order elastic constants of Al-7075 was not determined. However, measurements of acoustoelastic constants on steel [12] and heat treatable aluminum alloys [13] indicate that these constants increase as the amounts of second phase precipitates in these alloys are increased. These results, nevertheless, show that the third order elastic constants in these alloys are likely to increase as a function of second phase precipitates, and, in turn, contribute to the increase of the acoustic nonlinearity parameter which is opposite to that observed in metal-matrix composites.

Conclusions

The second and third order elastic constants as well as the acoustic nonlinearity parameter have been determined in metal-matrix composites consisting of SiC-particles up to 20% volume fraction and Al-7064 or Al-8091. The results show that the acoustic nonlinearity parameter is significantly influenced by the volume fraction of the second phase reinforcement present in the composite. The third order elastic constants m and n remain unchanged while the constant l as well as the nonlinearity parameter decrease as the volume fraction of SiC-particles is increased. This behavior can be explained in terms of the increase of the effective second order elastic constants and the decrease of the effective third order elastic constants with reinforcement. This argument can also be used to explain the increase in the acoustic nonlinearity parameter as a function of second phase precipitates observed by Razvi et al. in the aluminum alloy 7075.

Acknowledgements. The authors would like to acknowledge many useful discussions with Mr. E. Schneider from the Fraunhofer Institut für zerstörungsfreie Prufverfahren. This work is sponsored by the Army Research Office under contract No. DAAL03-88-K-0096.

References

1. S. Razvi, P. Li, K. Salama, J.H. Cantrell, and W.T. Yost. In: *Review of Progress in Quantitative NDE*, vol. *6B*, edited by D.O. Thompson and D.E. Chimenti, p. 1403, Plenum, New York (1987)
2. W.T. Yost and J.H. Cantrell. In: *Review of Progress of Qunatitative NDE*, vol. 9B, edited by D.O. Thompson and D.E. Chimenti, p. 1669, Plenum Press (1990)
3. K. Brugger, Phys. Rev. **133A:**1611 (1964)
4. F.D. Murnaghan, *Finite Deformation of an Elastic Solid*, Wiley, New York, (1951)
5. D.S. Hughes and J.L. Kelly, Phys. Rev. **92:**1145 (1953)
6. R.N. Thurston and M.J. Shapiro, J. Acoust. Soc. Am **41:**1112 (1967)
7. J.H. Cantrell, W.T. Yost, S. Razvi, P. Li, and K. Salama, Proc. IEEE Ultrasonics Symposium, p. 1075 (1986)
8. E.P. Papadakis, J. Acoust. Soc. Am. **42:**1045 (1967)
9. M.A. Breazeale and J. Philip. In: *Physical Acoustics, Vol. XVII*, edited by W.P. Mason and R.N. Thurston, p. 1, Academic Press (1984)
10. M. Spies and K. Salama, Res. Nondestr. Eval. **1:**99 (1989)
11. K.K. Chawla, *Composite Materials*, Springer-Verlag, New York (1987)
12. J.S. Heyman, S.G. Allison, K. Salama, and S.L. Chu. In: *Nondestructive Evaluation-Applications to Materials Processing*, edited by O. Buck and M. Wolf, p. 177, ASM Publications (1984)
13. E. Schneider, S.L. Chu, and K. Salama. In: *Review of Progress in Quantitative NDE*, vol. *6B*, edited by D.O. Thompson and D.E. Chimenti, p. 867, Plenum, New York (1985)